MASTER OF SCIENCE THESIS

Study on the effect of trailing edge serrations

For laminar boundary layer instability noise

Mudit Gupta

FACULTY OF AEROSPACE ENGINEERING

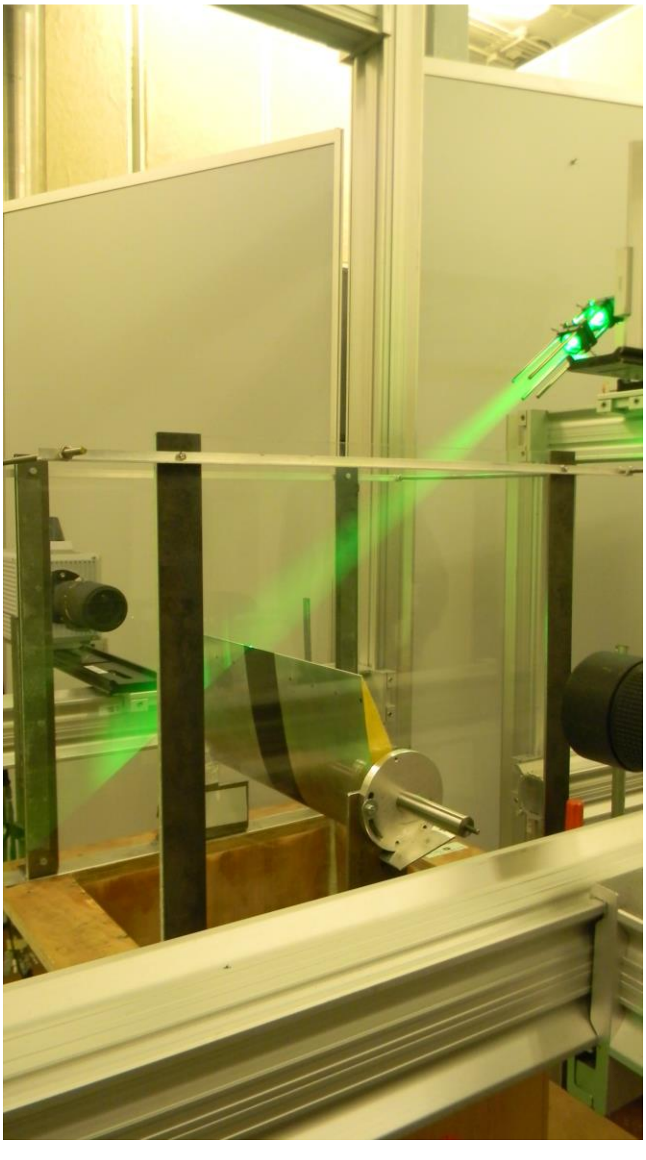

Faculty of Aerospace Engineering

Delft University of Technology

Faculty of Aerospace Engineering

Delft University of Technology

Master of Science Thesis

on

Study on the effect of trailing edge serrations

For obtaining the degree of Master of Science in Aerospace Engineering at the

Delft University of Technology

Author :	Supervisors:
M. Gupta	**Prof.dr. F. Scarano**
Student Number: 4299221	**J. Serpieri (MSc)**
	Dr.ir. S.Pröbsting

Aerodynamics

Faculty of Aerospace Engineering

Delft University of Technology

Date

Acknowledgement

I wish to record my sincere gratitude to thesis supervisors, Dr. Ir. Jacopo Serpieri, Dr. Ir. Stefan Pröbsting and Prof. Dr. Fulvio Scarano. Their inspiring guidance and affectionate encouragement throughout gave courage to finish the project. They provided me with maneuverability and freedom to work albeit keeping an eye on the progress. Without their patient and encouraging cooperation, this work could never have taken the present shape.

I would also like to thank my father, who supported me in thick and thin with his generous heart and warm smile. The student counsellor, Mr. John Stals and academic counsellors of aerospace department helped me though the anxious times I faced during my study. In the end, I would like to thank my friends and well-wishers for their emotional support which kept me going in tough times.

Abstract

Wings operated at low and moderate Reynolds number such as the ones of UAVs or the blades of small turbine and of compressors, can be the source of an aero-acoustic phenomenon called laminar boundary layer instability noise. The narrow band noise can be attenuated using trailing edge (TE) serrations (Chong et al. 2013, Moreau et al. 2012) but the mechanism behind tonal attenuation is yet to be investigated in detail. An experimental study ($1.32X10^5 < Re < 5.30X10^5$) is conducted in an open-jet low turbulence wind tunnel using NACA 0018 airfoil ($c = 0.20m$) with modified TE. The acoustic emission in the far field is recorded using far-field microphones whereas the developing field near the TE is studied using Time resolved planar particle image velocimetry and oil flow visualization techniques. Study showed the serration-3 ($2h = 20mm$, $\lambda = 10mm$) has maximum tonal noise attenuation and effect the point of separation of laminar separation bubble. The span-wise change in flow characteristics in case of serrations can be attributed to the effective chord-length of the wing at each span-wise position. Further span-wise correlation of chord-wise flow fluctuations show the flow being turbulent upstream of serration-3 TE modification.

Table of Contents

List of Figures

List of Tables

Abbreviations

Abbreviation	**Description**
Δt	time separation between two subsequent vector fields
U	free stream velocity
U	velocity component along the chord of the wing
V	velocity component along the span of the wing
W	velocity component along the normal to the chord plane
α_{geo}	geometric angle of attack
α_{eff}	corrected angle of attack
Re	Reynolds number
TE	trailing edge
TS	Tollmien-Schlichting
FOV	field of view
F	frequency
z_o	reference span wise station
C	wing chord length
PIV	particle image velocimetry

1. Introduction

Aero-acoustics is a specialised branch of acoustic science to study noise emitted from an object due to interaction between airflow and solid geometry. In last few years, with the introduction of guidelines to restrict noise near populated areas, the field of aero-acoustics has attracted researchers and engineers alike to attenuate noise. The field of aero-acoustics is quite wide in itself, so study presented here using experimental techniques, will focus on noise emitted by trailing edge of an airfoil in laminar flow within a certain Reynolds number range ($1.32X10^5 < Re < 5.3X10^5$). The noise emitted by airfoil under such conditions with moderate angle of attack in referred as laminar boundary layer (LBL) instability noise. The LBL instability noise is produced due to coupling of hydrodynamic instabilities and acoustic waves and the interaction of locked hydrodynamic instabilities in transitional stage with trailing edge. The coupling between acoustic waves and hydrodynamic instabilities is referred as acoustic feedback loop or just feedback loop in literature.

1.1 Background

Aero-acoustics have become a major area of research with governments taxing companies such as airlines on noise emitted while conducting services especially near populated residential areas. Also military is taking more and more interest in developing drone technology and making them as silent as possible. Wind power holds the key to energy sustainability and with wind mills situated near highways and residential areas; it is paramount to attenuate the noise produced.

These technological developments have motivated researchers to develop mathematical models as well as conduct experimental study to understand the physics behind noise emitted by airfoils. The study conducted here, as mentioned above, narrows the study to the regime where LBL instability noise is emitted by trailing edge (TE) of an airfoil.

Figure 1-1: Climber removing trips from serrated blade

The emitted sound waves from TE can be narrow band or broad band in nature which are related to laminar and turbulent flow regimes on the airfoil respectively and also on angle of attack (AoA). Due to non-linearity of governing equations it is quite difficult to predict sound generated by the interaction of air flow and solid geometry (assuming no aero-elasticity). As the sound produced represents only a small fraction of energy in the air flow, prediction and the physics governing the sound becomes quite difficult. This in particular becomes dramatic in free space and at low sub-sonic speeds. The sound in itself is a small perturbation in the overall flow, thus it requires complex, high resolution, computational intensive mathematical models to resolve and study aero-acoustics using CFD techniques. To study this complex phenomenon experimentally, low turbulence wind tunnel becomes a necessity. Equipment such as high resolution micro-phones and techniques to capture high frequency flow field is also required to run a successful experimental campaign. The author is passionate to learn different experimental techniques, thus a path to study this problem experimentally is chosen. With this in mind and the literature studied, an experimental campaign is planned to study aero-acoustics. The experimental study undertaken in this thesis work focuses on LBL instability noise produced by the sharp trailing edge airfoils within a certain Reynolds number ($Re < 10^6$). In the last 50 years, a number of research papers have been published and this study adds to the available literature pertaining to the topic in question. The first major study was conducted by (Paterson *et al.*) to understand the narrow band noise produced by airfoils in medium range Reynolds number. A generic airfoil in laminar flow produces narrow band (tonal) noise at low to moderate Reynolds number which is accompanied by the formation of laminar separation bubble (LSB). At low Reynolds number LSB is formed on suction side of the airfoil. While at medium Reynolds number LSB is formed on the pressure side of the airfoil. The experimental study in the study is conducted in medium Reynolds number regime ($1.32X10^5 < Re < 5.3X10^5$). The LSB formed on pressure side plays a central role in narrow band noise produced at the trailing edge. The emitted discrete tones from the trailing edge overlap on a broadband hump Arbey&Bataille 1983 and have specific characteristics, which are explained in detail in section 'Literature review'.

Though the physics involved in the trailing edge noise for medium Reynolds number with moderate angle of attack (AoA) is under scrutiny and over the years many theories have been suggested (Paterson et al. 1973; Arbey&Bataille 1983; Lowson et al. 1994; Nash et al. 1999).Experimental studies have been conducted by simulating the noise in the wind tunnel (open and anechoic). The closed wind tunnel is not preferable due to resonance of sound waves. In these experiments different airfoil modifications are used such as porous surface on pressure side, different serrations, brushes attached at the trailing edge and cavity on a generic airfoil. The idea behind these modifications is to attenuate the tonal noise, thus segregating the acoustic waves from hydrodynamic waves and study them separately and in combination. This approach of decoupling acoustic and hydrodynamic waves helps in studying the feedback loop in detail. Complex CFD techniques such as DNS, large eddy methods are applied to simulate and understand the mechanism of the tonal noise and some mathematical studies used trailing edge (TE) modifications to understand the mechanism through which noise in generated. The current experimental thesis work uses a generic airfoil (NACA 0018) with specially designed trailing edge modifications, to accommodate serrations and flap. It has been known for some time that modified trailing edge of wing with saw-toothed serrations attenuates the tonal noise and in some cases completely suppresses it. This gives an opportunity to study the feedback mechanism and study the effect of acoustic waves on hydrodynamic instability separately. Chong et al. (2013) exploited aforementioned characteristic concluding that serrations do not affect the upstream flow but only locally near the trailing edge. This thesis work systematically studies the impact of TE serrations on the flow upstream of serrations on pressure side and, feedback loop using experimental tools. The study proposed to be conducted takes a critical view of work published by Chong *et al.* (2013) and experimentally checks the effect of serrations on span-wise coherence of vortex structure of flow.

1.2 Research objective overview

The study of feedback loop and the tonal noise emitted from the sharp trailing edge of the airfoil using serrations has been studied by many researchers using experimental (Paterson et al. 1973, Arbey&Battille et al. 1983, Lowson et al. 1994, Pröbsting et al. 2013) and computational (Desquesnes et al. 2007, Joworski et al. 2013, Jones et al. 2010, Kingman et al. 2009) techniques. Howe 1991 proposed a theoretical model to understand the impact of serrations on discrete tones but the experiments conducted do not concur with the proposed theory. The latest study conducted by Chong et al. (2013) proposed localized effect of serrations and the overall feedback loop remains unaltered. The work in the thesis focuses on the effects of trailing edge saw-toothed serrations on the noise emitted and, how it impacts the flow the airfoil. It will also try to study the mechanism behind the self-induced acoustic feedback loop (Paterson et al. 1973, McAlpline et al. 1999), the impact of sound waves on stream-wise hydrodynamic waves/instabilities (Tollmien-Schlichting wave) travelling down-stream towards trailing edge (TE) on pressure side of airfoil.

The study presented here takes a critical look on Chong et al. (2013), whether the serrations only affect the local flow on/ near the serrations or trailing edge serrations have a more global affect. Is the flow upstream of the trailing edge modified due to the TE serrations? With these questions in mind, the study also tries to the stipulate on the feedback loop. During the study, the results obtained are compared with the past studies to verify the results. Taking into account the research objectives, a study outline is also proposed in the following section.

1.3 Methodology

The LBL instability noise study was conducted using NACA 0018 airfoil with specially designed TE in TU Delfts's low turbulence V-tunnel situated in low speed lab. The airfoil's TE can accommodate different serrations and flap; specifics are provided in chapter 5. It has been known for some time that modified TE of wing with saw-toothed serrations attenuate the tonal noise and in some cases completely suppress it. This gives an opportunity to study the feedback mechanism and the effect of acoustic waves on hydrodynamic instability separately. Chong et al. 2013. The noise is measured using far-field microphones and the flow fields is captured using time resolved (TR) planar particle image velocimetry (2C-PIV) at different in stream-wise and span-wise planes, for various TE configurations. The oil-flow visualization technique is employed to study the effect of serrations on the laminar separation bubble (LSB). The study conducted takes a critical view of work published by Chong et al. 2013 and experimentally views the effects of serrations on span-wise coherence of vortex structure of the flow.

1.4 Thesis outline

The thesis is divided into sections and sub-sections with an objective to provide reader an easy and intuitive access to study presented. The thesis in whole is divided into five sections, including the current section of 'Introduction'. The following section of 'Literature study' provides an overview of the work published on LBL instability noise and related topics. The research studies published over the years have been chronologically studied and illustrated. The sub-section 'Research objective' provides a more detailed and precise questions brought up in this thesis work with intent to answer. 'Experimental set-up' section delineates, with diagrams, the modified airfoil and wind tunnel used in detail. The experimental techniques and statistical methods applied to generate information from data collected are mentioned in sub-section of 'Experimental set-up'. The information gathered after processing the data collected during experiments is plotted in section of 'Results and Discussions'. This section discusses and tries to relate as well as critically access the results with the works published in past. Conclusion forms the last section of the thesis work, highlighting important points and progress made over the previous published work.

Different experimental techniques are used to conduct the presented study. First acoustic measurements are taken with and without TE modifications. The results obtained helped in selecting the serration for which maximum attenuation of noise is obtained. Then, time resolved 2C PIV campaign is planned to capture flow domain for specific cases on the airfoil based on far-field acoustic results. The time resolved 2C PIV campaign is divided in two parts. First campaign is planned to capture flow field on pressure side of airfoil in span-wise direction to study the impact of TE serrations on hydrodynamic instabilities. The second campaign took the same cases but this time the flow field is captured in stream-wise direction to study the laminar/transitional boundary layer. In stream-wise 2C PIV campaign, two cameras are used with an intention to capture the separation of laminar separation bubble. In addition to serrations, TE attached with flap is taken as a base for a comparative study. After the processing and post processing of stream-wise time resolved 2C PIV, it is observed that the point of separation or the start of separation bubble could not be captured. This led to Oil-flow visualization technique which helped in studying, to an extent, the global flow dynamics on the pressure side of the airfoil.

2. Literature review

The previous chapter provided a brief introduction on aero-acoustics, why the field of aero-acoustics have become important in this day and age and raised few questions which the presented work has tried to tackle. It also mentioned briefly methodology followed and the thesis outline, giving reader an idea of the follow of information.

In this chapter, a detailed literature overview is presented with an intention to gain information on the works published pertaining to the questions raised. The section 2.1 starts with a brief description of different kinds of airfoil self-noise. The section 2.2 gives a brief overview of laminar separation bubble and coherent structures as they a major role in tonal noise. With that a detailed literature review is presented in this chapter. This study is concentrates on laminar boundary layer instability noise and its inherent properties. The section 2.3 sheds light on different aspect as well as outlines different theories presented over the years to explain the tonal noise behaviour. In the end section 2.4 elucidates the noise control approaches and how can they be used to study the tonal noise and its behaviour.

2.1 Airfoil self-noise

The airfoil self-noise is produced due to interaction between the airfoil and the turbulence produced in its own boundary layer and near wake. Airfoil-self noise depends on the Re, shape of airfoil, AoA and the turbulence level of the incoming flow. The mechanism with which airfoil self-noise is produced changes, as the aforementioned factors change and thus is helpful to study them separately. The airfoil self-noise can be segregated under six sub-headings depending on the mechanism with which noise is produced [S.Pröbsting (2016), Brook et al. (1989)].

1. Separation & Stall noise: Near stall (light tall) or separation noise corresponds to a high airfoil load and an attached mean flow over the airfoil. In light stall, the flow over the suction side of the airfoil separates and reattaches transitioning into the turbulent boundary layer (Moreau et al 2009). Stall (deep stall) occurs at high angles of attack where the flow separates near the leading edge, forming a shear layer on the suction of

the airfoil. Near stall or separation noise is broadband in nature and radiated noise can be attributed to the interaction of turbulent boundary layer with TE as a dominant source (Paterson et al 1974 'Isolated airfoil tip-vortex interaction'). In deep stall, the large scale vortices give rise to low frequency noise where the noise is radiated from the whole chord. Deep stall has noise of higher amplitude at lower frequencies as compared to light stall.

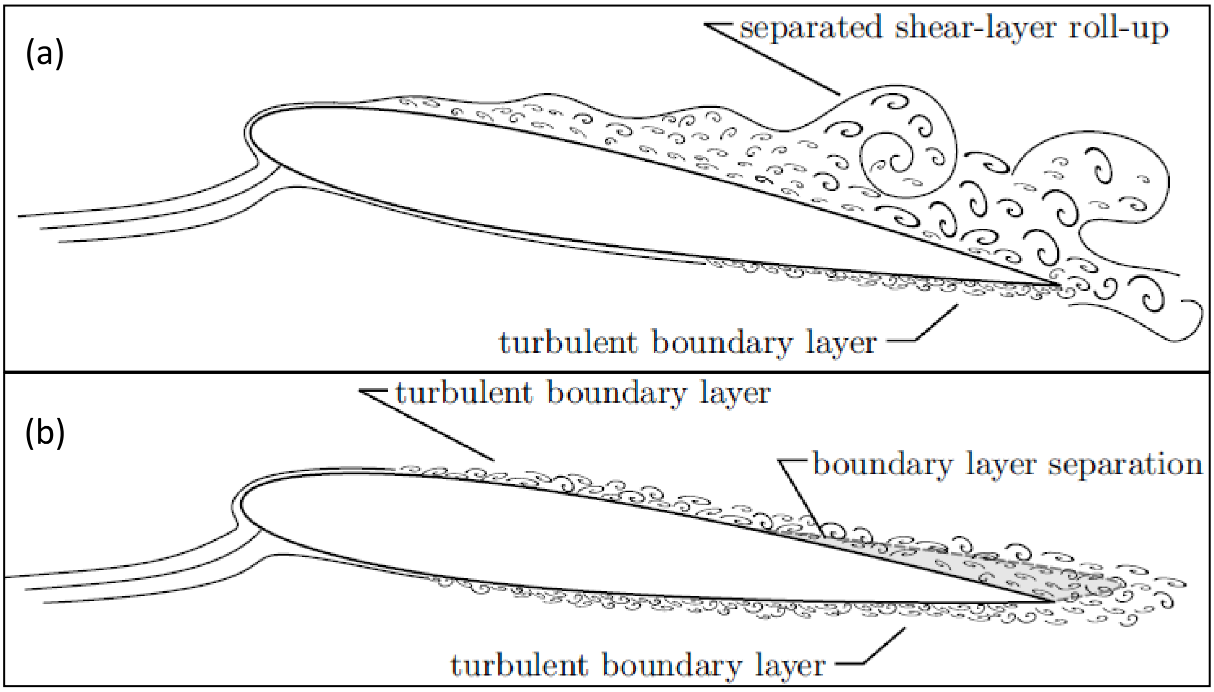

Figure 2-1: (a) Separation stall noise (b) Boundary layer separation noise (S.Pröbsting 2016)

2. <u>Tip-vortex formation noise:</u> Tip-vortex formation noise is unique as the wing span is finite as against to infinite assumed in other cases. Thus, tip-vortex formation noise is of high interest to control broadband noise generation in practical applications. The flow over the tip has certain vortex strength with a thick viscous core and recirculation flow in the vortex is highly turbulent (Brook et al. 1986). Turbulence interacts with wing tip giving rise to turbulent boundary layer trailing edge noise like characteristics, though three dimensional in nature.

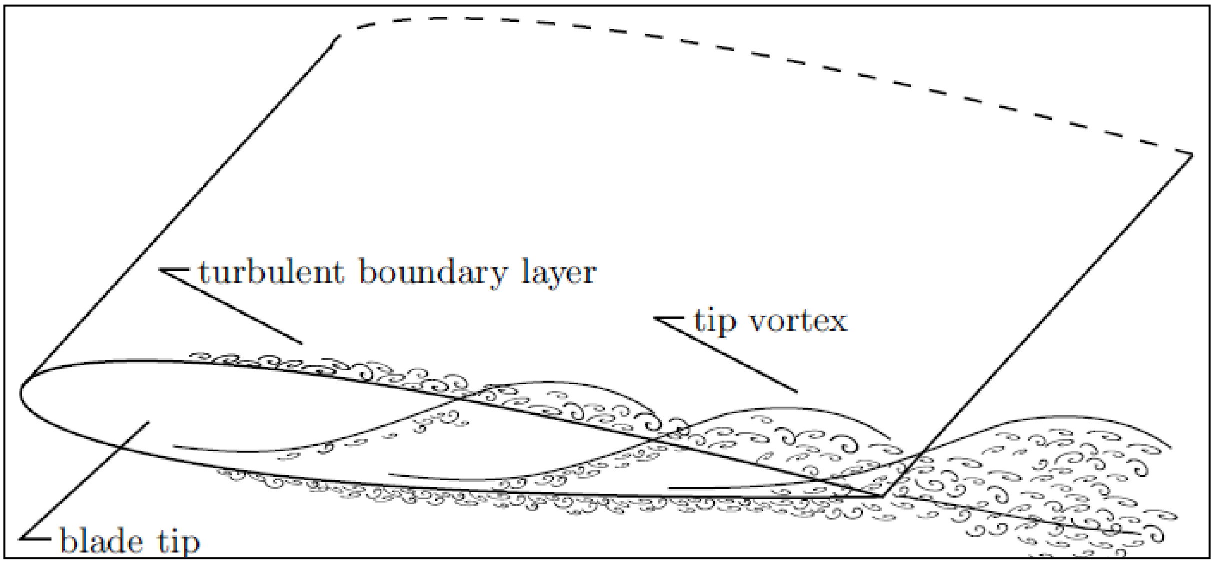

Figure 2-2: Tip noise (S.Pröbsting 2016)

3. <u>Turbulent boundary layer trailing edge noise (TBL-TE):</u> Turbulence can be seen as continuous stream of randomly oriented eddies of various sizes and intensities forming an energy cascade. The larger-scale eddies are affected by boundary conditions and predominantly control transportation and mixing. The smaller eddies are independent of geometry and can be seen as universal (Pope book). The energy cascade above mentioned act as a physical mechanism to dissipate energy imparted from the airfoil in the flow. Thus, turbulent flow contains fluctuating eddies which them self act as noise source and the turbulence noise amplifies when a closed boundary object like an airfoil is introduced. In a nominally non-turbulent high Re, the flow transition in BL occurs upstream of TE on PS or SS or both depending on AoA, free stream turbulence and shape of airfoil. When these disturbances in turbulent flow (stream of continuous eddies) are convected downstream, they interact with 'sharp' TE given the airfoil is not stalled. The sharp TE diffracts turbulence induced quad-pole noise when airfoil dimensions are large compared with radiated noise wavelength (c >>λ) and also partial energy of the flow is radiated through the noise emitted (Doolan 2006). The multi-scale randomised eddies present in turbulent BL interact with sharp TE radiate noise of high frequency broadband noise. The acoustic feedback loop is not applicable due to the incoherent nature of flow.

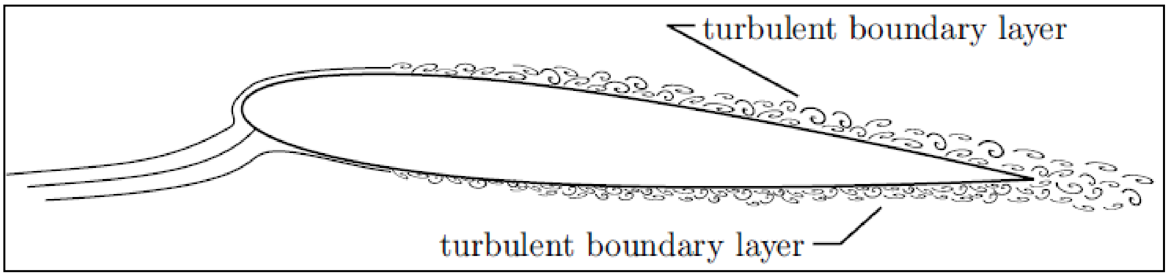

Figure 2-3: Turbulent boundary layer trailing edge interaction noise (S.Pröbsting 2016)

4. <u>Laminar boundary layer instability – trailing edge noise (LBL-TE):</u> The LBL-TE noise is generated when the flow is predominantly laminar over the pressure side of the airfoil for Re < 10^6. The noise produced (PS dominated) is narrow band in nature and is accompanied with formation of laminar separation bubble near the TE. The disturbances in the boundary layer convected downstream are magnified while passing over laminar separation bubble and span-wise coherent. These instabilities interact with sharp TE radiating tonal noise. The noise radiated travels upstream of the TE and interacts with the boundary layer instabilities. Many aero-acoustic feedback models have been suggested in past studies to explain the distinct characteristics associated with tonal noise over the Re and AoA. The LBL-TE noise is sensitive to AoA, turbulence intensity in free stream, shape of airfoil and Re. UAVs, ventilation fans etc. can produce tonal noise and such airfoils have to be treated to attenuate tonal noise.

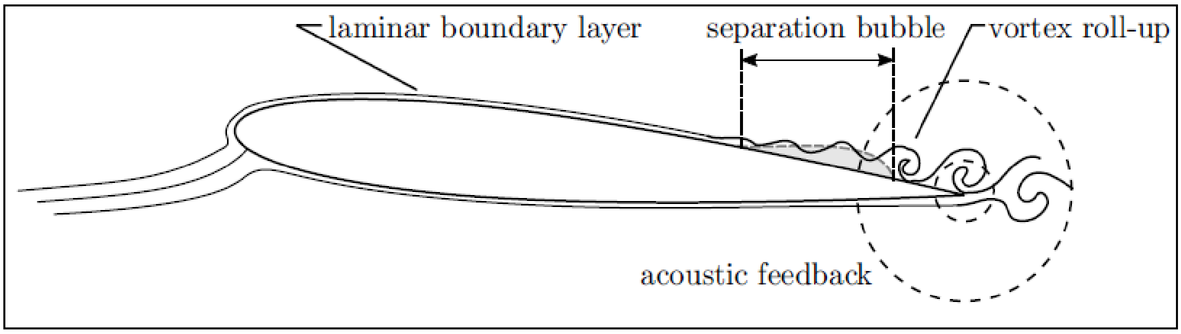

Figure 2-4: Laminar boundary layer instability noise (S.Pröbsting 2016)

5. <u>Trailing edge – bluntness noise:</u> When the TE of an airfoil is truncated with a certain thickness, it results in large scale vortex shedding over a region of re-circulating flow. Due to fixed scale of bluntness of TE, the noise is restricted to a narrow band of frequencies and in case if the shedding process is very periodic, it can even give rise to tonal noise. Though the process of tonal noise emitted from blunt edge is quite different as from the tonal noise emitted from sharp TE due to laminar boundary layer instability.

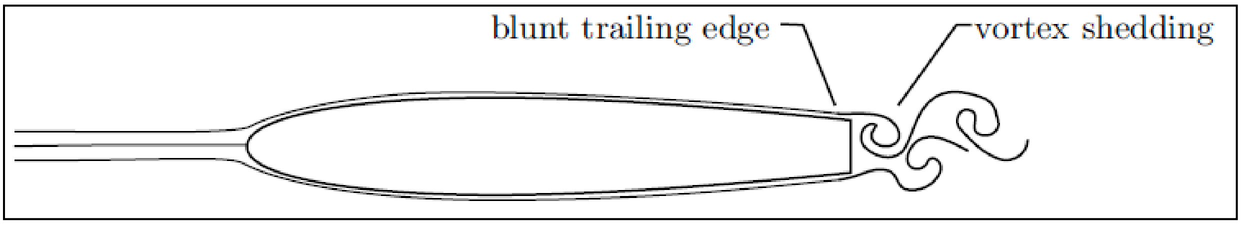

Figure 2-5: Trailing edge bluntness vortex shedding noise (S.Pröbsting 2016)

2.2 Laminar separation bubble

In previous published works, presence of laminar separation bubble near the TE of an airfoil, is reported as a necessity for the tonal noise to occur (McAlpine et al.1999, Nash et al 1999, Pröbsting et al. 2015). In this section, an over view is presented on the laminar separation bubble (LSB) and how flow parameters impact the tonal noise.

Laminar separation bubble (LSB) is reported to develop on airfoils operating at Re < $5*10^5$ (Lissaman 1983; Boutilier&Yarusevych 2012). In the aforementioned Re regime, a region of adverse pressure gradient is created on the surface of airfoil causing the laminar boundary layer (LBL) to separate, creating a region of reverse flow and re-attaches downstream as the flow transitions from laminar to turbulent. The area between the point of LBL separation (S) and the point of turbulent boundary layer (TBL) reattachment (R) is defined as LSB (Fig 2-6). The formation of LSB increases drag coefficient of an airfoil due to the presence of separated shear layer over the LSB. The separated shear layer (region: SS'T"R"RT'S) is inherently unstable and undergoes laminar to turbulent transition as the flow passes point of separation (O'Meara et al. 1987).

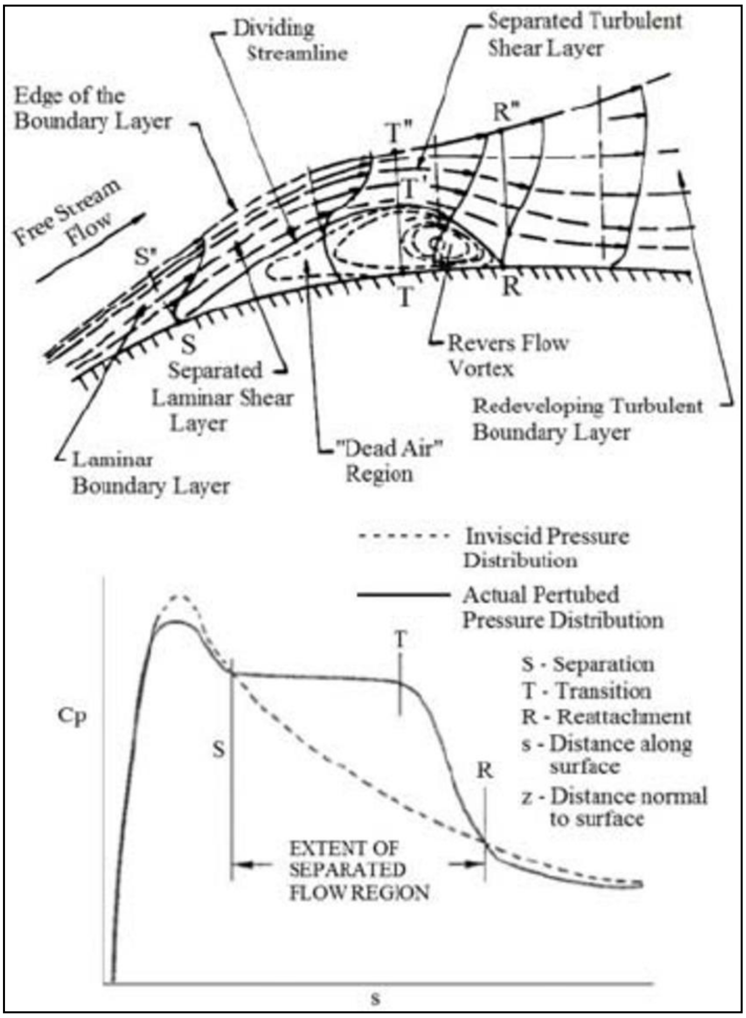

Figure 2-6: Schematic structure of the separation bubble in the flow around a blunt flat plate (Yaghoubi and Mahmoodi 2004)

The stable laminar flow with free stream turbulence enters the shear layer over the LSB, the small scale turbulent eddies get amplified and the flow enters the phase of transition. These turbulent structures, called TS-waves, are span-wise coherent and as TS-waves convect downstream, they are amplifies and roll-up into span-wise vortices into large structures gaining momentum. The span-wise vorticity is unstable and start to breakdown to give way to turbulent spots before the flow is transitioned into fully turbulent flow. A schematic diagram of this transition process is shown in fig 2-7. The region 2 (span-wise vorticity) in fig 2-8 plays a major role in tonal noise radiation from sharp TE of an airfoil. If the three regions of transition are bypassed and the laminar flow directly forms turbulent spots, then the process is called bypass transition.

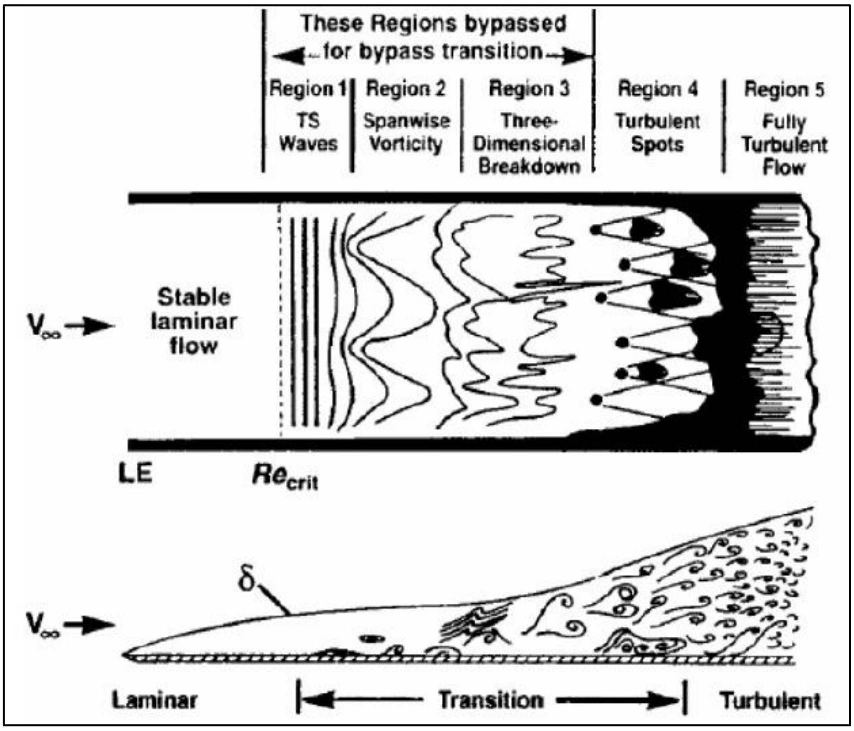

Figure 2-7: The natural transition process (Schlichting 1979)

The flow on PS is affected with change in AoA and Re for the cases pertaining to tonal noise. The shear layer on LSB is shown as the major contributor towards the amplification of TS waves travelling downstream. The easiest way to study the point of separation and reattachment is by using oil flow visualization technique, though it has its constraints being an intrusive technique shown in figure 2-8.

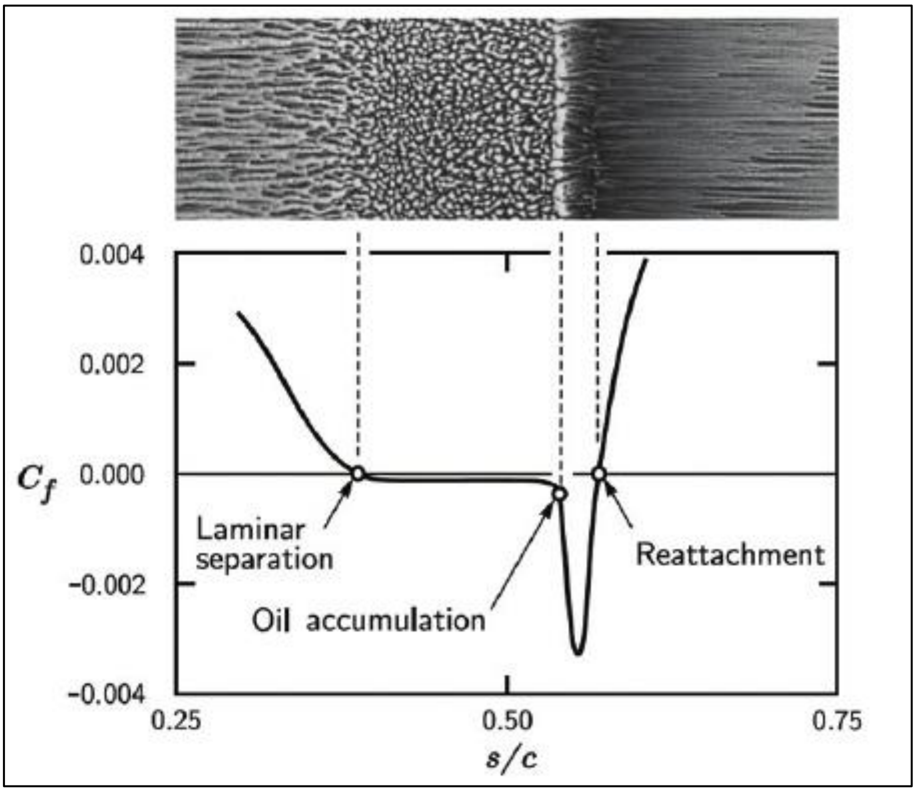

Figure 2-8: Conceptual visualization of LSB using oil flow visualization (Selig et al. 2011)

2.3 Laminar boundary layer instability noise

A number of experiments were conducted by in the beginning of 1970s (Smith et al. 1970; Hersh& Hayden 1971) showing that the discrete tones are emitted from isolated airfoils in a particular Reynolds number range at moderate AoA. Since then several studies have been conducted (Paterson et al.1973); Tam (1974); Arbey&Bataille (1983); Lowson et al. (1997); McAlpine et al. (1998); Nash et al. (1999); Desquesnes et al. (2007); Pröbsting et al. (2013)] to understand this phenomenon.

The first systematic study with intriguing results was conducted by (Paterson et al. 1973) on the NACA 0012 and NACA 0018 airfoils. The noise study was conducted in an anechoic wind tunnel. They observed that amplitude of narrow band sound (tonal noise) is higher for positive AoA as compared to zero or negative AoA. For a given positive AoA with increasing free stream velocity (U), tonal noise emitted increases to a maximum amplitude, reaches to a plateau and then decreases as these discrete tones become inseparable between the noise of airfoil and the wind tunnel. The tonal noise was detected up to AoA at which airfoil is expected to stall. The gradual decay of far-field noise is associated with transition from laminar to turbulent regime on the PS. As the flow was dominantly laminar for a given AoA on the airfoil, a trip wire was used to observe the effect of transition from laminar to turbulent flow on the tonal noise on both suction and pressure side. An intriguing observation was made; the tonal noise became undetectable when pressure side was tripped. This led to the conclusion, via some mechanism the tonal noise is pressure side dominated and boundary layer has to be laminar to generate tonal noise. Trip wire on suction side had no or undetectable impact on tonal noise. The results published by Paterson et al.(1973) are in concurrence with an earlier study published by (Hersh & Hayden, 1971)

Paterson et al. (1973) postulated the high amplitude tonal noise is related to vortex shedding at the trailing edge. They observed that frequencies of these discrete tones exhibited a ladder type variation, a piece-wise continuous function of the free stream velocity U, which increased locally following the power law f~0.8 and underwent a number of jumps as shown in fig 1-11. These discrete tones would jump with increasing U and at times have two distinct frequency tones at the same velocity keeping AoA constant. To further study the discrete tones further and come up with scaling law to define them, Paterson et al. (1973) made certain approximations. These assumptions were made to relate tonal noise to vortex shedding from the TE of airfoil:

i) Airfoil laminar boundary layer thickness (δ) approximated to flat plate boundary layer thickness.

$$\delta = \frac{5c}{Re^{0.5}} \tag{2.1}$$

ii) The airfoil vortex shedding approximated to bluff body vortex shedding as the tonal noise is central to δ on pressure side of airfoil. A Strouhal number (S) of 0.2 (for bluff body vortex shedding) is taken as reference for non-dimensional frequency scaling law.

$$S = 0.2 = \frac{2f\delta}{U} \tag{2.2}$$

Using these two assumptions, Paterson et al. 1973 put forth the frequency scaling law for discrete tones:

$$f = \frac{KU^{1.5}}{(c\nu)^{0.5}} \tag{2.3}$$

where K is a constant, . The scaling law derived from vortex model was able to predict the averaged evolution of frequency of the discrete tones for K=0.011 with overall vortex shedding of the airfoil. Though these assumptions were able to explain the dependency of shedding frequency of $U^{1.5}$ but could not explain individual frequency dependency of $U^{0.8}$ (ladder structure of discrete frequencies).

By cross-correlation of microphones on pressure side (PS) and suction side (SS), Paterson et al. Inferred the noise is dipolar in nature. Based on the micro-phone spacing (0.3 and 0.7), the measured delay between the signals suggested pressure disturbance was near TE. Hersh&Hayden (1971) postulated the dependency of tonal noise is relevant to overall thickness of airfoil. This observation was challenged by Paterson et al. (1973) by conducting experiments on NACA 0012 and NACA0018 and showing δ is the relevant dimension to define this noise regime.

Assumption of constancy of Strouhal number (in case of bluff body) was challenged by Tam 1974 as an airfoil has stream line body. The study proposed a self-excited feedback loop to explain discrete tones between acoustic waves, boundary layer and wake of airfoil as shown in fig 2-10. Tam's feedback loop consists of unstable boundary layer on pressure side of airfoil which forms a near wake flow on merging with suction side flow. The acoustic waves impinge on pressure side boundary layer initiating disturbances at trailing edge which travel downstream into wake. When these disturbances grow through wake instability, they cause the wake to vibrate laterally thus emitting acoustic waves from a highly localized region in the wake. These acoustic waves travel upstream impacting the pressure side boundary layer thus completing the loop. Taking experimental results of Paterson et al. (1973), he showed that discrete tonal frequency follows the law: $f = 6.85nU^{0.8}$, where n is an integer which corresponds to 180° phase condition necessary for such a feedback loop. Though the power law can vary and depends on the experimental conditions. Tam's argument is merely qualitative and does not account for $U^{3/2}$ law or transition of the maximum intensity from one tone to the other. Fink et al. (1975) provided another interpretation for the average frequency power law. He suggested that discrete tones are linked to laminar boundary layer instability on pressure side and performed boundary layer stability calculations by approximating pressure side as flat plate. However, the flat plate approximation itself makes this study qualitative and its inability to explain ladder type structure made this study inadequate.

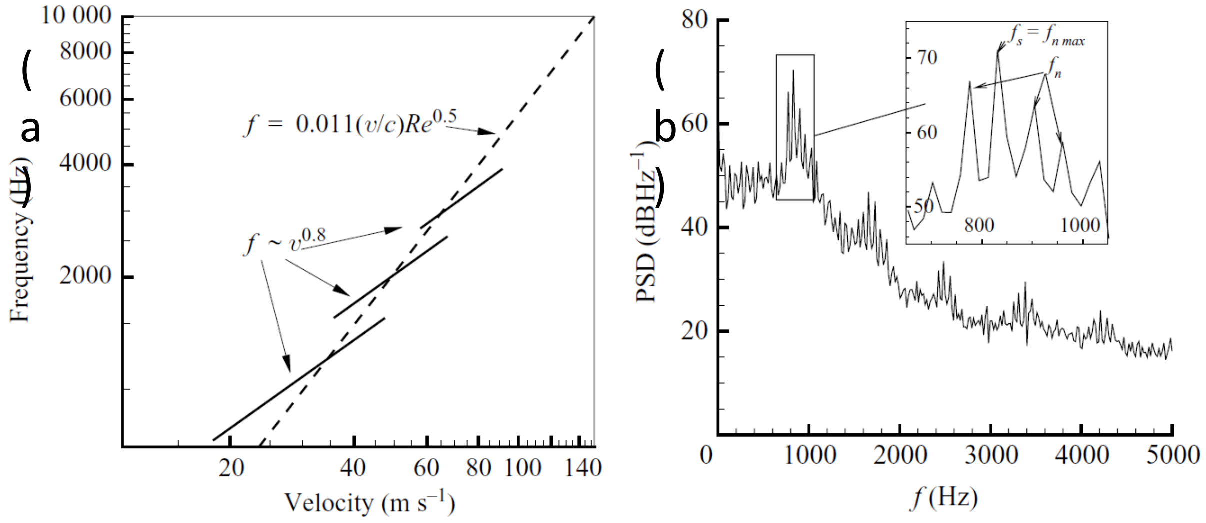

Figure 2-9: Typical radiated noise spectra: (a) NACA 0012.8, U = 20.2 m/s; (b) NACA 0012.16, U = 35m/s (from Arbey&Bataille(1983)); (c) the ladder type structure for discrete tones (Paterson et al. 1973).

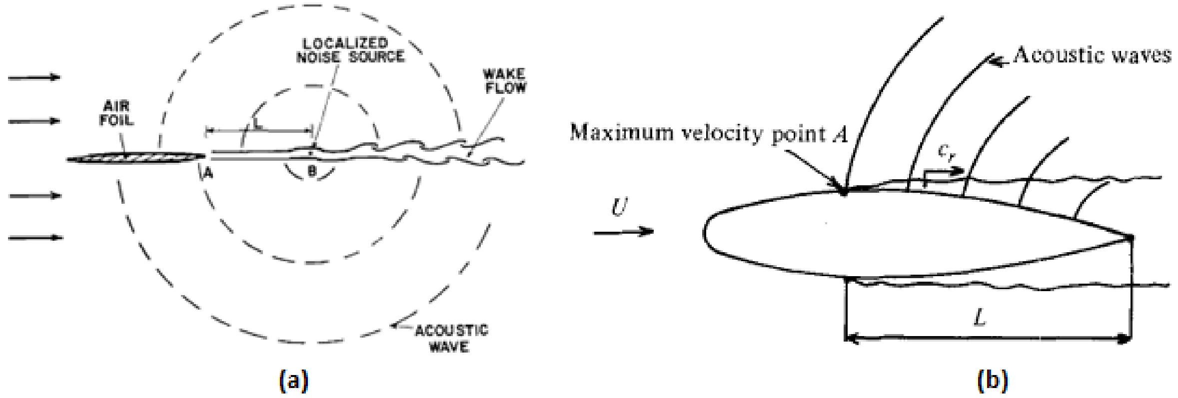

Figure 2-10: (a) Aero-acoustic feedback loop as suggested by Tam (1972) (from Tam (1972)); (b) Aero-acoustic feedback loop as suggested by Arbey&Bataille(1983).

Arbey&Bataille (1983) also investigated tonal noise generation on NACA 0012 of different chord lengths. Careful inspection of experimental data revealed that the peak frequency $f_{n,max}$ results from superposition of a broadband contribution around a frequency f_s and a set of regularly spaced discrete frequencies f_n. To analyze the peak frequency of broadband contribution f_s, they considered Strouhal number based on boundary layer displacement thickness at the trailing edge. After computing and analysing Strouhal number for different airfoils, they concluded that the Strouhal number remains to an extent constant and empirical relation for f_s coincides with $U^{3/2}$ power law for average frequencies. They also found a great similarity between the surface pressure spectrums at the trailing edge and far field acoustic spectrum. Thus confirming Fink et al. (1975)'s assumption that the broadband contribution of the spectrum is due to the diffraction of hydrodynamic instabilities of the boundary layer (Tollmien-Schlichting instabilities) by trailing edge. To explain discrete frequencies f_n, an aero-acoustic feedback loop was suggested which takes place inside unstable boundary layer. They postulated that the hydrodynamic instabilities, which are convected inside boundary layer at a certain velocity, are diffracted by the trailing edge generating acoustic waves. These acoustic waves then propagate upstream to a point of maximum velocity, A at a distance of L from trailing edge, where hydrodynamic instabilities are formed. If both hydrodynamic and acoustic signals are at 180° phase difference at this point, these disturbances amplify which again convect downstream thus completing loop. Though the point of formation of first instability is controversial. They also proposed a modified Tam et al. (1974)'s phase loop condition with an associated 180° phase shift:

$$\frac{f_n L}{c_r}\left(1+\frac{c_r}{c_o-u}\right)=n+1/2 \tag{2.4}$$

Lowson et al. (1994) observed that TS waves occur in boundary layer before the appearance of tonal noise. This proved that occurrence of TS waves is not the sufficient condition for acoustic noise. After performing calculations of boundary layer on NACA 0012 and experiments on NACA 0012 and NACA 23015, they showed a strong correlation between the presence of long laminar separation bubble on pressure side of the airfoil and the tonal noise. They suggested that length of laminar separation bubble on pressure side of profile is correlated to intensity of noise emitted. Using the information, Lowson et al. (1994) postulated a new mechanism for discrete tones suggesting that TS waves appear in the laminar boundary layer near leading edge of the airfoil. After laminar separation, the separated shear layer strongly amplifies the passing TS waves. Amplification of these TS waves stop at transition thus making noise level a function of length of laminar separation bubble. Then, these amplified TS waves diffract from trailing edge thus emitting sound waves which again travel upstream and re-inforce TS waves. This also explains the evolution of tone intensity with velocity for a constant angle of attack.

Nash et al. (1998) performed experiments on NACA 0012 airfoil using laser Doppler anemometry techniques. This non-invasive technique helped in acquiring data at very high frequencies without affecting the flow as compared to hot wire technique. They observed, to have tonal noise, there are certain conditions to be met

1. There must be region of separated flow or inflected flow near the trailing edge in order to amplify TS instabilities.
2. The separated or inflected flow should be close to trailing edge to maintain a periodic structure to the trailing edge for the instability waves to remain coherent.
3. The adverse pressure gradient at the trailing edge should not be too high to prevent transition.

Nash at al. (1998) also suggested a revised feedback loop for tonal noise generation based on vortex-shedding process. An adverse pressure gradient on the pressure of airfoil leads to inflection velocity profiles which develops into separated flow. This separated flow region is close to trailing edge where majority of boundary layer instabilities are amplified. Using laminar stability theory the frequency of the linear mode with maximum amplification is found which is close to the frequency of amplified TS wave. This discrete instability frequency continues to amplify downstream and begins to roll up into vortex. This rolled up vortex interacts with trailing edge resulting in oscillating flow around the airfoil of the same frequency as the most amplified instability. Then, this oscillating field extends upstream and selects the most amplified instability, thus completing the feedback loop.

McAlpine et al. (1999) concentrated on understanding the relationship between TS waves and tonal noise and concurs with Nash et al (1998) that the tone frequency is close to the most amplified frequency on the pressure side of airfoil.

Nakano et al. (2006) using NACA 0018 performed liquid crystal visualization, to capture separation and reattachment of laminar separation bubble, and particle image velocimetry. They observed that as angle of attack increases transition moves upstream on suction side while downstream on pressure side of profile. The turbulence intensity near trailing edge is higher on the pressure side than on suction side and near wake positive vorticity is observed on the pressure side while negative on the suction side of airfoil.

Desquesnes et al. (2007) proposed a new scheme to explain tonal noise mechanism. They proposed two aero-acoustic feedback loops, primary feedback loop on pressure side and a secondary feedback loop on suction side of the airfoil. They stated that a periodic amplitude modulation forced due to phase difference of hydrodynamic fluctuations on the pressure and suction side is the origin of regularly spaced discrete frequency peaks. Thus implying the interaction of most amplified instabilities from suction side and pressure side is a necessary condition for multiple tones. This conclusion has been challenged by Pröbsting et al. (2014) and Plogmann et al. (2013).

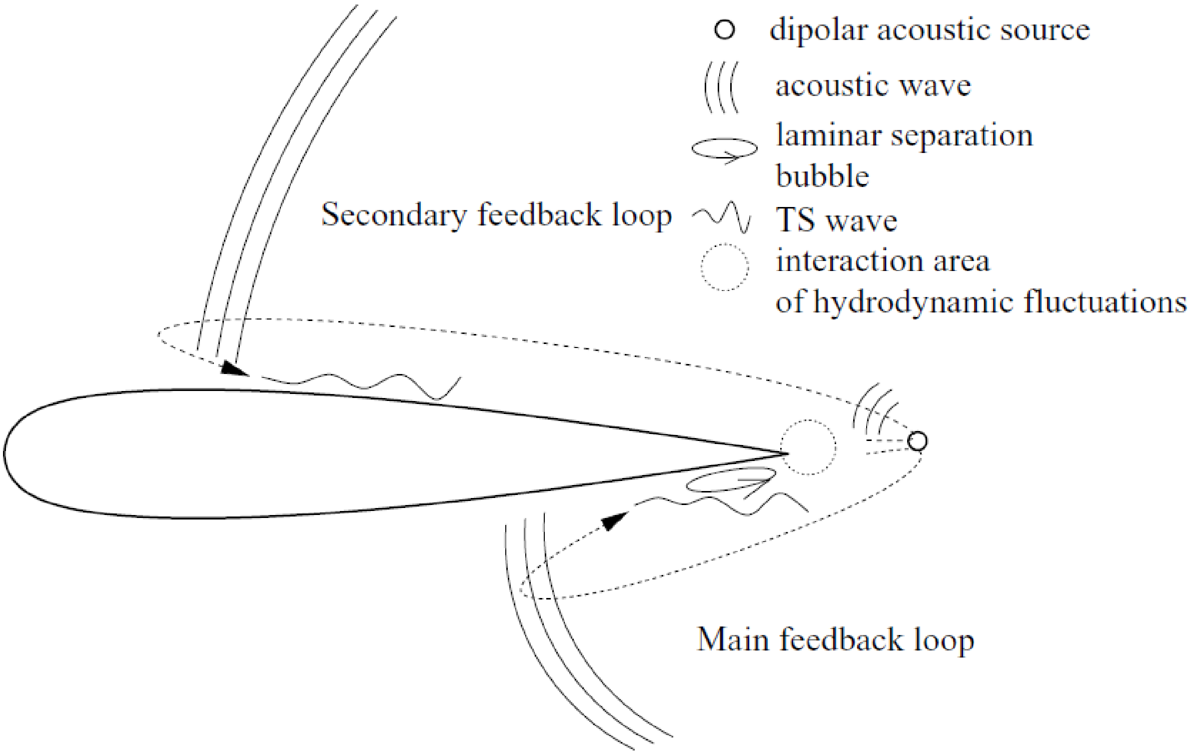

Figure 2-11: Scheme of tonal noise mechanism suggested by Desquesnes et al. (2007)

Timmer et al. (2008), performed experiments on NACA 0018 in closed loop low turbulence wind tunnel and showed that pressure side laminar separation bubble is responsible for tonal noise and this discrete tones can be eliminated by tripping the pressure side boundary layer. Thus, showing for NACA 0018, noise is pressure side dominated.

Plogmann et al. (2013) conducted experiments to examine the mechanism by which main tone frequency and regularly spaced side peaks at regular frequency spacing are selected. They also experimentally discarded the secondary feedback loop proposed by Desquesnes et al. 2007. Wall pressure measurements showed that the tonal noise is favored by a strong coherence of the vortices inside laminar separation bubble.

Probsting et al. (2014) showed experimentally that periodic amplitude modulation of the acoustic pressure in the far field is the cause for the presence of the multiple tones in the acoustic spectra, as suggested by Desquesnes et al. (2007) based on simulation. Further, they showed that the similar periodic amplitude modulation is present in the source field near the trailing edge linked to periodic modulation in strength of instability waves. Tripping the pressure side, while observing periodic amplitude modulation, concluded that an interaction between the two sides of the airfoil, or acoustic emission from the two sides, is not necessary for such amplitude modulation to occur in the source field.

2.4 Noise control approach and its application to study LBL instability noise

Sound from airfoil can be self-generated when an isolated airfoil is in a laminar flow or airfoil in a free stream with large vortex structures called vortex-structure interaction noise [Brooke (1989); N.Curle (1955)]. Sound can also be generated due to complex interaction in a multi-airfoil system. In a multi-airfoil system, an airfoil interacts with wake from another airfoil creating sound, like in a rotor of a helicopter when an airfoil cuts vortices in wake of the other airfoil called blade vortex interaction noise (Hardin&Lamkin 1987).

The current section will restrict itself with the noise control approach in case of LBL instability noise using trailing edge modifications and its application to study LBL instability noise and suggested feedback loop [Tam (1974); Arbey&Batille (1983), Lowson et al. (1994), Nash et al. (1999), Desquesnes et al. (2007), Pröbsting et al. (2013), Chong et al. (2014)]. In the previous section, studies [Nash et al. (1998); Lowson et al. (1994); Nakano et al. (2006); Probsting et al. (2013 & 2015)] have noted that LBS on PS plays a central role in amplification of disturbances in boundary layer and shear layer over the LSB is affected by the upwind travelling sound waves radiated from the TE. The attenuation of noise using TE modifications restricts the narrow band high amplitude noise from affecting upstream flow, thus breaking the suggested feedback loop. This presents an opportunity to study hydrodynamic instabilities in boundary layer of airfoil without feedback loop and, how the TE modifications and of kind, can successfully attenuate the tonal noise.

Trailing edge modifications can be brush (Chong et al. 2016) or serrations (Jones et al. 2009, Chong et al. 2014) to attenuate tonal noise. Again to restrict the literature review to the scope of the presented study, an overview of published studies with use TE saw-toothed serrations in regime of LBL-TE instability noise will be presented.

Moreau et al. 2013 conducted experimental study of flat-plate serrated trailing edge to explore noise reduction mechanism of saw toothed trailing edges at low to moderate Reynolds number ($1.6X10^5 < Re < 4.2X10^5$). They observed that experimental measurements do not agree with Howe 1991 theory both in terms of absolute noise levels and variation in noise reduction with free stream velocity and frequency. The maximum theoretical attenuation according to Howe 1991 for saw toothed serrations in radiated mean square pressure (decibels) is $10\log_{10}(1 + (4h/\lambda)^2)$. The mathematical model suggested is under the assumption that the statistics of the incoming boundary layer turbulence are not modified by the presence of serrations.

According to Howe (1991) mathematical model, narrow serrations should attenuate noise more than wider serrations. But contrary to the theory, wider serrations achieve higher noise attenuation against narrow serrations. The mean velocity profiles acquired using hot wire technique shows significant difference between smooth and serrated trailing edges. Thus, indicating that trailing edges affect flow structure near wake of airfoil. They observed greater wake flow deflection for serrated trailing edges as compared to smooth and this deflection increases with decreasing serration wavelength. They showed the assumption in Howe et al. (1991)'s theory that serrations do not affect the hydrodynamic properties is invalid and on the contrary trailing edge serrations alter the behaviour of the flow field about the trailing edge and thus directly affecting the noise emission.

In order to reduce laminar instability noise and analyse aero-acoustic feedback loops, Chong et al. (2013), used trailing edge saw-toothed serrations. They used a NACA 0012 airfoil with a changeable trailing edge which allowed them to investigate different serrations using the same airfoil. Free field noise measurements are done in an open jet wind tunnel using a far-field microphone. The geometric angle of attack was taken 15° which corresponded to 4.2° after applying wind tunnel corrections. To determine the point of separation a non-intrusive surface mounted hot-film arrays are used. This position of separation, experimentally acquired for different trailing edges, is then compared with XFOIL code for smooth trailing edge airfoil. It was seen that separation position predicted by XFOIL matches well with experiments. Thus, the global attributes of flow field around the airfoil remain unchanged. At last to measure mean and root mean square root fields in wake region of airfoil, PIV technique is employed. Using linear stability analysis, they compared the calculated Falkner

Skan velocity profile with the measured velocity profile at the airfoil's pressure surface. This comparison showed that the serrations do not affect the separation point of the flow on airfoil and thus any potential changes in noise spectra can solely be due to dynamics of the local flow within saw-tooth serrations. They observe that there is increased level of noise reduction with increasing angle of serration. Using hot wire anemometry, boundary layer profiles at several stream wise locations are measured with smooth as well as with different trailing edges. They observe that in case of serrated trailing edge, the boundary layer velocity excess at the near wall region become more significant, resulting in stable boundary layer. They also observed that flow over a serration has larger turbulent intensity level as compared to smooth trailing edge, thus implying that the boundary layer on a serrated trailing edge is turbulent and less likely to separate. They observed if the point of separation is after the serration root, the bypass transition will occur making boundary layer turbulent-like and on the other hand if point of separation is before serration root, boundary layer will have same characteristics as smooth trailing edge counterpart. With these observations Chong et al. (2013) concluded that the saw-toothed geometry at trailing edge reduces two dimensionality of TS-waves but also inhibits amplification process that is supposed to take place after point of separation. But no experiments were conducted span-wise of the airfoil to show the effects of serrated trailing edge on the two dimensionality of TS waves. No quality experimental data is collected upstream of trailing edge to study the effect of trailing edge modifications on the amplification of TS waves after point of separation and on NACA 0018.

3. Research proposal

In past, the researchers have used different techniques; hot-wire anemometry (Paterson et al. 1973), laser Doppler anemometry (Lowson et al. 1994, Nash et al. 1996), surface mounted pressure arrays (Chong et al. (2014)), averaged PIV (Nakano et al. 2006, Chong et al. 2014) etc. to capture hydrodynamic disturbances in laminar/transitional boundary layer. The literature presents many models (Paterson et al. 1973; Tam 1974; Fink 1975; Arbey&Batallie 1984; Lowson et al. 1994; Nash et al. 1999; Desquesnes et al. 2007) to describe the physics of the narrow band width sound waves emitted by the airfoil in low to medium Reynolds number range (50,000<Re<200,000) at moderate AoA. But none of these models have been verified and accepted by scientific community. The problem faced while analysing the physics behind noise generated is how in feedback loop *(if there is)* the acoustic pressure waves actually affect the TS waves and their amplification. To counter the problem, researchers thought to attenuate the TE noise, thus separating the high amplitude acoustic waves from hydrodynamics waves. This can be done using TE serrations and analyse the flow without acoustic effect on hydrodynamic instability. The idea of breaking up the problem looked innovative as Howe et al. (1991)'s mathematical model, assuming that level of turbulence intensity remains un-affected while using trailing edge serrations, suggested that the noise attenuation is only because of the dispersion of acoustic waves on interaction with trailing edge. Moreau et al. (2013) did experiments using saw-toothed serrations to verify the assumption and concluded that the modified trailing edge has an upstream effect contradicting Howe et al. (1991)'s theory. Chong et al. (2013) used an airfoil with detachable trailing edge to experimentally study the effects of different saw-toothed serrations when attached to TE. They concluded that the flow over the serrations are affected but the global characteristics such as separation point of LSB remain the same and two dimensionality of TS waves is reduced with inhibited amplification of TS waves after point of separation on pressure side of airfoil, forcing the flow to by-pass transition(ref fig.2) to turbulent. Though these conclusions are derived and are not supported with proof.

The experimental study planned in the thesis is to verify the derived conclusions made by Chong et al. (2013) and to further study the feedback loop in LBL instability noise.

The first step is to select the saw-toothed serrations and make a comparative study between different trailing edges; far-field acoustic measurements are proposed to be conducted using an airfoil with detachable trailing edge. After selecting the serrations to be used in the study which provides maximum attenuation of tonal noise, time-resolved particle image velocimetry (PIV) technique is proposed to capture flow upstream of the trailing edge and, resolved enough to capture high frequency boundary layer instabilities. To verify the impact on span-wise coherent TS waves, a span-wise 2C-PIV measurement campaign is proposed at different displacements from the surface of airfoil. These measurements will also be used to further study the flow domain and through correlation analysis, upstream effect of serrations can be studied in detail. To check the second derived conclusion made by Chong et al. (2013) on global flow dynamics, oil flow and stream-wise PIV measurements are proposed. These proposed experimental studies and derived results will provide us with enough information to conclude whether the TE serrations' impact is local or global. It will also help in understanding the feedback loop in question and what role it plays in LBL instability noise emission.

4. Experimental techniques & data reduction methods

During the study, different experimental techniques are used to measure the self - airfoil noise as well as the flow topology of the flow on and over the surface of NACA 0018. These days different kinds of microphone can be found in day to day appliances. To measure rich and high frequency tones in the far field, microphone is used and to measure flow over the surface of wing on PS, Planar Particle Image Velocimetry (2C PIV) technique is applied. Oil flow visualization, one of the most primitive flow visualization techniques, is applied to visualize surface flow patterns.

In this chapter, concise background of the experimental techniques, used during the study, is provided. Section 4.1 provides an over-view of the microphone used and data reduction methods applied. 2-C PIV is applied to measure velocity vectors on different planes in vicinity of the TE as proposed in Chapter 2. Section 4.2.2 discusses principle of 2C-PIV concisely and how various instruments involved work in synchronization to give requisite output. The chapter ends with a discussion on oil flow visualization in Section 4.2.1.

4.1 Microphone measurements

Microphones are quite common to find in regular mobile phones, laptops and other devices. Microphones are a type of transducers which convert acoustical energy (sound waves) into electrical energy (audio signal). There are different kinds of microphones depending on the type of conversion technology or the application they are designed for. Though all the microphones share one commonality that is diaphragm. The incident sound waves vibrate the diaphragm and in turn the vibrational energy in diaphragm is converted to a suitable signal.

In the proposed study it is required to study the noise emitted from the wing. A condenser type microphone also called capacitor or electrostatic microphone is used to record acoustic noise

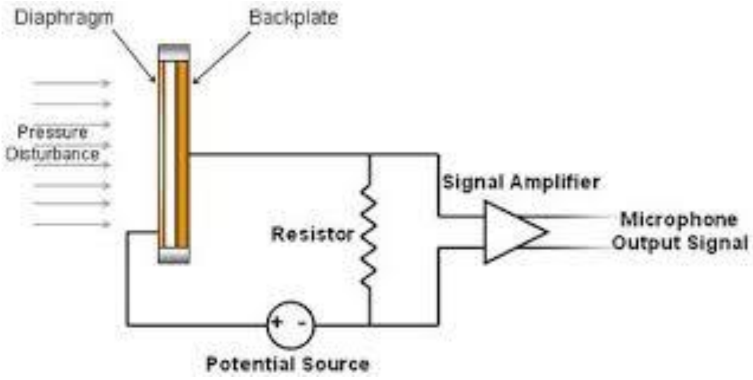

Figure 4-1: Schematic diagram of condenser microphone

4.2 Flow visualization

The flow visualization started not as a scientific tool but a form of art to study the nature. Leonardo da Vinci, a truly remarkable polymath, could perhaps be called as a hydrologist was fascinated with water and flow. In one of his manuscripts he writes (translated by The Project Gutenberg EBook of The Notebooks of Leonardo Da Vinci), "*Observe the motion of the surface of the water which resembles that of hair, and has two motions, of which one goes on with the flow of the surface, the other forms the lines of the eddies; thus the water forms eddying whirlpools one part of which are due to the impetus of the principal current and the other to the incidental motion and return flow.*" P. 389, the *CodiceAltantico.* Over time, the flow visualization matured and became a scientific tool to study complex fluid flow problems in both bounded and un-bounded boundary conditions.

Figure 4-2: A rigid obstacle in flowing water creates wake turbulence, a fact noted and sketched by Leonardo da Vinci in 1509 Bingham (2007)

Flow visualization, even in this day and age, forms the backbone of experimental techniques to study flow physics in hydrodynamic, aerodynamic etc. fields. Though it comes with its own challenges as rightly quoted by Hussian (1981), "*Flow visualization presents excessive information but very little hard data, and hot-wires or Laser Doppler Anemometry (LDA) give some hard data but very little flow physics*". Contrary to the above quotation, recent technical developments in laser, optics, image processing, digital photography and computers have enabled the scientific community to extract 'hard data' enabling to study the flow physics in greater detail. The majority of the thesis work presented uses two of the flow visualization experimental techniques:

1. Photochromic dye (oil) flow visualization technique
2. Planar Particle Image Velocimetry (2C-PIV)

which are elaborated concisely in the following sub-sections.

4.2.1 Photochromic dye (oil) flow visualization

Photochromic dye flow visualization (one of many oil film techniques), reported by Popovich&Hummel (1967), is a surface flow visualization technique with addition of photochromic materials in the liquid solution. Photochromism is defined as the reversible transition of a chemical substance between two states, A and B, exhibiting noticeably different absorption spectra of photon wavelength (Agard-AG-302, pp.25). Such substances called 'pyridines' show two states A (transparent), high absorption rate of Ultraviolet radiation (UV) and and B (opaque), high absorption rate of visible range of light wavelength. The transition from A to B is stimulated by UV making the pyridine induced liquid opaque thus giving an opportunity to study the physics of the surface flow and after sometime transitioning back to state A. Photochromic substances are insoluble expect in organic liquids. Concentration of photochromic substances has to be adjusted according to the experimental conditions as low concentration will give weak dye while too high concentration will cause an unwanted temperature increase of the surface fluid because only a fraction of UV radiation is used to stimulate state B and remaining is converted to heat.

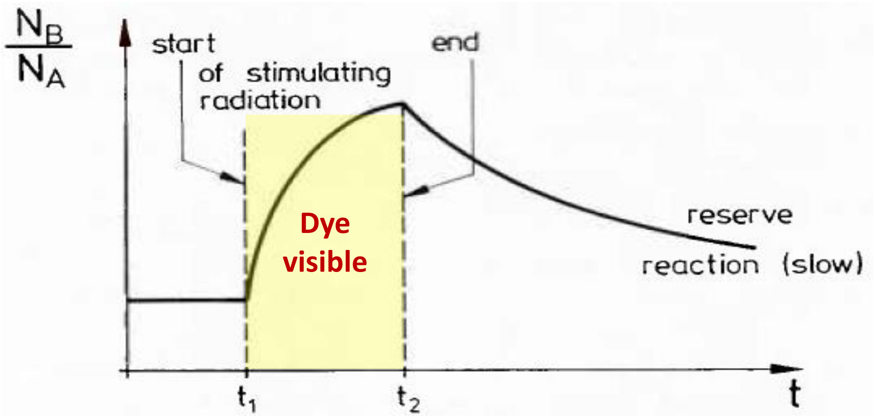

Figure 4-3: Principle of the transition of the photo-chromic material between two states of different absorption, A & B. N_A , N_B= Number of molecules in states A and B, respectively; t = time. (Agard-AG-302, pp.25-26)

The oil film techniques is influenced by various physical processes such as mass, momentum and heat transfer but strongly depend on state of flow on the surface; laminar or turbulent, attached or separated. Thus, such techniques are quite useful to study the points of separation and re-attachment of the flow. Though simple in application, oil film technique is an intrusive technique as the boundary conditions need to be fulfilled by air-oil interface where no slip is void as the two fluids have the same velocity. Squire (1962, pp.7-28) investigated the effect of motion of thin oil sheet relative the body surface on the boundary layer of the flow. He proposes the velocity u at the interface:

$$u(y=h) = \frac{\mu_{air}}{\mu_{oil}}\left\{-\frac{h^2}{2}\left(\frac{1}{\mu_{air}}\frac{dp}{dx} + h\left[\frac{\partial u_{air}}{\partial y}\right]_{y=h}\right)\right\} \tag{4.1}$$

Where *h* is oil film thickness and *p* is pressure. Since the ratio of $^{\mu_{air}}/_{\mu_{oil}}$ is quite small, the u (y=h) can be negected except for the cases where $^{dp}/_{dx}$ becomes quite large. This situation can arise at the points of separation and re-attachment, especially if the separation is induced by shock wave. A percentage error calculation is such cases is not mentioned with respect to location of separation and reattachment. Thus, it is important to interpret such results with great care.

4.2.2 Particle Image Velocimetry

Particle image velocimetry (PIV) , in past decade, have become a very useful and effective technique for flow analysis. In past laser doppler velocimetry (LDV) would use tracer particles in the flow to measure the velocity vectors at a point in the flow. On the other hand, PIV can measure the velocity vector field over a plane and even in a volume (tomographic PIV). This is be made possible by technological advances in high energy laser optics, high speed processor cameras and modern day computing power.

The principle of PIV is based on tracing the particles introduced in the flow and measuring their displacements at short intervals. PIV is a complex system made of various sub-systems. A schematic diagram of 2C-PIV is shown in fig 4-4 with doubled pulsed laser as source of illumination, cylindrical or spherical lenses to produce the sheet or volume of light, tracer particles introduced in to the flow through seeder, CCD camera capturing the images at definite time intervals, a storage device to store the images taken and a computer based program to correlate and generate the velocity field vectors in the field of view (FOV). The following sub-sections will provide a short introduction on each of the sub-systems used and techniques involved which makes the 2C-PIV technique successful (Raffel 2006).

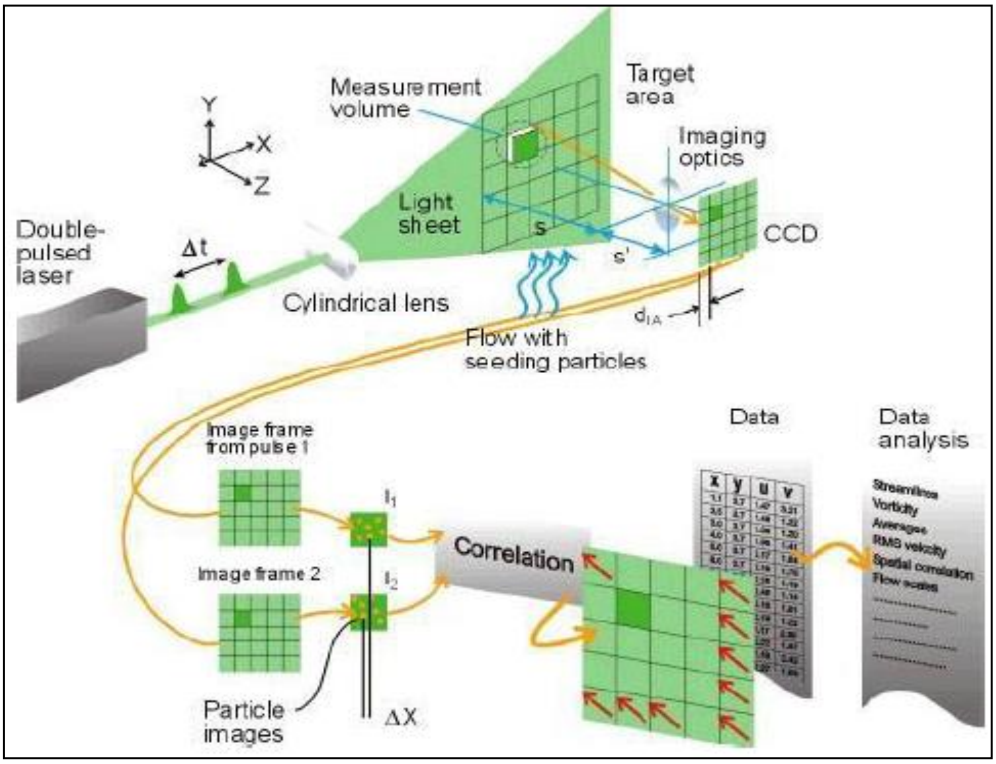

Figure 4-4: Schematic diagram of 2C-PIV with various components

4.2.2.1 Illumination

The measurement principle in PIV measurement is the measurement of small displacement of tracer particles with a time interval of Δt (pulse duration). Thus, the tracer particles are illuminated and measured twice and to achieve it, certain requirements have to be met.

a) The particle images should not appear as streaks but as circular dots. This is achieved when particle displacement is significantly smaller than the particle size.

$$\Delta t = \frac{d_\tau}{VM} \tag{4.2}$$

Where d_τ is particle image diameter, V is the velocity, and M is the mass of the tracer particle.

b) Particles lying in the thin sheet of light are all in focus of the camera. The position in the depth is controlled by the sheet of light

c) The illumination source intensity must illuminate the particles in the light sheet to be captured by the digital imaging devices.

Dual pulsed lasers are used to as illumination source as they emit collimated, monochromatic light beam that can be shaped into thin sheet and can be fired at very short pulse durations. Dual pulsed laser consist of two separate and independent laser which can be fired at a required pulse duration.

Light sheet formation optics play an important role to shape the circular cross-section monochromatic light (λ=532 nm) into thin sheet. The optics required are generally a set of cylindrical (focal length f_1) and spherical (focal length f_2) lenses adjusted in a manner to obtain constant or variable width light sheet. In the present study variable width laser sheet is used which is applied to illuminate large areas. The desired sheet width can be obtained at a distance L as a function of f_1.

$$D = 2Ltan\theta + d = d\left[\frac{L}{f_1} + 1\right] \tag{4.3}$$

Where d and D are initial and final width of laser sheet respectively and θ is width divergence angle. The minimum thickness of laser sheet is called laser sheet width:

$$w = 2\frac{2.44\lambda f_2}{d} \tag{4.4}$$

Laser sheets overlap, from dual pulse laser, is an important factor in the quality of results obtained. It is important to achive at least 80% overlap to obtain satisfactory results.

4.2.2.2 Flow seeding

Microscopic particles are introduced in the flow stream as tracers with appropriate concentration (10^9 to 10^{12} particles/m^3) not affecting the flow properties. The mass ration

$m_{fluid}/m_{particles}$ governs the concentration of micron size particles in air flow, which should not exceed 10^{-3}. The tracers particles used should have two properties:

a) Tracer particles, when introduced in the flow randomly, should follow the local flow faithfully. This requires knowledge of mechanical properties of small particles in the flow. The properties required for tracer particles are pointed below:
   i. Condition of buoyancy neutral particles $(\rho_p - \rho_f)/\rho_f \ll 1$
   ii. The particle time response τ_p should be smaller than the smallest time scale of the flow (critical for turbulent flows).

$$\tau_p = d_p^2 \frac{\rho_p}{18\mu} \tag{4.5}$$

The particle stokes number (S_k) is the most critical when applying PIV technique to map velocity vector field for turbulent flows.

$$particle\ stokes\ number = \frac{particle\ responce\ time}{flow\ characteristic\ time}$$

S_k< 0.1 returns acceptable flow tracing accuracy with error below 1%.

   iii. Health, safety and envirnmental aspects should also be kept in mind before choosing the tracer particles.

b) Tracer particles when illuminated should be clearly detected by the digital imaging devices, require the particles to scatter light efficiently. The scattering efficiency can be quantified by:
   i. ratio of reflective index n/n_f,,
   ii. the wavelength of lightλ^{-4},
   iii. particle diameter d_p

Seeding concentration in the flow is very important step in achieving correct velocity field vectors and for aerodynamic flows, the typical seeding concentration is 10 particles/mm^3. The procedure of dispersing the seeding/tracer particles should not disturb the flow and should provide a homogenous seeding concentration in the flow.

4.2.2.3 Imaging

The image of the tracer particle is formed on the image sensor of the camera via lens. The imaging system is characterised by the focal length f, f-stop ($f_\#$) $f_\#$ = f/D (D is aperture diameter of the lens) and image magnification M.

$$\frac{1}{f} = \frac{1}{d_i} + \frac{1}{d_o}\ ;\ M = \frac{d_i}{d_o} \tag{4.6}$$

Magnification factor can be evaluated as:

$$M = \frac{sensor\ size}{imaged\ object\ size} = \frac{pixel\ size\ \times number\ of\ pixels\ in\ the\ sensor}{FOV}$$

Where FOV is field of view.

Thus the particle images would have a diameter:

$$d_{geom.} = M.d_p \tag{4.7}$$

Where d_p is effective particle diameter. But diffraction effects the minimum particle diameter:

$$d_{diff} = 2.44\lambda(1+M)f_{\#} \tag{4.8}$$

An acceptable approximation of the resulting particle image diameter d_τ is:

$$d_\tau = \sqrt{\left(Md_p\right)^2 + \left(d_{diff}\right)^2} \tag{4.9}$$

The d_τ follows the above equation only for the particles in focus, i.e. when the light sheet thickness Δz_0 is smaller than the focal length δz of the optical system given by:

$$\delta z = 4.88\lambda f_{\#}^2 \left(\frac{M+1}{M}\right)^2 \tag{4.10}$$

Focal depth is the range in which the particles are in focus. Typical values of image seeding density ranges between 0.02 to 0.2 ppp. The image density N_I represents the most probable number of particle images present in the interrogation window:

$$N_I = \frac{C\ \Delta z_0}{M_0^2} \times D_I^2 \tag{4.11}$$

where C is tracer concentration.

The digital image recording is done using charged coupled device (CCD) digital camera. The most high speed cameras suitable for time-resolved PIV have CMOS sensors with active pixel sensor (APS) technology architecture. To record and save large amount of data in seconds, cameras have inbuilt 25GB solid state memory. After the recording, the data from camera's internal memory is transferred to the computer.

4.2.2.4 Processing of particle image motion

The processing of particle images are done in four steps.

1. Image windowing: The entire image is partitioned into small cells each containing at least 10 tracer particles. Every interrogation window evaluates the local velocity vector.
2. Cross-correlation: A statistical tracking operator is applied to the corresponding windows, thus returning a discrete cross-correlation map, whose peak position relative to the origin gives average particle image displacement.
3. Correlated peak sub-pixel interpolation: The highest correlation peak is selected as the corresponding particle motion.
4. Divide by time and scaling: Results from (3) gives particle motion in terms of pixel shift. The velocity is obtained by dividing known time separation between laser pulses and multiplying by the size of the pixel and dividing by the imaging magnification.

There are few optimization rules to be kept in mind while processing the images:

1. The maximum in-plane displacement should be smaller than ¼ of the interrogation window size.
2. The maximum out-plane displacement of the tracer particles should be less than ¼ of the laser sheet waist.
3. The maximum in-plane variation of particle image displacement inside the interrogation window should not exceed the particle image diameter.

4.3 Data reduction methods

The measurements were taken at 4500Hz frequency which allows to perform correlation analysis on time resolved vector fields.

Correlation function is a statistical technique between random variables at different points in space or time which indicates how the random variables co-vary with one another on average across space and time and thus, can provide information and conditions between two sample points to be effectively uncorrelated. In the present study, a cross-correlation function is defined for u’ (stream-wise velocity fluctuations) which varies in time. A line is selected in chord-wise direction with 148 discrete u’ values and each of these 148 discrete u’ is correlated in time with each discrete 256 u’ values in span-wise direction.

$$u_o^{'} = u^{'}(x_i, z_0, t)$$

$$u_{ik}^{'} = u^{'}(x_i, z_k, t)$$

Where, I = 1 to 148, k = 1 to 256 and t = 0.

In continuous form correlation function can be written as:

$$G_{u_o',u_{ik}'}(x_i,z_0,\tau) = \frac{1}{T}\lim_{T\to\infty}\int_0^T u'(x_i,z_0,t)u'(x_i,z_k,t+\tau)dt \tag{4.12}$$

Where $\tau$is an incremental step in time.

The function generated is then normalized by standard deviation, $\sigma_{u(x_i,z_0)} and \sigma_{u(x_i,z_k)}$ providing the value of normalized correlation function between -1 (uncorrelated) and +1 (correlated).

$$-1 \leq g_{u_o',u_{ik}'}(x_i,z_0,\tau) = \frac{G_{u_o',u_{ik}'}(x_i,z_0,\tau)}{\sigma_{u(x_i,z_0)}\sigma_{u(x_i,z_k)}} \leq 1 \tag{4.13}$$

Correlation function applied on u' shows the extent of coherence of flow structures in z direction with time, the larger the value of $g_{u_o',u_{ik}'}(x_i,z_0,\tau)$ more coherent are the flow structures. The coherence of these span-wise structures or vortices are directly related to the strength of tonal noise emitted by the wing.

5. Experimental set up

Experiments were conducted in a low-speed V-tunnel facility at Delft University of Technology. The facility is an open-section low-turbulence wind tunnel with a square cross-section of 400X400mm, operating from 5ms^{-1} to 45 ms^{-1} with free stream turbulence intensity below 1%.

5.1 Airfoil & serrations

The flow over NACA 0018 airfoil, chord length 200mm and wing span 400mm, with Reynolds number ranging from 1.33 X 10^{5}to 5.33 X 10^{5} is investigated. This profile is selected to contribute to limited data available on thick airfoil profiles in tonal noise investigation. Such airfoils are used in wind turbines to with stand large forces and moments. NACA 0018 profile has been used by [Nakano et al. (2007), Timmer et al. (2008), Yasusevych et al. (2009), Boutilier et al. (2012)] in the published studies investigating tonal noise. In this experiment airfoil model is machined from aluminium block, using CNC, to with stand heavy loads. In order to investigate the effect of different TE geometries on flow regime and, the airfoil model is designed with replaceable TE to install different trailing edge geometries with ease. In current experiment, four different modified TE geometries are used of which three are saw-toothed serrations (S1, S2& S3) (fig 5-2) and a flat plate which acts as a flap (S4). Saw-toothed serrations have three main associated geometric parameters, tip-to-root distance (2h), wavelength (λ) and serration angle (ε) as shown in fig 5-3, whose values are given in Table 5-1. The straight TE without any modifications acts as a base line case.

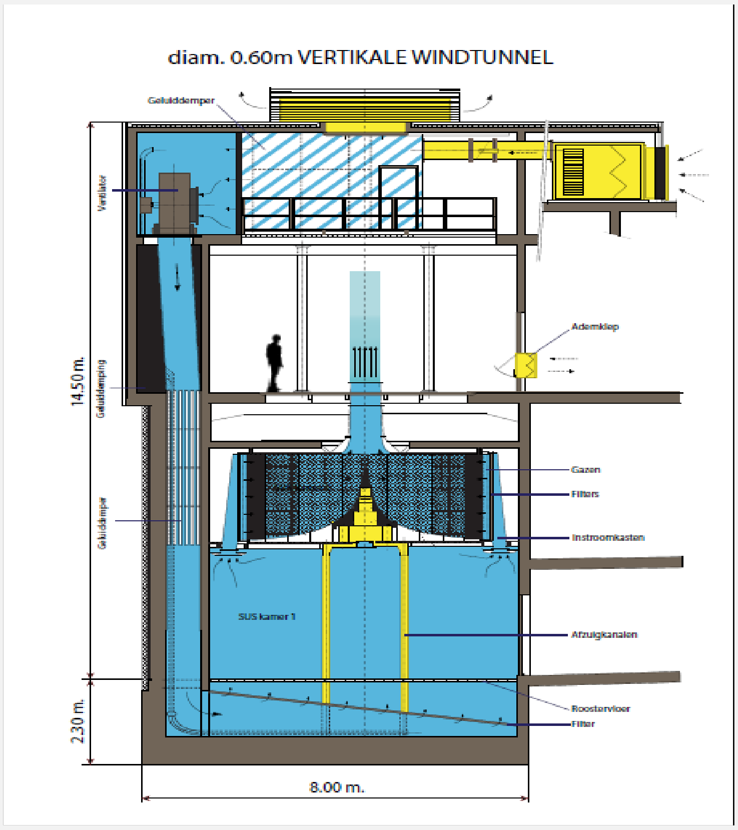

Figure 5-1: University of TU Delft, V-tunnel facility

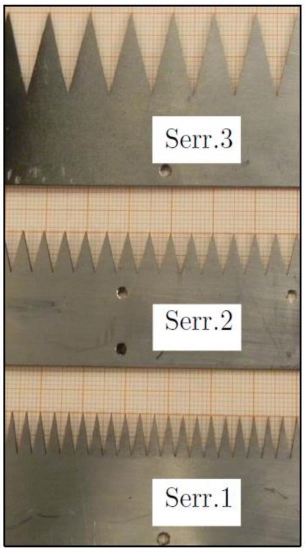

Figure 5-2: TE serrations used

Reference	tip-to-root distance (2h) [mm]	wavelength (λ) [mm]	serration angle (ε)
S1	10	3	8.5˚
S2	10	5	14˚
S3	20	10	14˚

Table 5-1: Geometric parameters of the serrations

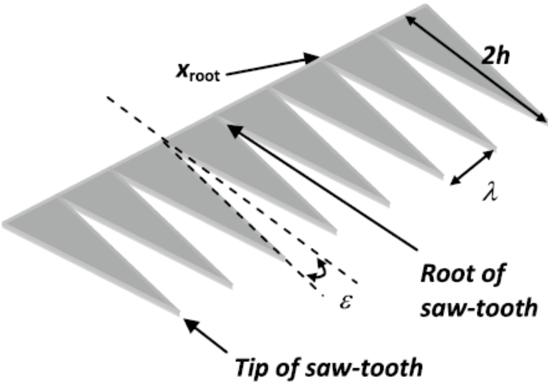

Figure 5-3: Geometric parameters of saw toothed serrations [Chong et al. 2013]

A flow diagram of experimental setup is shown in fig 5-4. The experimental setup can be sub-divided into four parts. The first part is the wind tunnel on which the NACA 0018 airfoil is mounted and the experiments are conducted. The second part is acoustic noise recording radiated from the airfoil TE. The analog signals is received by an analog to digital convertor which then in turn is connected to the computer. The computer is the third part of the setup which acts as controller as well as data recorder for both PIV and microphone measurements. The fourth part is 2C-PIV system which consists of seeder, digital high speed cameras, double pulsed laser with its power source and high speed controller to align the time of laser bursts and camera shutter. The high speed controller is made by Davis and the software used to control as well as to obtain vector fields is also Davis software.

5.2 Acoustic measurements

LinearX M51 microphone is installed at 1350mm from TE aligned to the centre of the wing and at the same height as the trailing edge from ground when positioned at zero degree angle of attack. The acoustic measurements were performed at the frequency of 51.2 KHz for a period of 15.625 sec. These measurements were repeated for 4, 7, 10, and 13 degree angles of attack with free stream velocity (U) varying from 10ms^{-1} to 40ms^{-1} and for the mentioned TE geometries. The V-tunnel facility, though not an anechoic equipped facility, has low overall background noise. Noise data were gathered using 24-bit National Instrument analogue to digital card. The microphones were calibrated with a GRAS piston phone and calibration constant was calculated for each microphone. Using these calibration constants digital data were converted into pressure and then averaged over hamming window (over size of 5120 points) to obtain power spectral density in db., with reference pressure of 20 X 10^{-6} Pa.

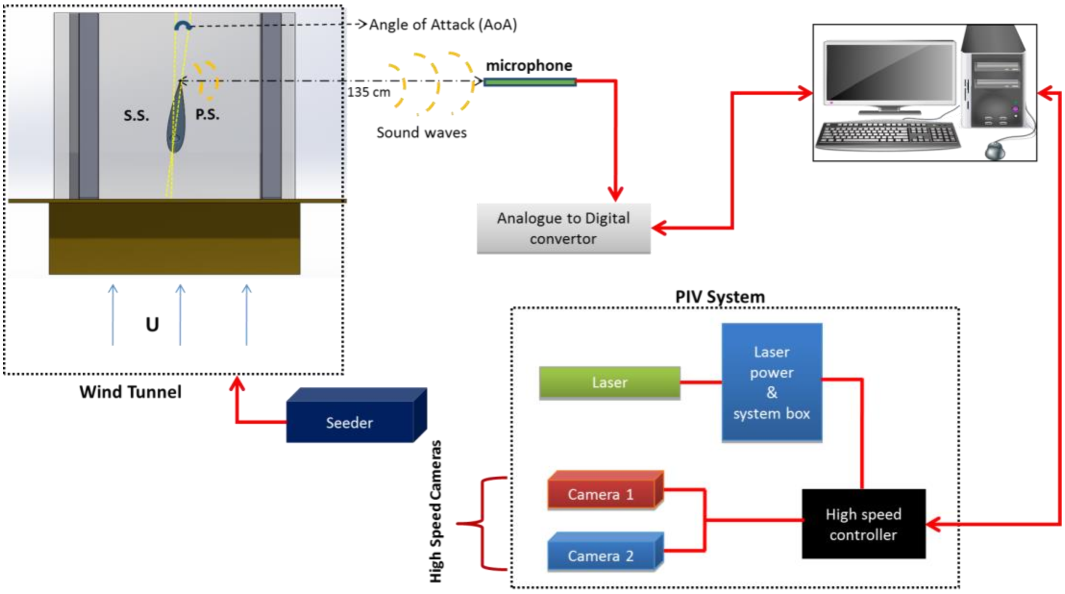

Figure 5-4: Schematic diagram of the NACA 0018 mounted tunnel with PIV system and microphone

5.3 Photo-chromic dye (oil) flow visualisation

Photo-chromic dye flow visualisation is used to capture the points of separation and reattachment of LSB on the PS of the airfoil. The photo-chromic dye is made using paraffin, petroleum and fluorescent pigment of aluminium oxide. A schematic diagram of the experimental set-up for oil flow visualization is shown in fig 5-5. The camera lens is focused on the surface of the airfoil on the PS and the camera's image sensor is set parallel to the airfoil chord. The mounted airfoil is cleaned to remove any dust particles which might cause aberrations and then a very thin of dye is applied on the PS of airfoil after rotating to AoA 7°. The UV light lamp is setup in a manner to give consistent exposure to the oil film.

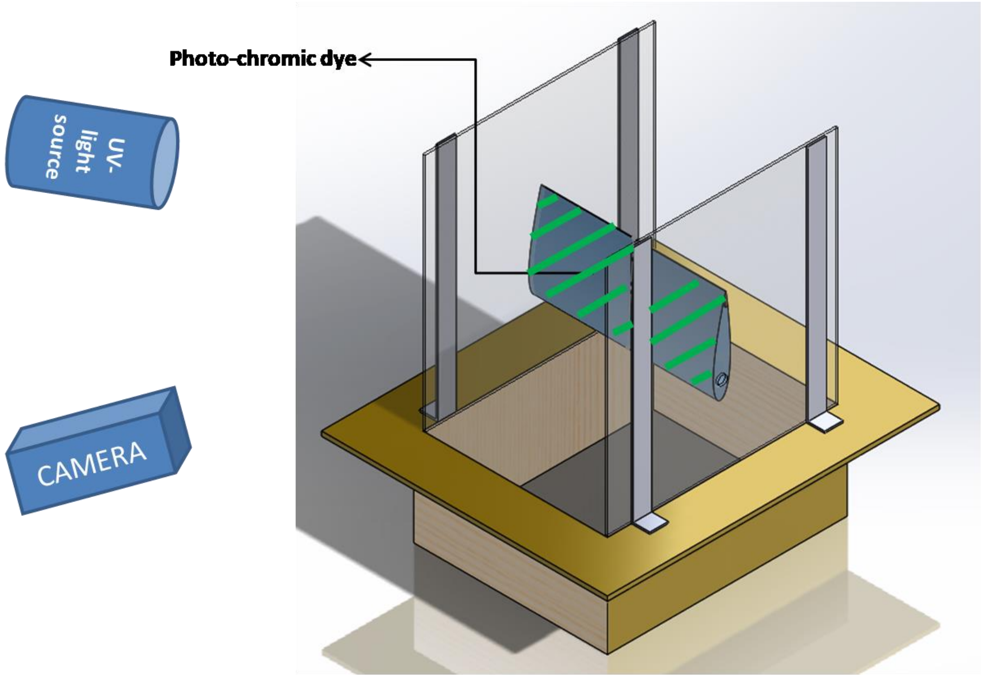

Figure 5-5: Schematic diagram of photo-chromic dye visualisation on PS of airfoil

5.4 Two component particle image velocimetry (2C-PIV)

Two different 2C-PIV setups were used to analyse flow, one in plane perpendicular to surface of airfoil i.e x-y plane and the other parallel to surface of airfoil i.e in x-z plane, near trailing edge of airfoil as shown in fig 5-6 & fig 5-7. The airfoil was rotated at 7˚ angle of attack and images were taken at velocity of 15ms^{-1} and 25ms^{-1} free stream velocity in both cases. To avoid reflection of laser light from airfoil surface, the FOV was painted black. Four different trailing edge configurations were used (smooth, S2, S3 and flap) and images were taken on pressure side of airfoil close to trailing edge. To analyse flow in both x-y and x-z plane near trailing edge of airfoil, PIV setup consisted of:

a. Photron *FASTCAM SA1.1* high speed cameras with Nikon micro-nikkor 105mm lenses for magnification. These cameras feature a maximum operating frequency, when used in single frame and at full sensor, of 5.4 KHz.

b. LaVisionHighSpeed Controller to synchronize illumination and imaging device and a work station installed with LaVision DAVIS 8 to store images. LaVision DAVIS 8 is used to process these images and calculate velocity vector fields.

c. Nd:YLF laser (QuantronixDarwinDuo) is used for illumination. The emitted light wavelength is 532nm.

d. *SAFEX F2010* fog generator is used as seeder to introduce particles in the free stream flow of the wind tunnel. The particles produced by the fog generator have a mean diameter of 1µm.

5.4.1 Wall normal configuration

2C-PIV experimental setup in x-y plane: The schematic of the setup (not to scale) is shown in fig 5-6. It consists of two high speed high-speed cameras (448 X 1024), on either side of the airfoil capturing two FOV with a certain overlap. They were placed on opposite side of airfoil taking images through clear acrylic glass plates. The two cameras were used with an intention to capture a large field of view and were aligned in such a way that post-processed vector fields can be stitched together to one field. The laser was placed at a certain height from trailing edge to minimize reflection from surface. The laser light sheet was formed using opportune set of lenses. The magnification of the camera was 0.4545. $f_{\#}$ were adjusted to have an optimal focus and diameter of imaged particles. The images were taken at a frequency of 4500 Hz in double frame and 4500 double set images were taken for every case. For mean and rms fields the images were taken at a frequency of 125 Hz in double frame and 1000 double set images were taken for every case.

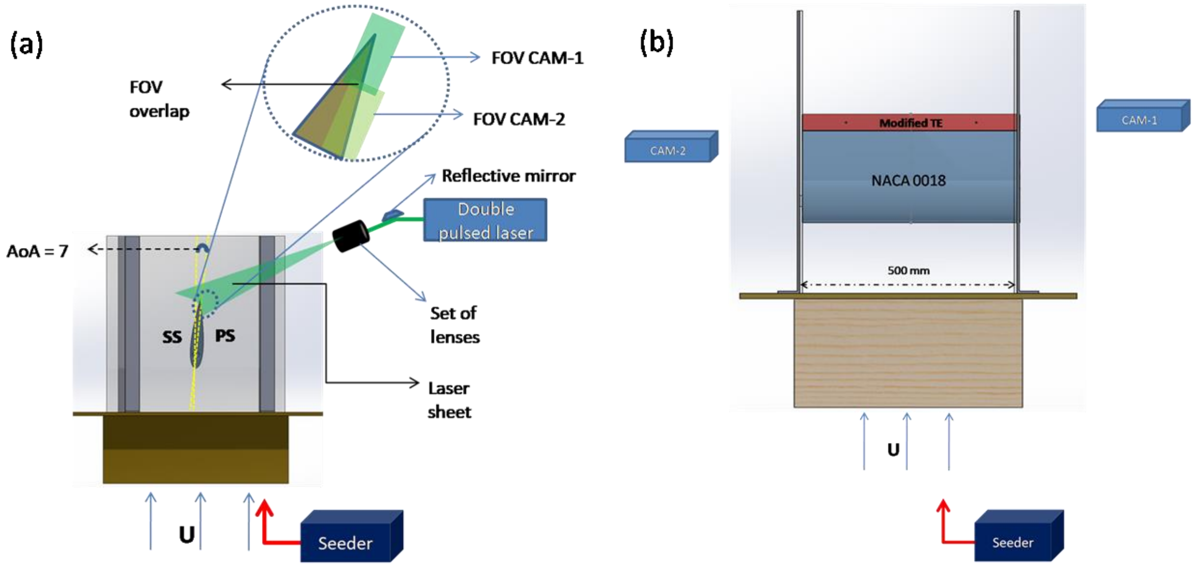

Figure 5-6: Schematics of 2C-PIV setup in x-y plane (stream-wise) (a) end view (b) front view.

5.4.2 Wall parallel configuration

2C-PIV experimental setup in x-z plane: The schematic diagram for the wall parallel configuration setup (not to scale) is shown in fig 5-7. The setup consists of one high speed camera (1024X592) capturing images of the field of view. To capture x-z plane velocity fields inside boundary layer near the trailing edge, measurements were made at 3mm height from the surface of the airfoil near the TE. This was achieved by carefully moving the laser sheet at the required perpendicular distance from the surface and aligning it parallel to the airfoil profile. The magnification of the camera was 0.4545. The $f_{\#}$ was adjusted of the camera lens to get an optimal focus and diameter of imaged particles. The images were taken at a frequency of 4500 Hz in double frame and 4500 double set images were taken for every case for time resolved PIV. For mean and rms fields the images were taken at a frequency of 125 Hz in double frame and 1000 double set images were taken for every case.

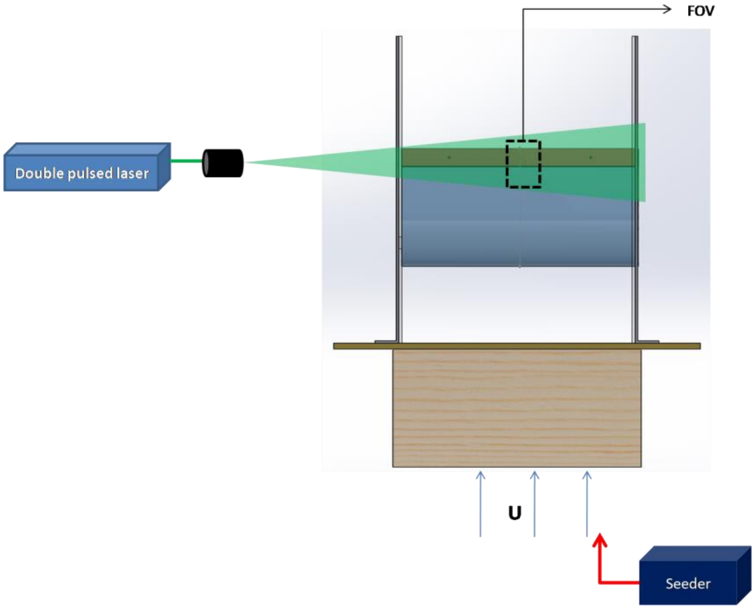

Figure 5-7: Schematics of 2C-PIV setup in x-z plane (span-wise)

6. Results & Discussions

The acoustic experiments are conducted on NACA 0018 airfoil from Re = $1.32X10^5$ to $5.30 X10^5$. The acoustic signal from the airfoil below Re = $1.32X10^5$ is inseparable from acoustic signal from the wind tunnel and acoustic signal above Re = $5.30X10^5$ contains disturbance from the open jet and surroundings. These two practical restrictions, open jet velocity between $10ms^{-1}$ to $40ms^{-1}$, dictate the boundary conditions of the experiment. Acoustic experiments are conducted on different airfoil geometric AoA ranging from 4° to 13°. Due to wind tunnel blockage, the effective AoA is reduced (Brooke et al. 1984) and are tabled below.

α_t	α_{eff}
4	2
7	3.5
10	5
13	6.51

Table 6-1: Effective angle of attack after applying wind tunnel corrections

The acoustic results are compiled, compared against the literature and explanation is given for the behaviour in section 6.1. Acoustic results are followed with oil flow visualization results for all four TE configurations at free stream $U=25ms^{-1}$ at geometric AoA=7° on the PS. The oil flow visualization shows an approximate point of separation and also the length of separation bubble. It also provides a visual of global mean field velocity over the airfoil surface. Section 6.2 contains oil flow visualization results along with boundary layer profiles at different chord-wise stations obtained from PIV experiments. Section 6.3 presents instantaneous as well as statistical flow field results at geometric AoA=7° and free stream $U=25ms^{-1}$ for four TE configurations.

6.1 Acoustic emissions

Acoustic measurements are performed in free field conditions in an open jet wind-tunnel as discussed in Chapter 4. The section is divided into three sub-sections. First sub-section presents effects of varying angles of attack, geometric AoA = 4°, 7°, 10°, 13°, on acoustic emissions with velocity from $10ms^{-1}$ to $40ms^{-1}$(Re = $1.32X10^5$ to $5.3X10^5$). Second sub-section corresponds to effect of tripping of BL on PS, SS and both sides, keeping AoA constant at 7°

with free stream velocity ranging between 10ms^{-1} to 40ms^{-1}. Third sub-section presents effect of TE modifications on self-noise radiation. For this case a constant AoA=7° is selected with U=25ms^{-1}(Re = 3.05e4), to keep the study succinct and the free stream velocity is varied between 10ms^{-1} and 40ms^{-1}.

In the following sub-sections, spectral maps of acoustic pressure auto spectra are plotted. These plots are truncated at frequency of 3500Hz showing only the first harmonics which helps in zooming into finer structures of the plots.

6.1.1 Effect of changing angle of attack and effects of forced transition

Acoustic measurements are done at different AoA with free stream velocity between 10 ms^{-1} and 40ms^{-1}, sampled with a resolution of 1ms^{-1}. The acoustic pressure power spectral density PSD (with reference to $(20 \text{ X}10^{-6})^2$ Pa^2/Hz) is plotted with background noise PSD subtracted on spectral maps for above mentioned cases. Sound pressure levels of dominant tones are sufficiently high to be seen on spectral maps. The tones plotted on spectral maps, after first group of dominant tones, are harmonics presenting themselves at twice the frequency of the preceding tone and are less in intensity with increasing frequency. A distinctive narrowband 'ladder-type' structure (Paterson et al. 1973) is observed varying with frequency, as a piecewise continuous function of the free stream velocity which increased locally according to $f \sim U^{0.85}$ and undergoes a number of jumps. At certain velocities two or more distinct frequencies are observed for the same velocity (Paterson et al. 1973, Lowson et al. (1994), Arbey&Battille 1984).

The boundary layer is forced to transition using carborundum (Silicon Carbide) particles (average height 36µm) randomly placed on double sided tape of width 10mm. The tripping tape is placed upstream to the point of separation. Approximate point of separation is measured by oil flow visualization (section 6.2.2) at chord-wise position x/c = 0.2. Paterson et al. (1973), Plogmann et al. (2012) and more recently by Pröbsting et al. (2013) used forced transition to identify the side of the wing mainly responsible for tonal nose emission.

The wing is tripped on case by case basis on suction side, pressure side and then both sides to compare it with clean cases. The self-noise radiated from the wing is measured for geometric AoA 4°, 7°, 10°, 13° and spectral maps of acoustic pressure auto spectra (subtracted background noise) are plotted for each shown in Figure 6-1; 6-2; 6-3; 6-4 respectively.

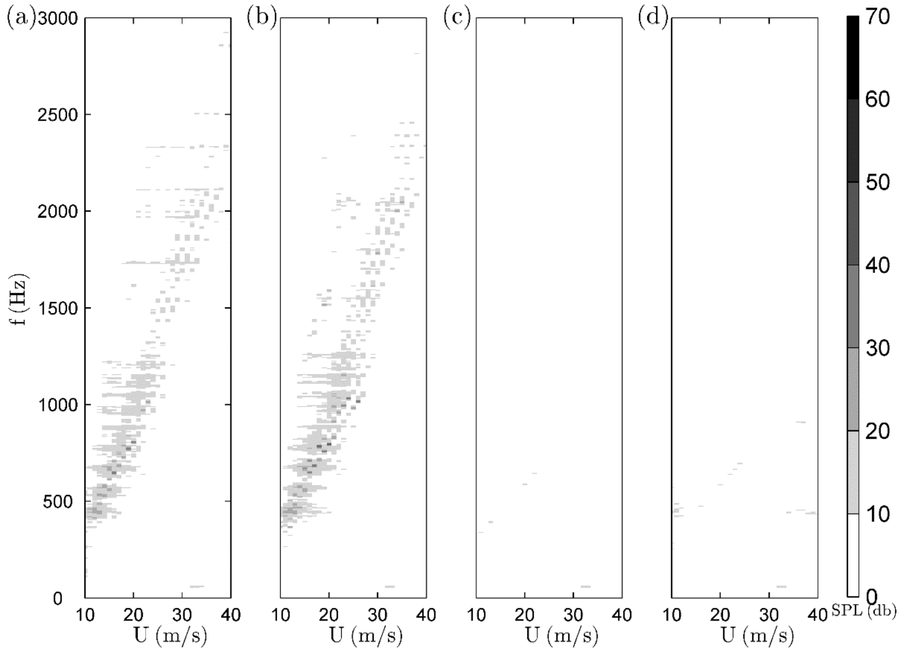

Figure 6-1: Narrowband SPL [dB., reference 20µPa] AoA 4° (a) without forced transition, (b) forced transition SS, (c) forced transition PS, (d) forced transition PS+SS

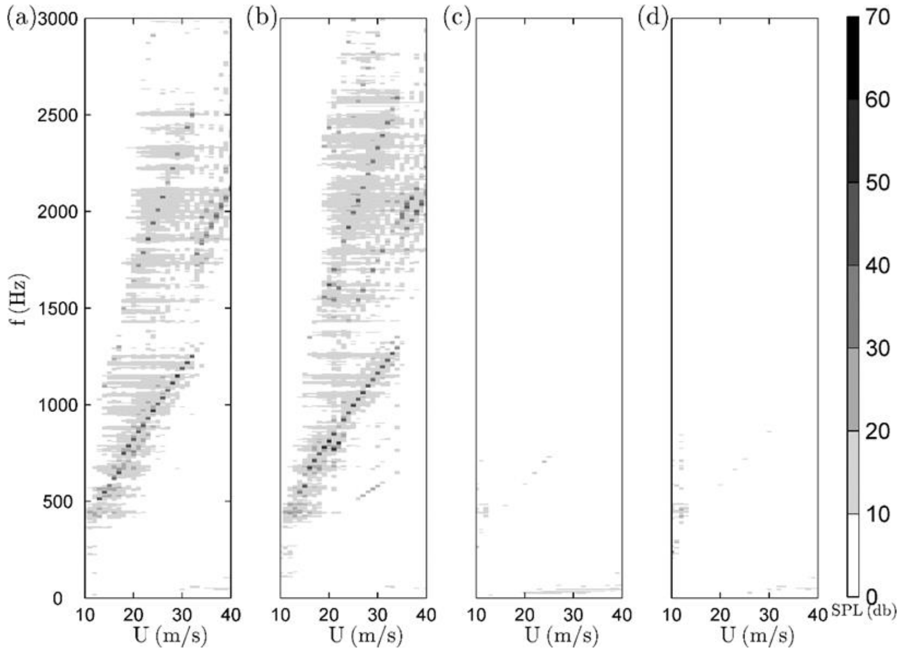

Figure 6-2: Narrowband SPL [dB., reference 20µPa] for AoA 7° (a) without forced transition, (b) forced transition SS, (c) forced transition PS, (d) forced transition PS+SS

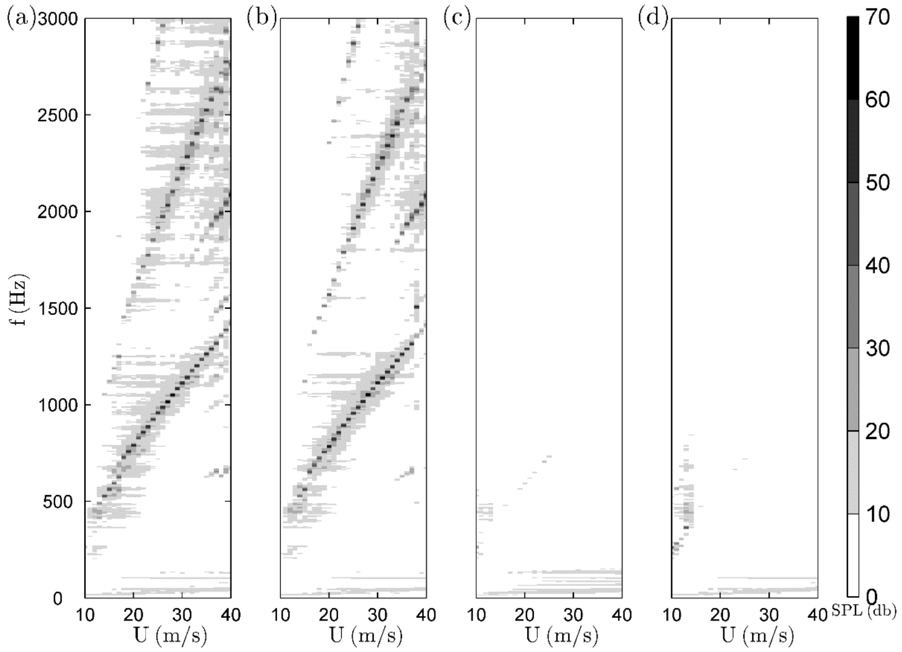

Figure 6-3: Narrowband SPL [dB., reference 20μPa] for AoA 10° (a) without forced transition, (b) forced transition SS, (c) forced transition PS, (d) forced transition PS+SS

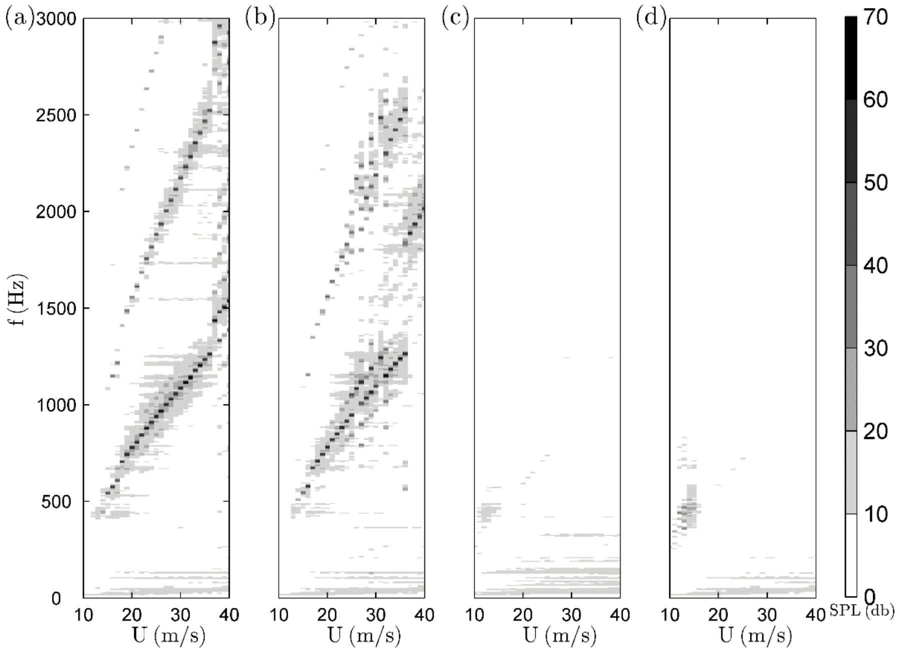

Figure 6-4: Narrowband SPL [dB., reference 20μPa] noise maps for AoA 13° (a) without forced transition, (b) forced transition SS, (c) forced transition PS, (d) forced transition PS+SS

As discussed in chapter 2, the disturbances (TS-waves) in the laminar boundary layer of different frequencies move downstream in the boundary layer of the wing. The laminar separation bubble is unique to this regime, present close to trailing edge on pressure side of the wing. The LSB plays an important role in amplifying these TS-waves which lock-on to a particular frequency depending on the angle of attack and free stream Reynolds number. Locked-on and amplified TS-waves, roll-up as the flow transitions, interact with TE and emit tonal noise at same frequency as with locked-on TS-wave frequency. Clean and SS-tripped spectral plots show strong tonal noise and SS forced transition has no effect on tonal noise. Forced transition of PS and PS-SS attenuates tonal noise, thus showing tonal noise in NACA 0018 for the considered range of angles of attack and Reynolds number is PS dominated. This finding is concurrent with the studies published by Paterson et al. (1973), Arbey&Battille (1984), Pröbsting et al. (2013).

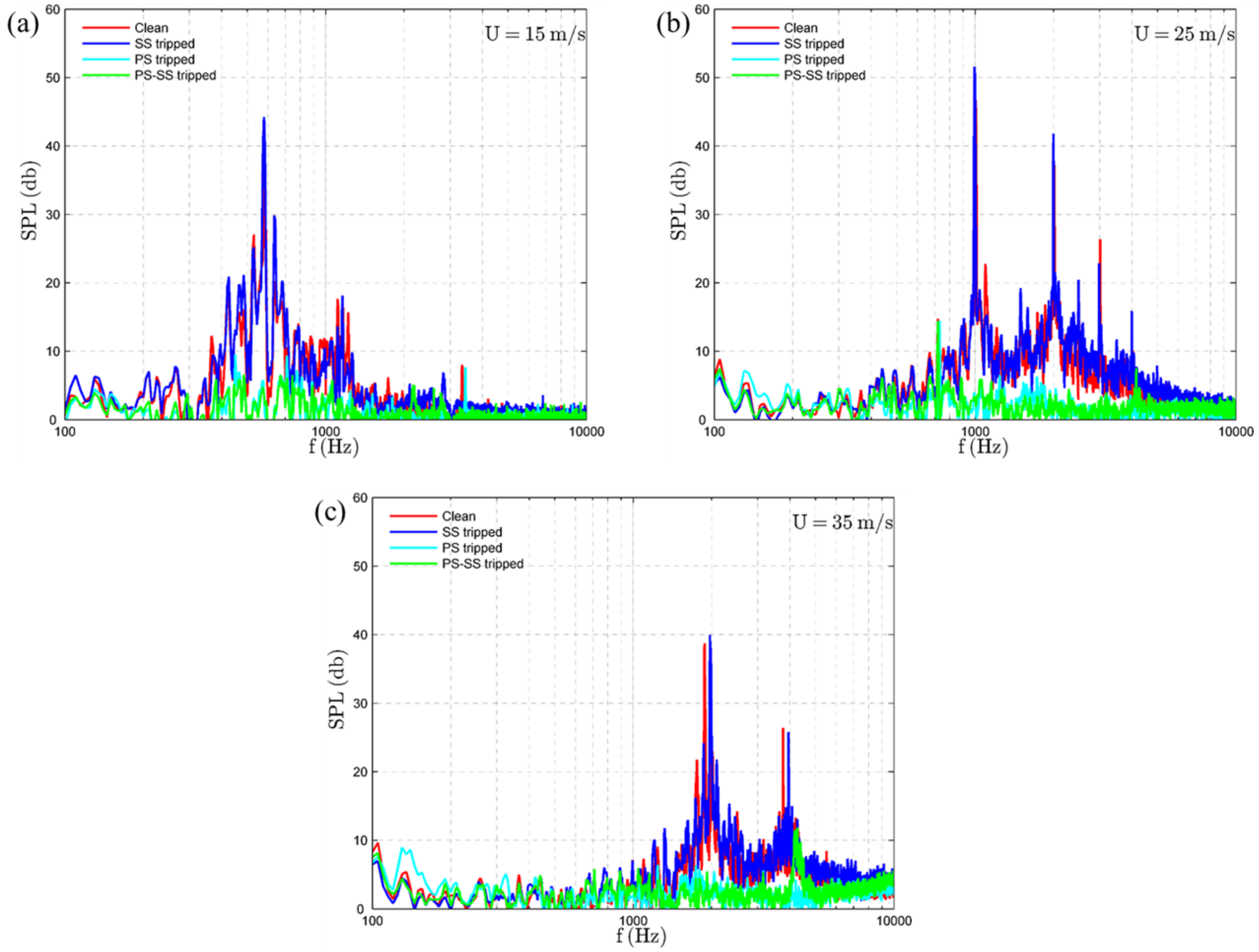

Figure 6-5: Narrowband SPL [dB., reference 20µPa], geometric AoA 7° (a) U = 15ms^{-1} (Re = 1.98e5)(b) U = 25 ms^{-1} (Re = 3.31e5)(c) U = 35 ms^{-1} (Re = 4.63e5)

Fig 6-5 clearly shows the drop in sound pressure level for PS and PS-SS tripped to the level of background noise levels. The SPL level for U=25 ms^{-1}without forced transition features SPL about 75db and for SS tripped SPL is around 80db at 1kHz which drops to wind tunnel background noise level of about 35 db. The harmonics are present at 2KHz and 3KHz with decreasing amplitude. Same trend is observed for cases U=15 ms^{-1} and U=35 ms^{-1} where tripped boundary layer on PS truncates narrowband tones to a level where they are indistinguishable from wind-tunnel background noise. By forcing the laminar boundary layer to transition to turbulent on PS, the feedback loop is stopped by early transition using tripping tapes before it interacts with TE. However, it is observed that PS tripped and PS+SS tripped have no dominant tones in all angles of attack which underlines the tonal emitted is PS dominated for these flow cases.

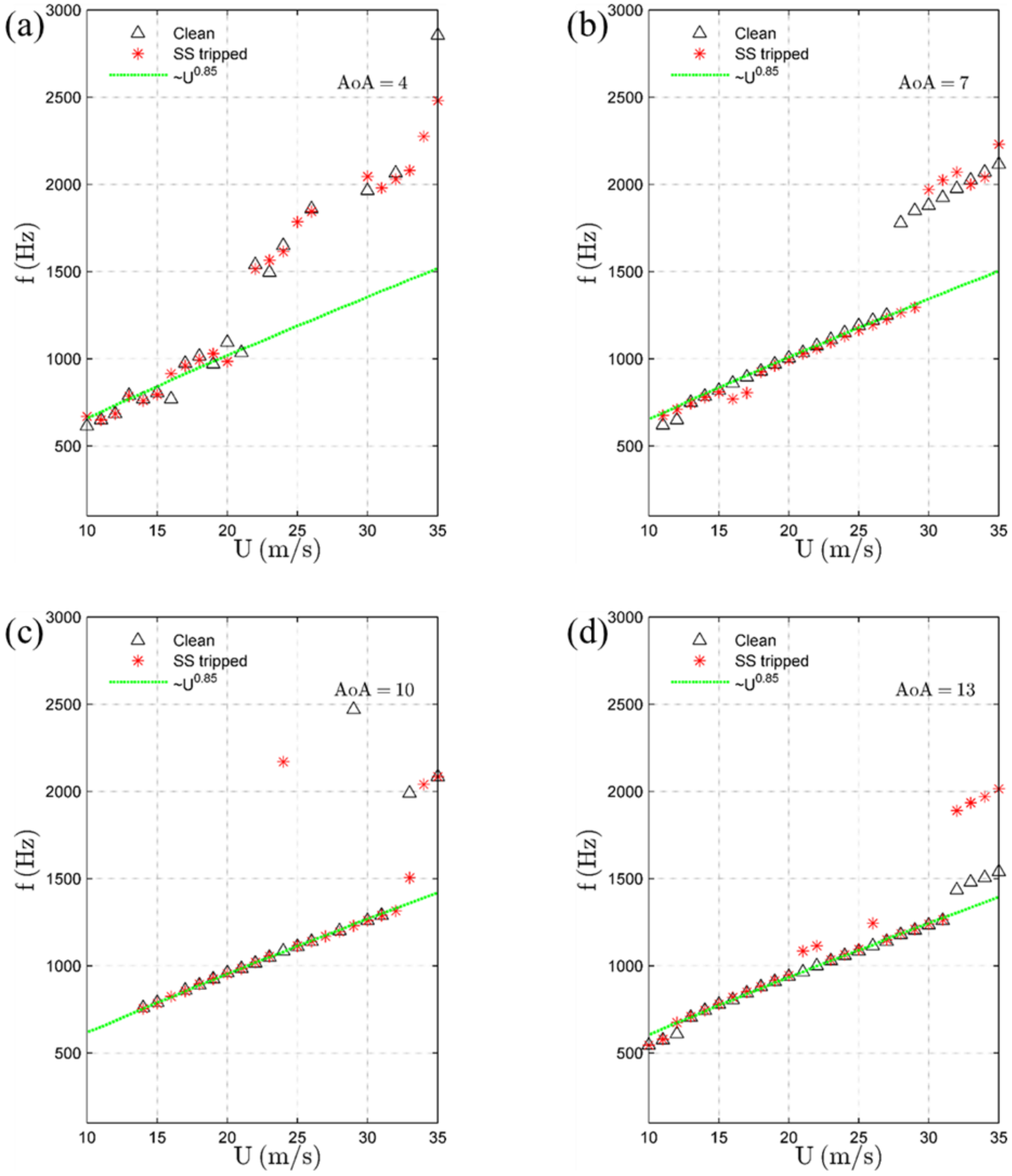

Figure 6-6: Variation of primary tone frequency f_{nmax}varying $U^{0.85}$, geometric AoA (a) 4°, (b) 7°, (c) 10°, (d) 13°

Paterson et al. plotted a curve fit with f_{nmax} varying with $U^{0.8}$, though in Fig 6-6 it is not the case and the power factor is 0.85 which is in line with Arbey&Bataille (1984). It also shows the ladder structure (Paterson et al. (1973)) as the frequency jumps to higher values at a certain velocities for different AoA.

6.1.2 Effect of trailing edge geometry

After determining the tonal noise is dominated by the flow events on the PS, next step is to attach TE modifications. The boundary layer on the suction side is forced to transition by the same tripping device to avoid eventual interactions of the unsteady flow events between the two sides of the wing. The case AoA 7° is selected to further study the effects of TE modifications on tonal noise being the flow case that showed stronger acoustic tonal emissions. Fig 6-7 (a) shows the spectral SPL map for straight TE and other three TE modifications. Fig 6-7(b) is the spectral SPL map with a flap attached emitting tones of low amplitude at comparable frequencies as the smooth TE. Fig 6-7(c) shows spectral SPL map for serration 2 attached to TE of the wing with tonal noise attenuated as compared to smooth as well as flap cases. Serration 3 spectral SPL map shows the strongest attenuation of tonal noise at velocities over 20ms^{-1}. The amplitude of tones in the case serration 3 have partially or completely attenuated as compared to straight TE. To study the effect of serrations on the flow evolution, oil flow visualization and 2C-PIV experiment results are discussed in the later sections.

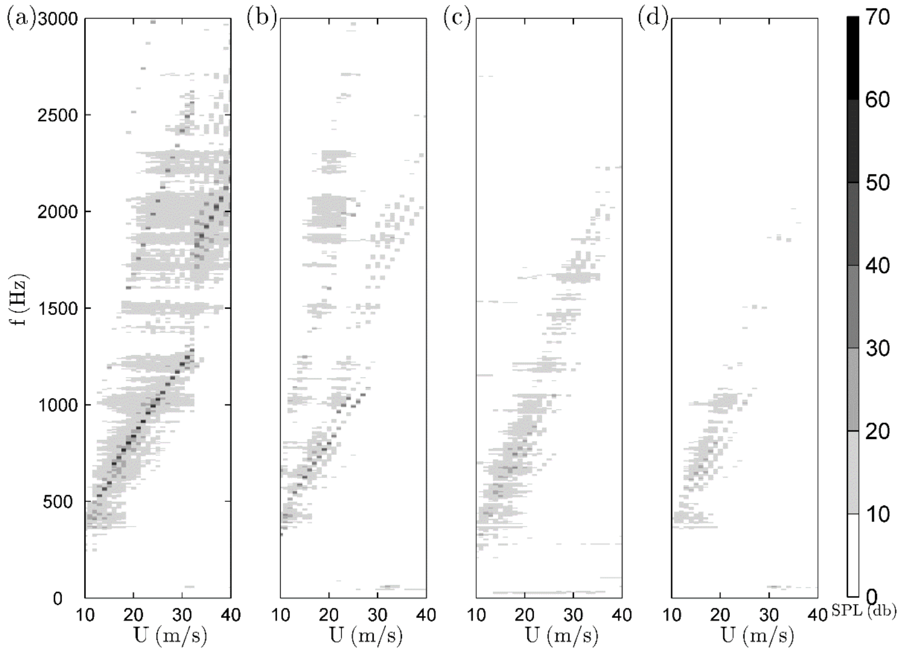

Figure 6-7: Narrowband SPL [dB., reference 20µPa] for AoA 7° (a) straight TE, (b) flap, (c) serration 2, (d) serration 3.

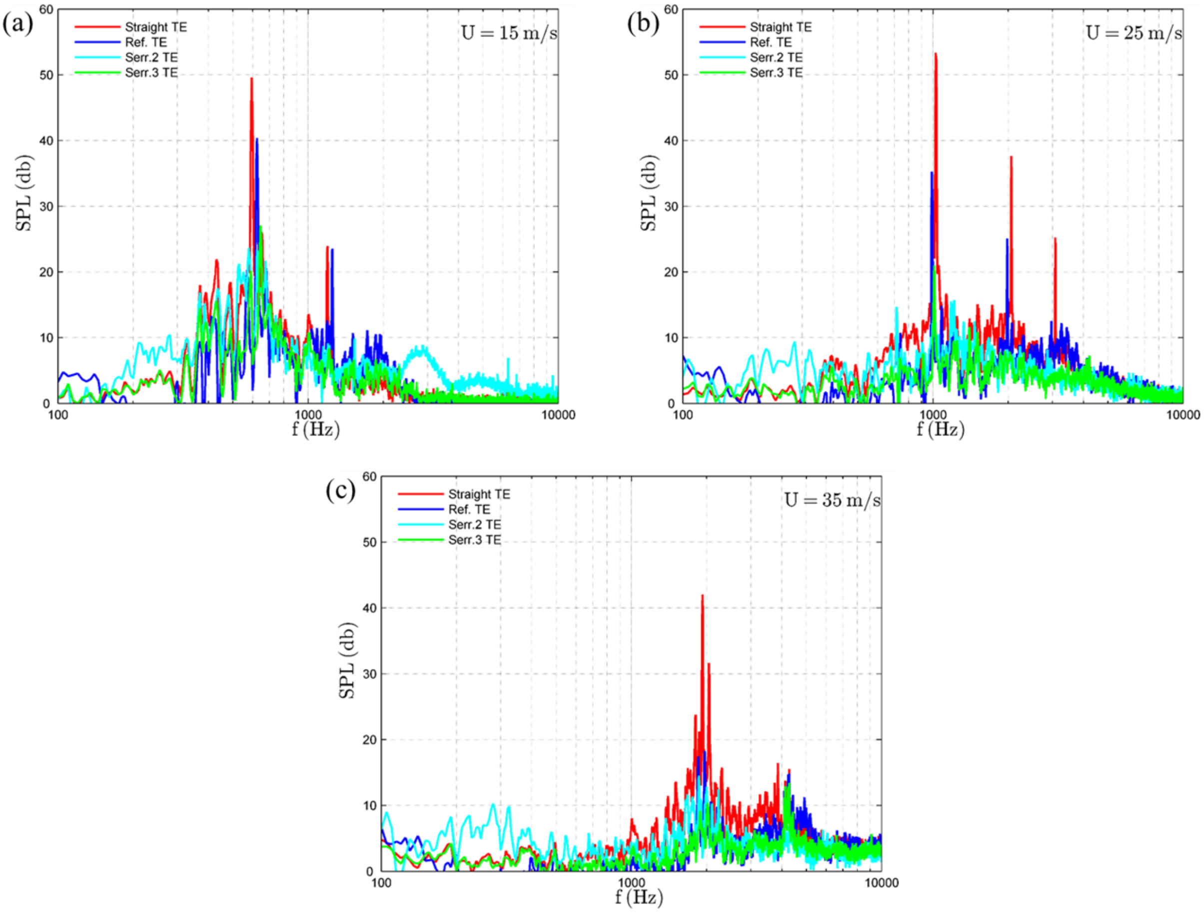

Figure 6-8: Narrowband SPL [dB., reference 20µPa], geometric AoA 7°, SS tripped (a) U = 15ms^{-1} (Re = 1.98e5)(b) U = 25 ms^{-1} (Re = 3.31e5)(c) U = 35 ms^{-1} (Re = 4.63e5)

From the noise maps in fig 6-7, it is concluded, the TE modifications definitely attenuate the tonal noise. In fig 6-8, spectra are plotted at AoA 7° for U=15 ms^{-1}, 25ms^{-1} and 35ms^{-1} to make a comparative study. In case of U=25 ms^{-1}, two harmonics can be seen at 2 kHz and 3 kHz for straight TE. Serration 3 TE modification has the most noise attenuation of 30 dB compared to the straight TE geometry as shown in fig 6-8 (b). Due to the clear distinctions in noise attenuation, the AoA 7° with U=25 ms^{-1} is selected to study the flow domain in detail using photo-chromic oil flow visualization and time resolved (TR) 2C-PIV.

6.2 Flow field structure & evolution

The acoustic study of airfoil tonal noise using forced transition technique is concurrent with the previously published studies [Paterson et al. (1973), Arbey&Battille (1984), Probsting et al. (2013)], affirming the tonal noise emitted and its mechanism is PS dominated. It is also shown that the serration-3 TE geometry attenuates the tonal noise by 30 dB for AoA 7 at U = 25ms^{-1}. To study the effects of saw-toothed serrations on self-noise radiation from wing as well as to study the flow domain, a base line case of AoA7° is selected. To keep the study succinct, flow field study is constrained to free stream velocity to U = 25 ms^{-1} and AoA 7°. Applying oil flow visualization technique and time resolved 2C-PIV techniques are applied to further study the flow in detail. The results from these experiments are presented in the following sections.

6.2.1 Surface flow visualization & boundary layer profiles

The Oil flow visualization with photo-chromic dye (Aluminium oxide) is performed in order to study the position of separation and reattachment of LSB on the PS of the wing. Such techniques have been shown to be a useful to study LSB in case of tonal noise [Nakano et al. (2006)].

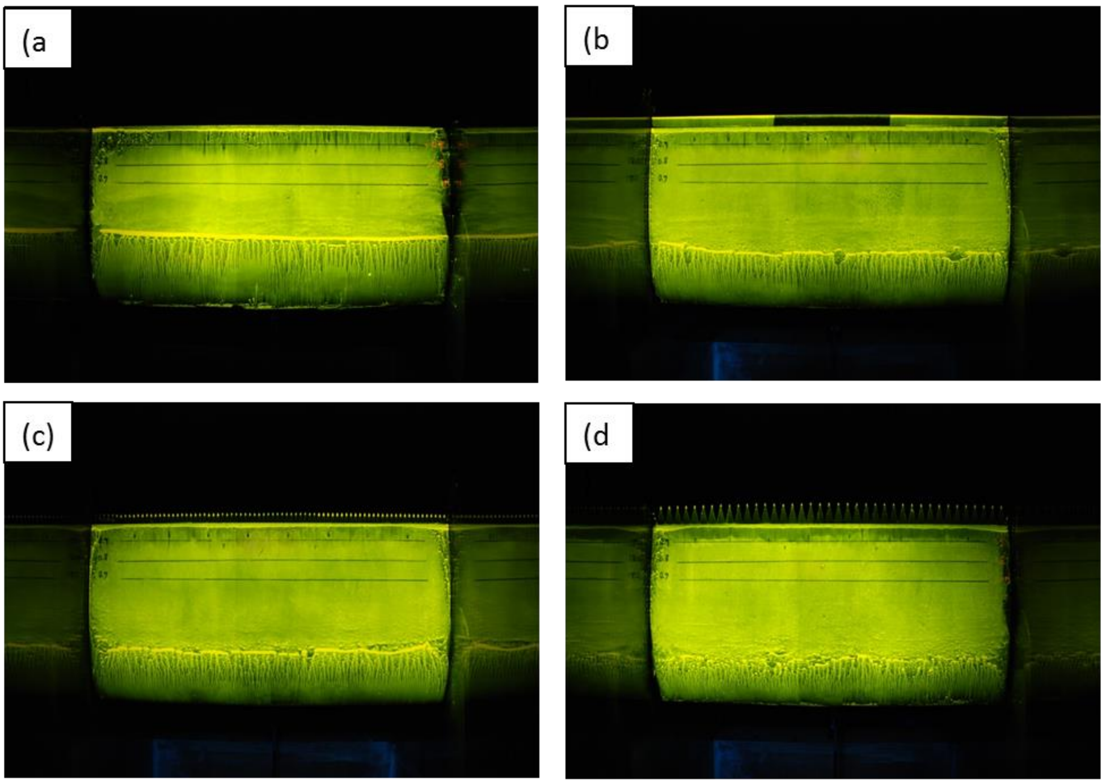

Figure 6-9: Oil flow visualization pictures for four different cases at AoA 7° and U =25ms^{-1} with (a) Straight TE (b) flap (c) Serration 2 & (d) Serration 3.

The oil flow visualization is done to determine qualitatively global effect of the serrations on the upstream flow on the PS of wing surface. Three lines are drawn on the model at 0.7c, 0.8c and 0.9c respectively which act as scale for calibrating the captured image in physical space. In the images taken (fig 6-9), it is interesting to compare the length of laminar separation bubble (LSB) and flow characteristics near the line of separation for each case. For better visualization of flow characrteristics, the image's bit map is scanned and prominent edges are detected and plotted using *inkscape 0.91*. The results are plotted in fig 6-10.

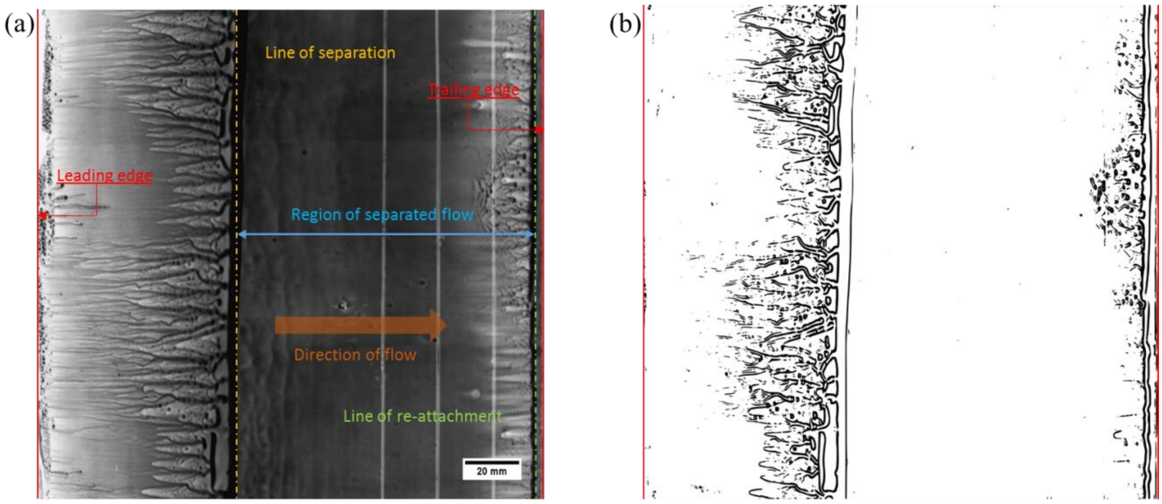

Figure 6-10: Span-wise truncated oil flow visualization plots for straight TE (a) flow field description (b) colour inverse

Straight TE emits high tonal noise at AoA 7° and Re = $3.3X10^5$ as shown in fig 6-8 (b). Oil flow visulaization for the straight TE case is presented in fig 6-10(a) with line of separation, line of re-attachment and region of laminar separation bubble. The flow on the PS convecting downstream (flow from left to right) separates due to adverse pressure gradient forming a spanwise separation line. The separated flow region is the laminar separatio bubble. The flow reattaches as the flow transitions from laminar to turbulent regime.The length of separation bubble is 110mm. In fig 6-10 (b), the prominant edges are plotted which provides rich visual detail. The NACA 0018 has a strong span-wise separation with reattchment close to TE. The results concur with Nakano et al. 2006.

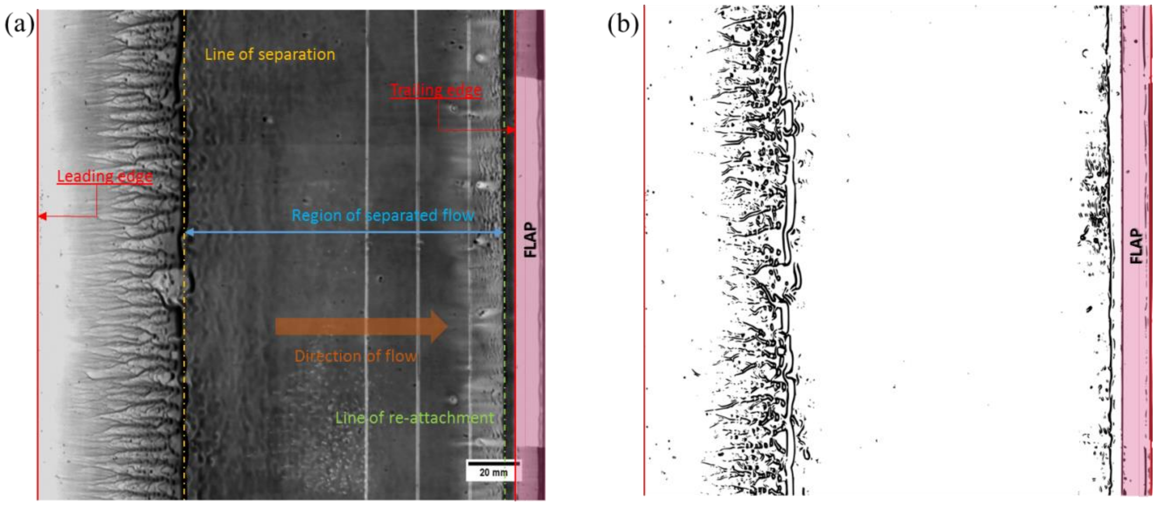

Figure 6-11: Span-wise truncated oil flow visualization plots for reference plate (flap) TE (a) flow field description (b) colour inverse

The reference plate (flap) TE case emits tonal noise at AoA 7° and Re = $3.3\text{X}10^5$, refer to figure 6-8 (b). The flap has effect on the upstream flow of airfoil with weak separation starting upstream as compared to straight TE case. The length of separation bubble changed to 130mm in length. The weak separation can be seen in fig 6-11 (b) as the span-wise line of separation is sporadic.

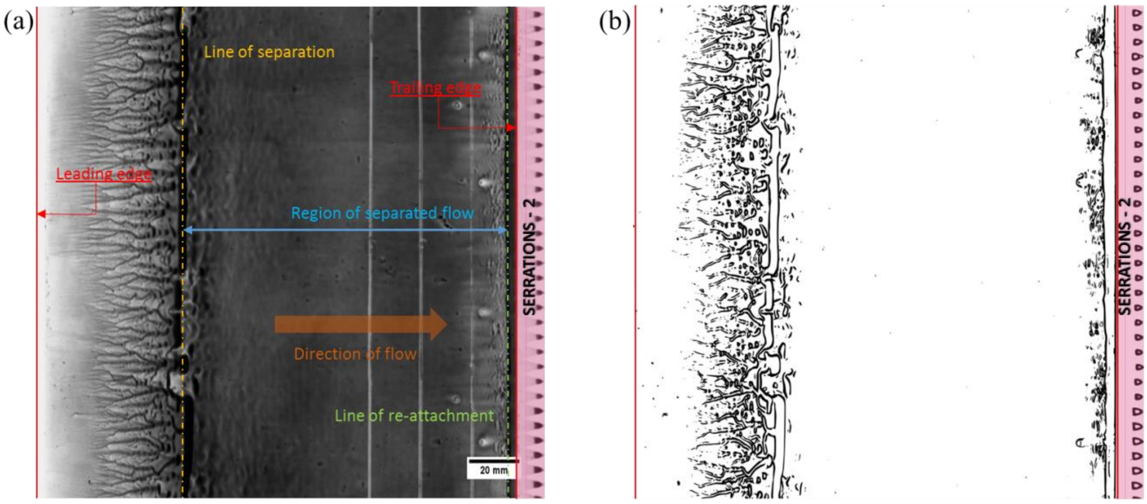

Figure 6-12: Span-wise truncated oil flow visualization plots for straight TE (a) flow field description (b) colour inverse

The serration 2 TE does not completely attenuate the tonal noise as can be seen in fig 6-8 (b) for AoA 7° and Re = $3.3\text{X}10^5$. The serrations affect the upstream flow making separation sporadic and changing the length of separation bubble. The length of separated flow is 134mm and the span-wise line of separation is weak as compared to base case of straight trailing edge, presented in fig 6-10(b). The oil flow visualisation are comparable for serration-2 and flap.

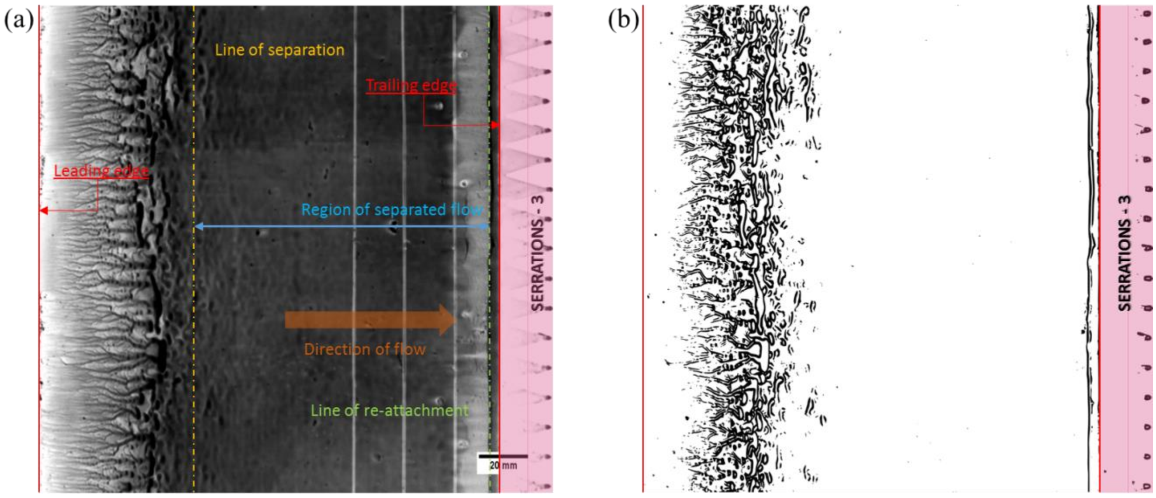

Figure 6-13: Span-wise truncated oil flow visualization plots for serration 3 TE (a) flow field description (b) colour inverse

The serration 3 TE completely attenuates the tonal noise as can be seen in fig 6-8 (b) for AoA 7° and Re3.2e5. The span-wise line of separation is broken and discontinuous with weak separation upstream of the flow. The length of separated flow is 138mm, largest for serration 3 among all the four cases. The distinct span-wise line of separation has disappeared and the separation is discontinuous even in stream-wise direction as shown in fig 6-13 (b).

The oil flow visualization for all four cases provide a clear picture of the serrations affecting flow upstream of TE. To study effect of TE modifications in detail, BL profiles are plotted for straight, flap and at root, tip position for serrations. To present different cases for span-wise and orthogonal measurements, a nomenclature method is introduced. The cases will be referred to the nomenclature described in the table below for here on.

TE modifications Measurement plane	Wall-parallel(span-wise) 2C-PIV measurement	Wall-normal (orthogonal) 2C-PIV measurement
Straight TE	A-1	A-2
Serration 3 TE	B-1	B-2
Serration 2 TE	C-1	C-2
Flap	D-1	D-2

Table 6-2: Nomenclature of the different cases for PIV measurements.

The laboratory coordinate axis is rotated about z-axis to make the x-axis along the surface of wing (x*-axis) and y-axis normal to the surface (y*-axis) at each chord-wise position. Boundary layer (BL) profiles are plotted using the mean x*-axis velocity fields of camera-1 (camera frame close to TE of the wing). The PIV measurements close to or at the surface of wing are erroneous with non-physical discrepancies such as non-zero velocity at the wall. These non-physical anomalies can be due to lack of particles close to wing surface or reflection from the surface in certain cases; thus inaccurate correlation. To correct these anomalies close to surface and to satisfy the no-slip boundary condition at the wing surface, a spline based interpolation is used. At each vector station along the x*-axis, velocity is set to zero at the wall. The three vector points in y*-axis (wall normal direction) adjacent to wall are deleted at every station and cubic spline interpolation method is used to re-calculate the velocity vectors to satisfy no slip condition at the wing surface. The mean velocity profiles are plotted at six different stations; x/c = 0.875, 0.900, 0.925, 0.950, 0.975, 0.999.

Comparison is made between BL profiles for different cases to determine the effect of TE modifications on the BL characteristics. The A-2 case presented in fig 6-14 (a) has LSB point of reattachment is before x/c = 0.95. The stations x/c = 0.875, 0.900, 0.925 have negative tangential velocity component showing presence of LSB.

Fig 6-14 (b), presents D-2 case with flap attached to the TE of the wing, features a more advanced transition state with turbulence onset at x/c = 0.999 as compared to A-2 case. At station x/c = 0.925, reverse flow is waning as compared to A-2, pointing towards higher momentum in the BL. This observation is in-line with the partial tonal noise attenuation for case D-2 (Probsting et al. 2013). The point of reattachment is before x/c = 0.950.

The BL profile for case B-2_{root} , presented in fig 6-14 (c) , is comparable with A-2 case. The partial similarity between BL profiles can be attributed to the fact that the chord length is same at the root of serration; thus length of LSB and its characteristics. The reverse flow velocity close to the wing surface at stations x/c = 0.875, 0.900, 0.925 is greater as compared to A-2. " Higher reverse flow velocities in LSB lead to more intense shear layer, amplifying TS-waves at a greater rate". The point of reattachment is before x/c = 0.950.

The point of reattachment for case B-2_{tip}, presented in fig 6-14 (d), is before x/c = 0.950. The BL profile has transitioned towards turbulent regime compared with BL profile of B-2_{root}. It is interesting to note at x/c = 0.999, BL profile is similar to that of D-2. The flow is 3-D in nature upstream of TE with varying BL profiles when compared station to station between B-2_{root} and B-2_{tip}.

In fig 6-14 (e), at x/c = 0.875, case C-2_{root}, has non-physical BL profile close to wing surface. It is the only chord-wise station that cubic-spline interpolation gives erroneous results. The cause can be the reflection, at or around station in question, from wing surface making the correlation to calculate the vector field in the window inaccurate. The BL-profiles for both cases, shown in Fig 6-14(e), (f), C-$2_{root\ \&\ tip}$ are quite similar and are also comparable to case D-2. The point of re-attachment is before station x/c = 0.950.

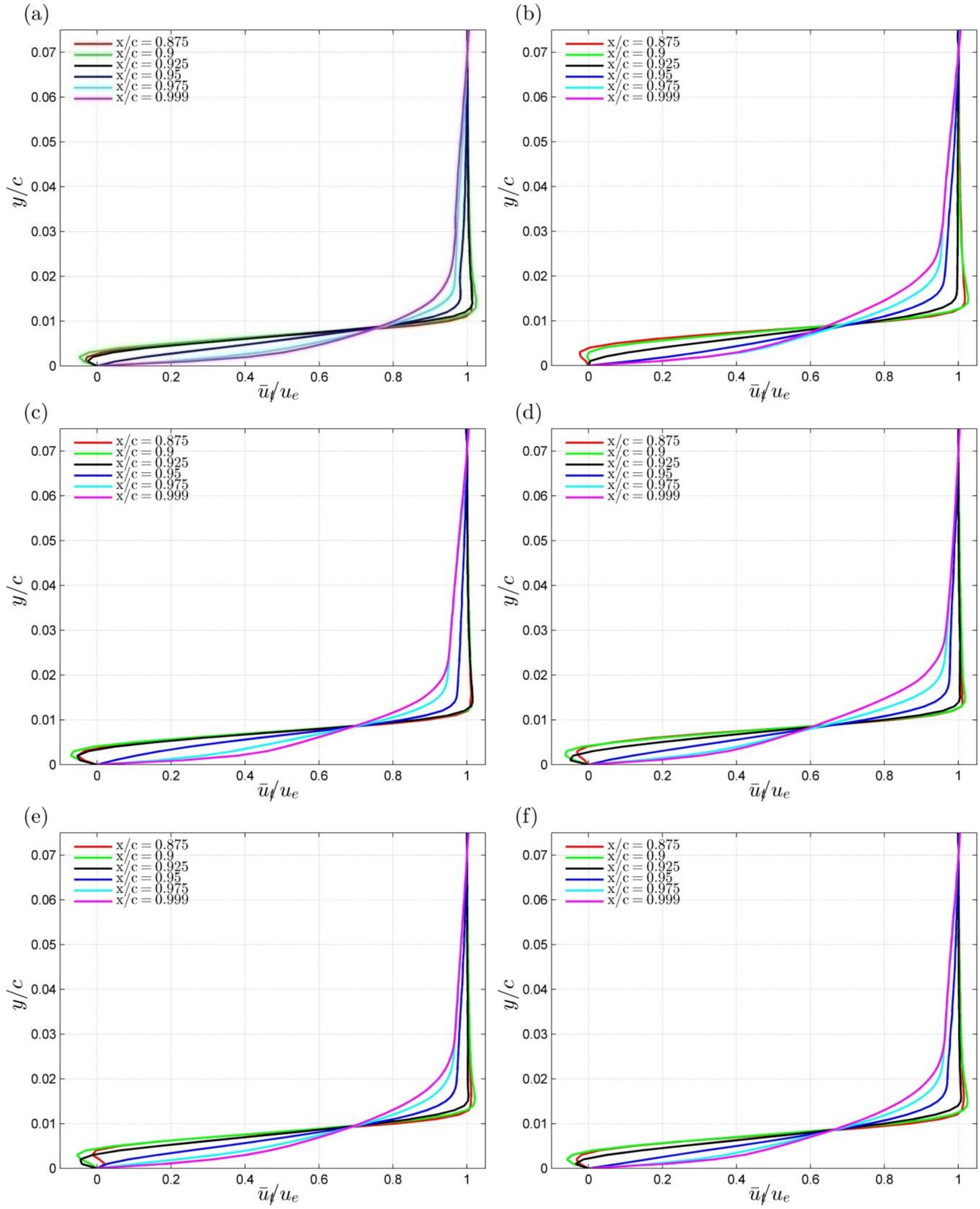

Figure 6-14: Boundary layer profiles at different chord positions (x/c = 0.875, 0.9, 0.925, 0.95, 0.975, 0.999) for (a) configuration A – 2, (b) configuration D – 2, (c) for configuration B – 2 at root of serration, (d) for configuration B – 2 at tip of serration, (e) for configuration C – 2 at root of serration, (f) for configuration C – 2 at tip of serration

6.2.2 Time-resolved flow evolution

Time resolved 2C-PIV is performed at a frequency 4.5 kHz on the PS of the wing near TE. The PIV is performed on two different planes near TE of wing, tangential and orthogonal to the surface, described as span-wise configuration (1) and stream-wise configuration (2) respectively. In the literature it has been hypothesised that the TS waves travelling downstream lock onto a particular frequency and are amplified while passing through the shear layer over the LSB (Pröbsting et al.). These disturbances (TS-waves) convect downstream, role-up to form span-wise coherent structures before interacting with the TE. With the use of time resolved PIV, study of aforementioned span-wise coherent structures and effects of TE modifications on the flow upstream of trailing edge has been made possible. Section 6.2.2.1 presents three instantaneous time frames for each case in span and stream wise configurations at a time difference of 222µs. The base case of U = 25ms^{-1} and AoA = 7°, for all cases, is chosen to compare and study the effects of modified trailing edges. The specifications of the experimental setup for both stream-wise and span-wise configuration have been mentioned in the Chapter 5. Different colour schemes are followed to distinguish between span-wise and stream-wise velocity configuration.

6.2.2.1 Instantenuous visualization

In span-wise configuration, TE is at 0 on x-axis, and the velocity fields plotted are approximately at span-wise centre of the wing to minimise interference in flow from the side plates of the experimental setup. For the ease of presentation, the velocity fields plotted have a length to breadth spatial ratio of 5:1. Fig 6-15 shows velocity vector field for straight TE in span-wise configuration. The velocity field vectors are close to zero at x/c = 0.9, thus in region 1 of TS waves (fig 2.7). As the TS-waves transverse downstream, entering into the span-wise vorticity phase, the positive and negative alternative velocity bands form span-wise vorticity (2-D disturbances) which are being amplified in the shear layer above the LSB. These bands are shear layer rollup vortices travelling towards TE with a certain convective velocity. Close to the TE, span-wise coherent vortices interact with the TE. The TS-wave evolution observed is in line with the narrow band dominated noise emitted by straight TE.

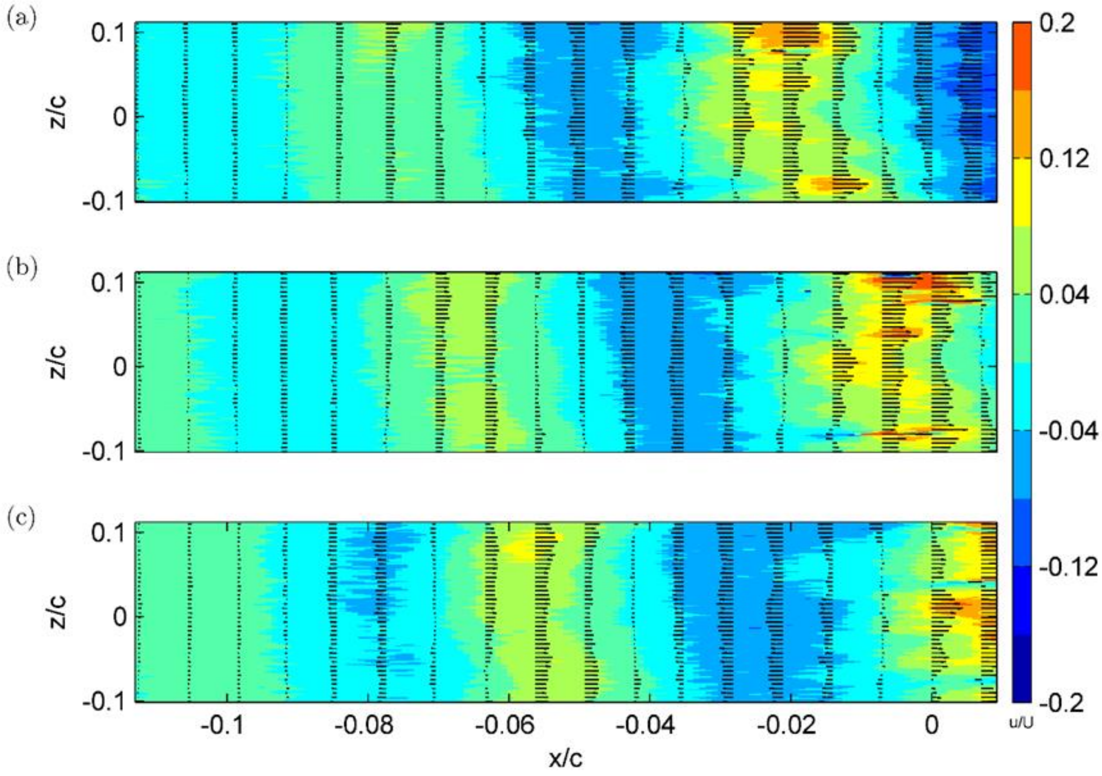

Figure 6-15: Velocity vector field (y – position = 3 mm & configuration A - 1) of 'u' at three time instances (a) t_o, (b) $t_o + \Delta t$& (c) $t_o + 2\Delta t$ with $\Delta t = 222\ \mu s$

The configuration B-1 in fig 6-16 present quite a different velocity profile as compared to configuration A-1. The configuration B-1 has the maximum tonal noise attenuation effect which is due to change in flow characteristics. Span-wise coherent structures are non-existent in B-1 configuration as the velocity vectors are both positive and negative at each chord positions on the wing. The flow, upstream of x/c = 0.9, is already in the third phase of transition with 3-D breakdown. It is of interest to know what forced an earlier onset of 3-D breakdown as compared to A-1 case. Clues can be found in the oil flow visualization of B-1 case in fig 6-13. The unstable LSB and point of separation forces the TS-waves to enter the 3-D breakdown phase and as the disturbances approach TE, x/c = 0.98, turbulent spots starts to form. Furthermore, the boundary layer shows a higher degree of turbulence close to TE of the wing. Fig 6-13 shows an unstable laminar separation bubble which plays a part in span-wise non-coherent TS-waves which amplify degree of turbulence while passing through the shear layer of LSB towards serrations. The unstable separation point restricts the feedback loop from locking on to a particular frequency. As the flow transitions from laminar to turbulent upstream of the TE, there is complete attenuation of tonal noise at U = 25 ms^{-1}, AoA 7°. Thus the lack of periodic shedding of span-wise coherent vortices and high degree of turbulence might play a central role in attenuation of narrow bandwidth noise.

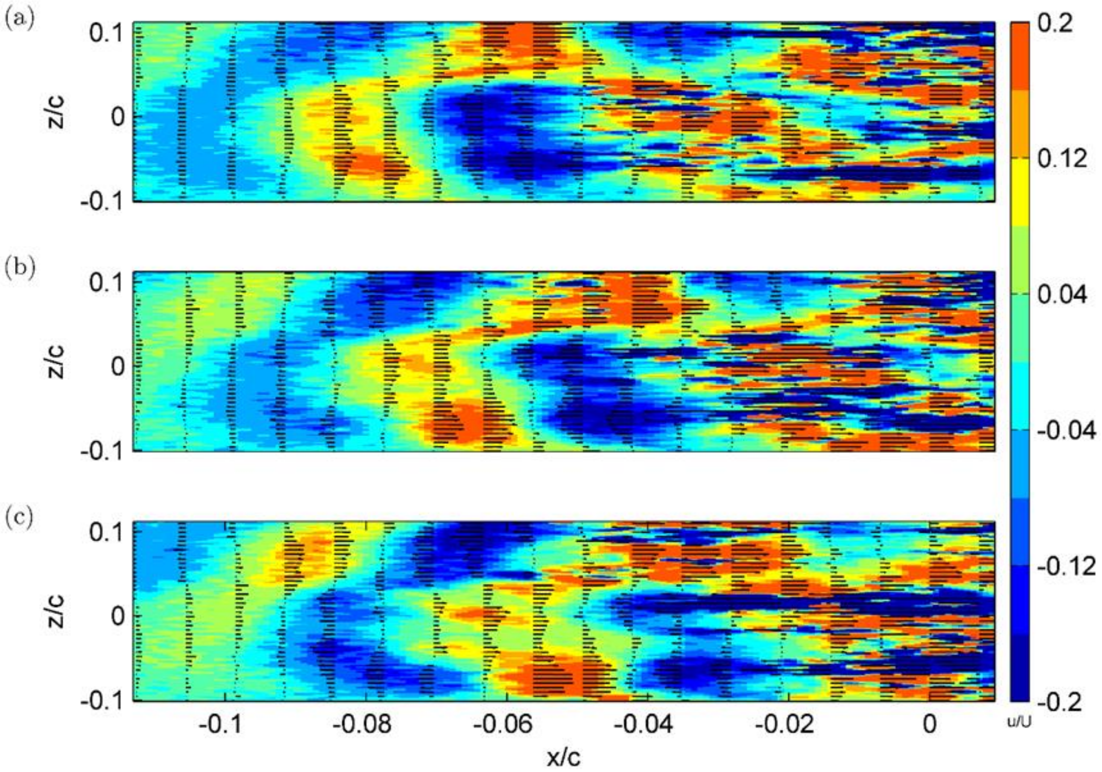

Figure 6-16: Velocity vector field (y – position = 3 mm & configuration B - 1) of ‘u’ at three time instances (a) t_o, (b) $t_o + \Delta t$& (c) $t_o + 2\Delta t$ with Δt = 222 µs

Serration 2 and flap have a varying degree of noise attenuation as shown in fig 6-8 (b). Configuration C shows less degree of turbulence as compared to configuration B and D which is concurrent to the noise attenuation characteristics for the respective cases.

The span-wise time evolution of velocity fields shows that the flow upstream of TE has higher degree of turbulence as compared to non-serrated trailing edges. As shown in oil flow visualization, the separation in configuration-B is weak and occurs upstream as compared to separation in configuration-A. This could be due to inability of TS-waves to lock on to a certain frequency.

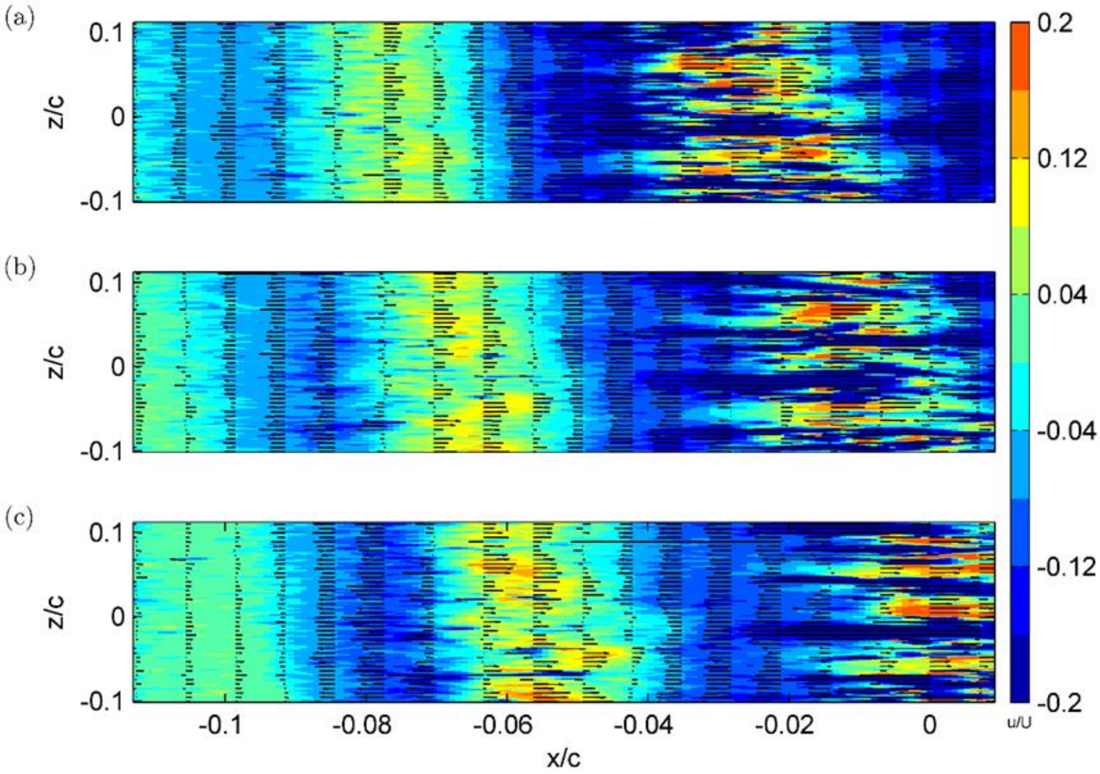

Figure 6-17: Velocity vector field (y – position = 3 mm & configuration D - 1) of ‘u’ at three time instances (a) t_o, (b) $t_o + \Delta t$& (c) $t_o + 2\Delta t$ with Δt = 222 µs

In stream-wise configuration, LSB is observed on the PS near the TE similar to the case of straight TE case.

In stream-wise configuration, images are taken from either side of the wing to capture the flow on the upstream positions of the wing and to also have maximum resolution with the available lenses. These two images are then overlapped into a single frame for optimised presentation. The grey portion presents the masked region of wing, black region is masked due to shadow. In stream-wise frames, a LSB is observed on PS as suggested in literature. The TS waves cross-over the LSB, amplify and roll-up to form vortices as they interact with trailing edge in a periodic manner. The rolling up of the disturbances and formation of these vortices is clearly observed for the straight TE case. These vortices interact with TE and are then shed in wake of the wing regularly.

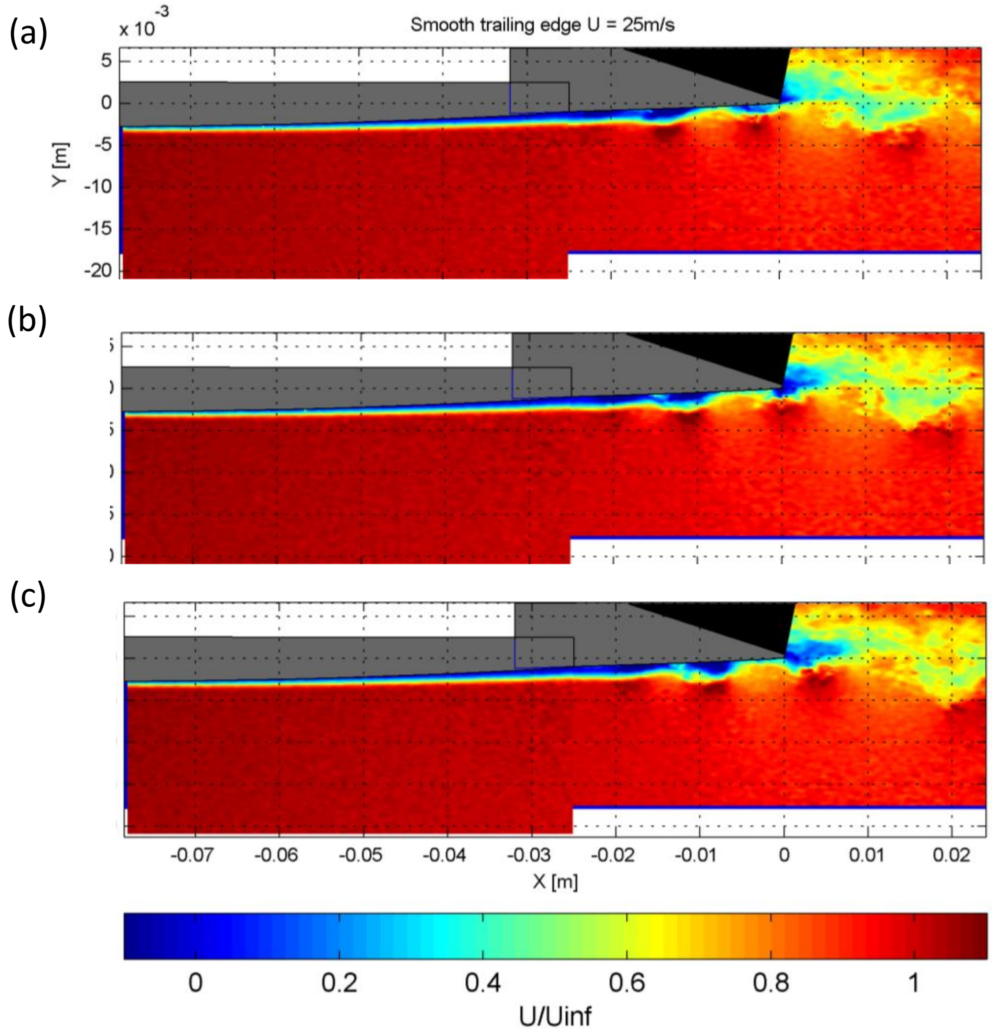

Figure 6-18: Velocity field (span-wise centre of wing & configuration A – 2; AoA 7°& U = 25 ms^{-1} of 'u' at three time instances (a) t_o, (b) $t_o + \Delta t$& (c) $t_o + 2\Delta t$ with $\Delta t = 222$ µs

In all the fields in figure 6-18 & 6-19, it is possible to notice a shallow region of separated flow close to the wall extending from the beginning of the domain up to few mm before the TE. The separation bubble at the trailing edge was individuated by McAlpine et al. (1999) to be necessary for acoustic tonal radiation. Difference between the two investigated flows is what happens from this location going downstream: the straight TE case shows the formation of vortices, shed from the upper bound of the bubble and convected by the flow. For the serrated case, the flow is more turbulent with little distinguishable periodical structures. It seems that the add-on TE geometry causes a sudden enhancement of the three-dimensionality of the flow fluctuations. Chong et al. (2014) in their recent study on the effect of these geometries on tonal noise flows, commented similar findings by showing that the serrated trailing edges can be effective in reducing the radiated noise by means of two different mechanisms: they shorten the separated region thus leading to less amplified instability waves and they strongly reduce the coherence of the shed waves past the trailing edge. The results of the TR-PIV of vortex shedding frequency, presented in fig 6-20, confirms the second observation by giving a clear picture of the flow domain.

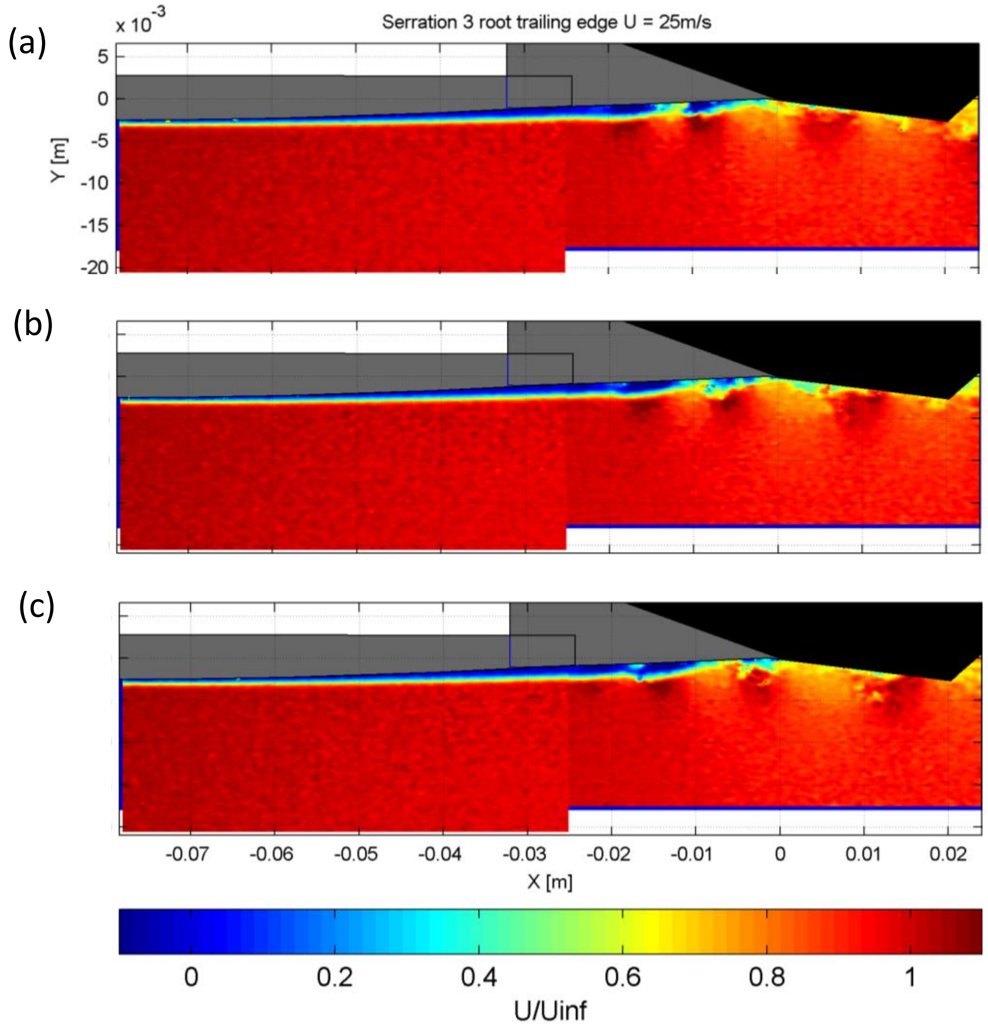

Figure 6-19: Velocity field (span-wise centre of wing & configuration A – 2; AoA 7°& U = 25 ms^{-1} of 'u' at three time instances (a) t_o, (b) $t_o + \Delta t$& (c) $t_o + 2\Delta t$ with $\Delta t = 222$ µs

6.2.2.2 Vortex shedding frequency

The auto spectral power density analysis on velocity field is performed to correlate dominant frequency of acoustic waves emitted and locked on TS-waves travelling downstream for all the span-wise configurations. The spectral analysis is done at the span-wise position of Z = 0 and Y = 3mm in the velocity fields. Fig 6-20 (a) has a dominant frequency at 1000Hz with its harmonic at 2000 Hz. The velocity auto spectral power density frequency coincides with the tonal noise frequency. The above conclusion is true for the remaining cases. In fig 6-20 (b), the case B-1 has no dominant frequency. It can be concluded that the TS-waves do not lock to any specific frequency for wing configuration with serration 3 TE modification. Thus, the tonal noise is attenuated. The spectral analysis of velocity field shows a definite change in upstream flow on pressure side of the wing. The observed results are coherent with the conclusion made in section 6.1.2.

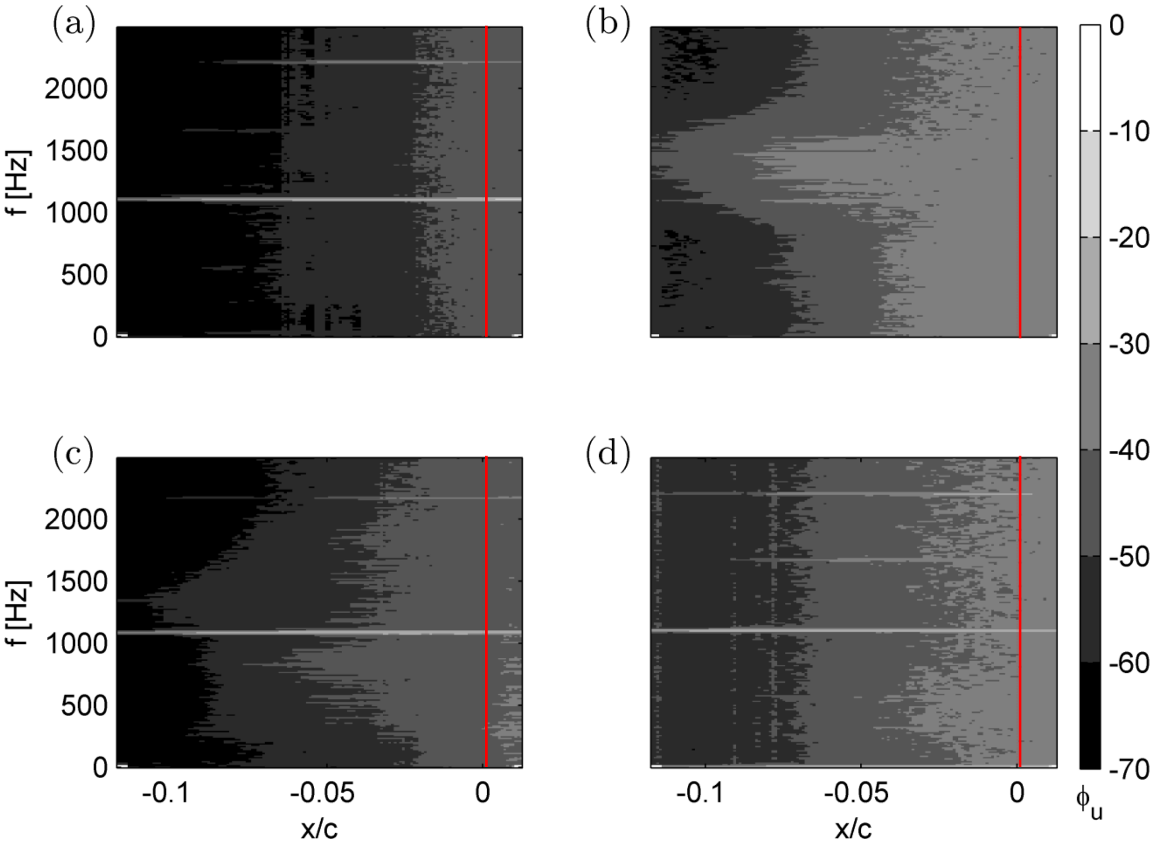

Figure 6-20: Auto spectral power density of the stream velocity component sampled along Z = 0 for the configuration A-1 (a), configuration B-1 (b), configuration C-1 (c),configuration D-1 (d) at Y = 3mm from airfoil pressure side surface. The red line is at trailing edge of NACA 0018.

6.2.3 Statistical characteristics of flow field

The time resolved PIV are taken at high frequency of 4.5 kHz and total dual-frames taken are 4500. So, the flow captured is for 1sec in total for time-resolved PIV. To study the statistical characteristics of the flow, the frequency is set to 125Hz and the measurements are taken for 5 sec. Field of view (FOV), in case of span-wise 2C-PIV, is larger as compared to instantaneous flow field to capture statistical characteristics. The span-wise flow field is captured at 3mm from the surface of the wing. ‘Jet’ color sheme is used to present span-wise statistical characteristics. The TE is located at the origin. The origin on z-axis is located at the span-wise centre of the wing.

As explained in experimental set-up, two cameras are used to capture flow upstream of the TE. The FOV close to TE is of interest to study change in flow dynamics upstream of TE, thus only CAM-1 images are processed. The laboratory frame is rotated about z-axis to obtain surface attached, curvilinear coordinate system, represented as x_c-y_c axis, with x_c-axis is along the surface of the wing. The new origin is located at the leading edge of the wing. Body-fitted coordinate system is advantageous for comparative study as well as to calculate the BL characteristics. The black dashed line drawn in stream-wise plots show the location of statistical flow characteristics plotted in span-wise location at a height of 3 mm from the surface of the airfoil.

6.2.3.1 Velocity mean & fluctutaion fields

The field of view in span-wise configuration (1) is small as compared to stream-wise configuration (2). The span-wise configuration shows the mean and rms velocity fields close to TE. In Fig 6-22 (a) U_m/U is decreasing steadily as the flow approaches the TE. The same can be seen in figure 6-23 (a) as the span-wise plane (represented by black dotted line) enters the shear layer as the BL transitions from laminar to turbulent. Thus, approaching the TE, there is a change in BL profile of the flow due to the amplification of the disturbances. In figure 6-22 (b), W_m/U is quite low as compared to V_m/U in fig 6-23 (b) near the TE. Low values of W_m shows that the flow is mostly two-dimensional, span-wise coherent, and breaks into three-dimensional only when interacts with the TE. This finding is in line with the literature [(Lowson et al. (1994), Nash et al.(1999)], and also fits well with the results showed in the previous sections. U_{rms}/U, fluctuations/perturbations, in fig 6-22 (c) are amplified significantly in 2%c upstream of the TE while W_{rms}/U in fig 6-22 (d) remain comparatively low even when close to the TE, signifying the two dimensionality of coherent structures. U_{rms}/U in figure 6-23 (c) shows the perturbations are amplified in the shear layer above the LSB as they approach the TE. These perturbations grow significantly from x/c = 0.9 and the flow in BL gain momentum as it transitions from laminar to turbulent, thus shrinking the LSB before interacting with TE. In fig 6-23 (d) features the same trend, major amplification of v’ starts around x/c = 0.90. Results presented here and the discussion above leads to the conclusion that the fluctuations in the shear layer start to roll up into significant span-wise coherent structures from approximately x/c = 0.90.

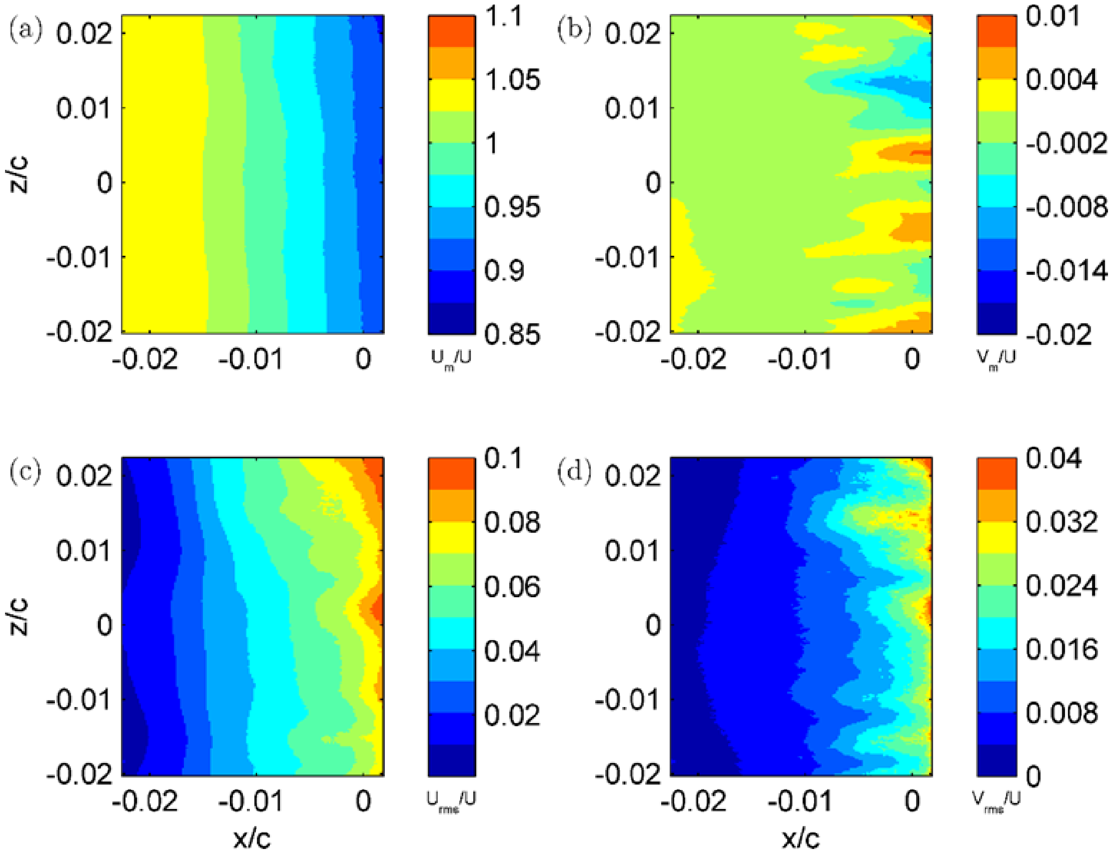

Figure 6-21: Mean and fluctuation velocity plots for configuration A-1

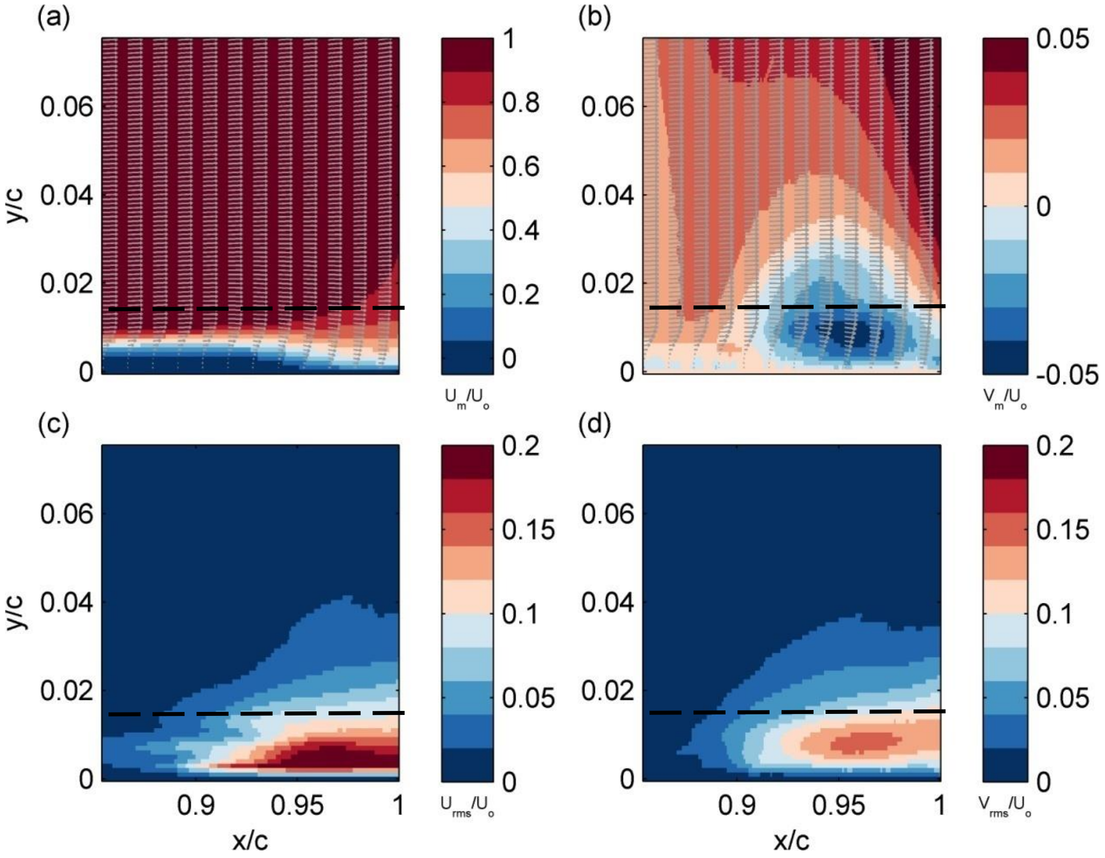

Figure 6-22: Mean and fluctuation velocity plots for configuration A-2

The configuration 'D', TE with flap, has some interesting observations to make when compared to straight TE, configuration 'A'. In fig 6-25 (a), the shear layer is more pronounced as compared to fig 6-23 (a) and the LSB reattaches upstream as compared to straight TE. Fig 6-24 (a) shows the change in U_m/U as the measurement plane (shown with black dotted line in fig 6-25(a) passes through different sub-layers of shear layer. The point of re-attachment moves upstream due to the flap attached at TE, the region of $(V_m/U)_{max}$ in fig 6-25 (b) moves upstream as compared to $(V_m/U)_{max}$ in fig 6-23 (b). This point towards the latter stages of transition where two-dimensional TS-waves break down into three-dimensional perturbations. The same can be deduced from the fig 6-24 (b) as close to the TE, there are spots where W_m becomes significant. The regions of $(U_{rms}/U)_{max}$ in fig 6-25 (c) shifts upstream and it is interesting to note that region $U_{rms} = 0.2U$ does not extend to TE as in case of $(U_{rms}/U)_{configuration-A}$. The v' perturbations start to amplify at about 0.9c, fig 6-25 (d), which is comparable to straight TE, fig 6-23 (d). As against the amplification of two-dimensional perturbations near the TE in case of straight TE, the amplification is three-dimensional seen in fig 6-24 (d). The W_{rms} attains a comparable value to the U_{rms} for flap, thus pointing towards higher turbulence. The breakdown of turbulence can also be seen in instantaneous velocity fields of flap in fig 6-18, giving way to 3rd phase of transition. Hence, the attenuation of narrowband (tonal) noise in case of TE modification with flap, fig 6-7.

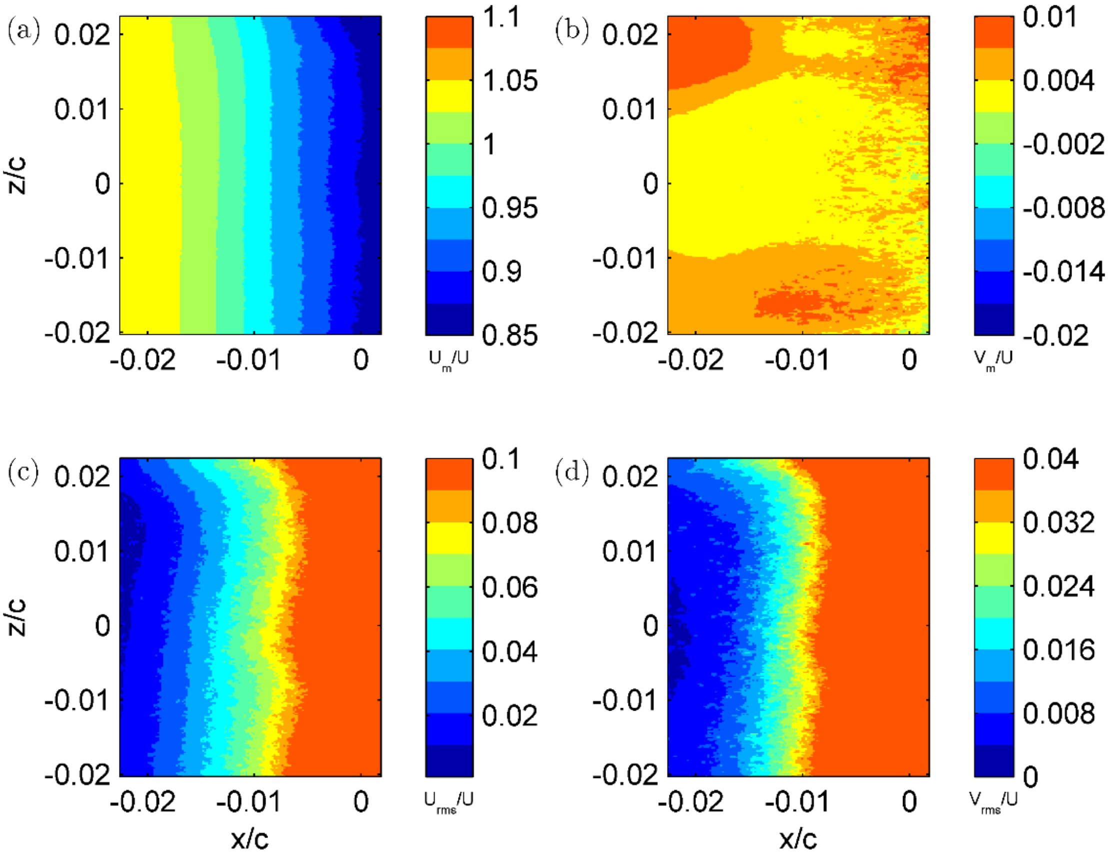

Figure 6-23: Mean fields and fluctuations plots for configuration D – 1

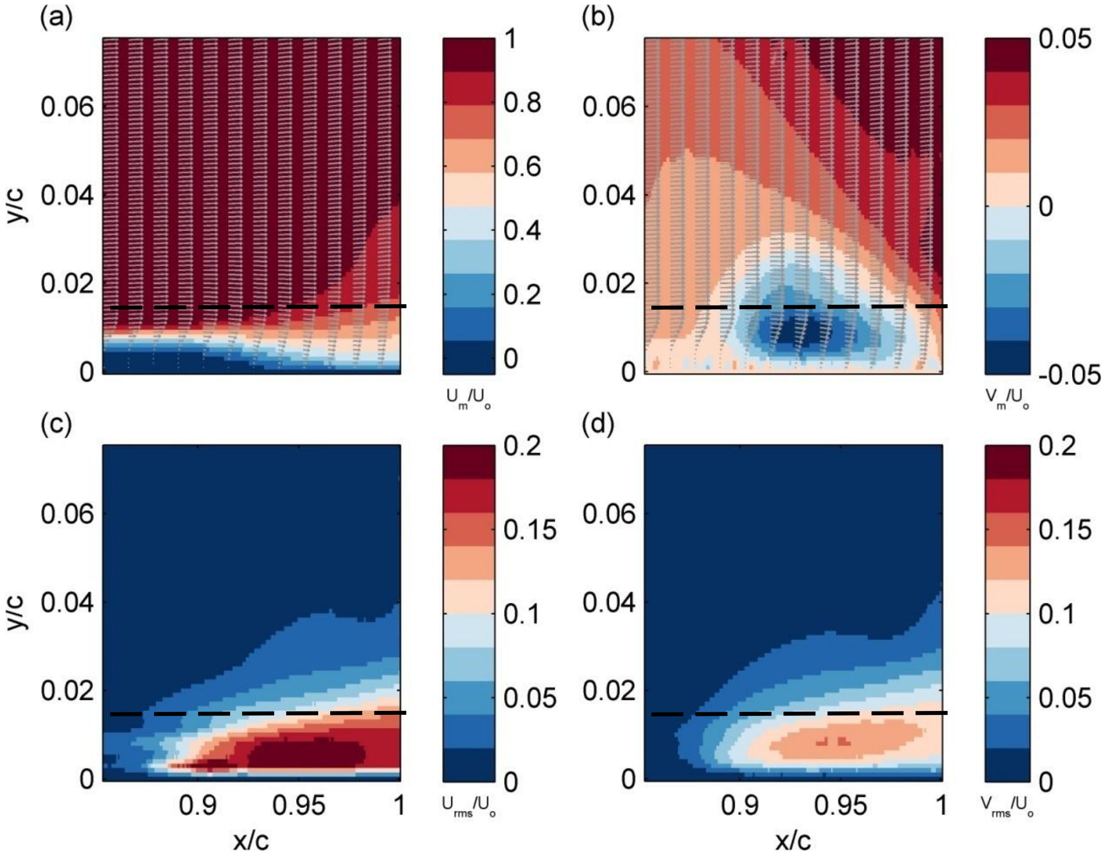

Figure 6-24: Mean and fluctuation velocity plots for configuration D – 2

To study the effect of serration 3 (configuration 'B'), the stream-wise mean and rms velocities are plotted at the tip and the root of serration. At these two localized points, the effective chord length is different, for the tip c=0.21 m and the root c=0.20 m. Fig 6-26 (a) shows the drop in mean velocity much more upstream as compared to other cases presented. As the span-wise plane enters, shown by dotted lines in fig 6-27 & fig 6-28, the shear layer the U_m/U drops. W_m/U varies drastically upstream of TE, showing that lack of span-wise coherent structures. The W_{rms}/U in fig 6-26 (d), fluctuations in span-wise is strong, thus the flow attained a three dimensional character upstream of TE. This behaviour can also be seen in fig 6-16 from instantaneous velocity fields.

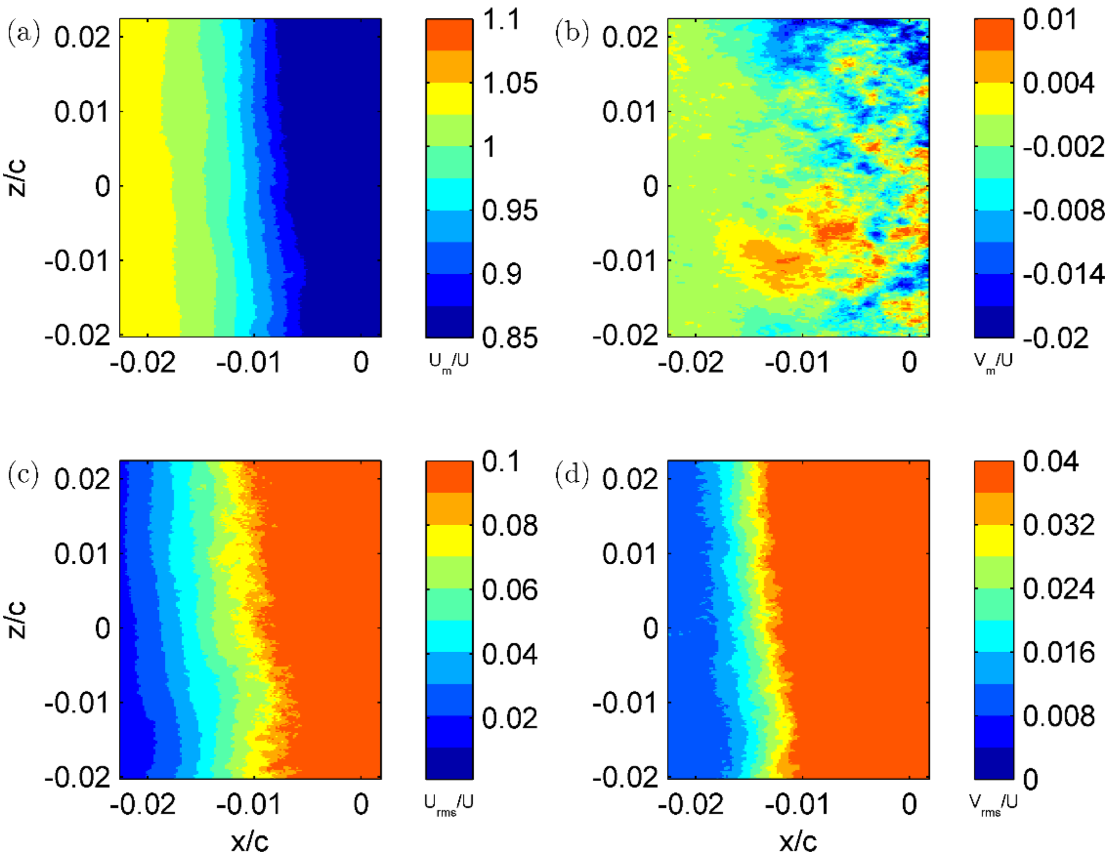

Figure 6-25: Mean fields and fluctuations plots for configuration B – 1

It is interesting to note the change in mean and rms velocity fields in stream-wise configuration between the tip and the root. The stream-wise localised statistical velocity fields for tip are comparable to statistical velocity fields of flap due to the comparable chord length and the same is for the localised statistical velocity fields for the root as compared to straight TE statistical velocity fields. The Um/U in fig 6-27 (a) shows a thicker BL near the TE while Um/U in fig 6-28 (a) shows less pronounced BL near the TE. The localised effective chord length at the tip shifts the region of V_m/U, in fig 6-27 (b) upstream as compared to root V_m/U in fig 6-28(b). The rms velocities also behave accordingly to the localised chord length. These localised rms fluctuations at every span wise location makes the span-wise coherent structures inherently unstable, thus attenuating the narrow band noise and breaking the proposed feedback loop.

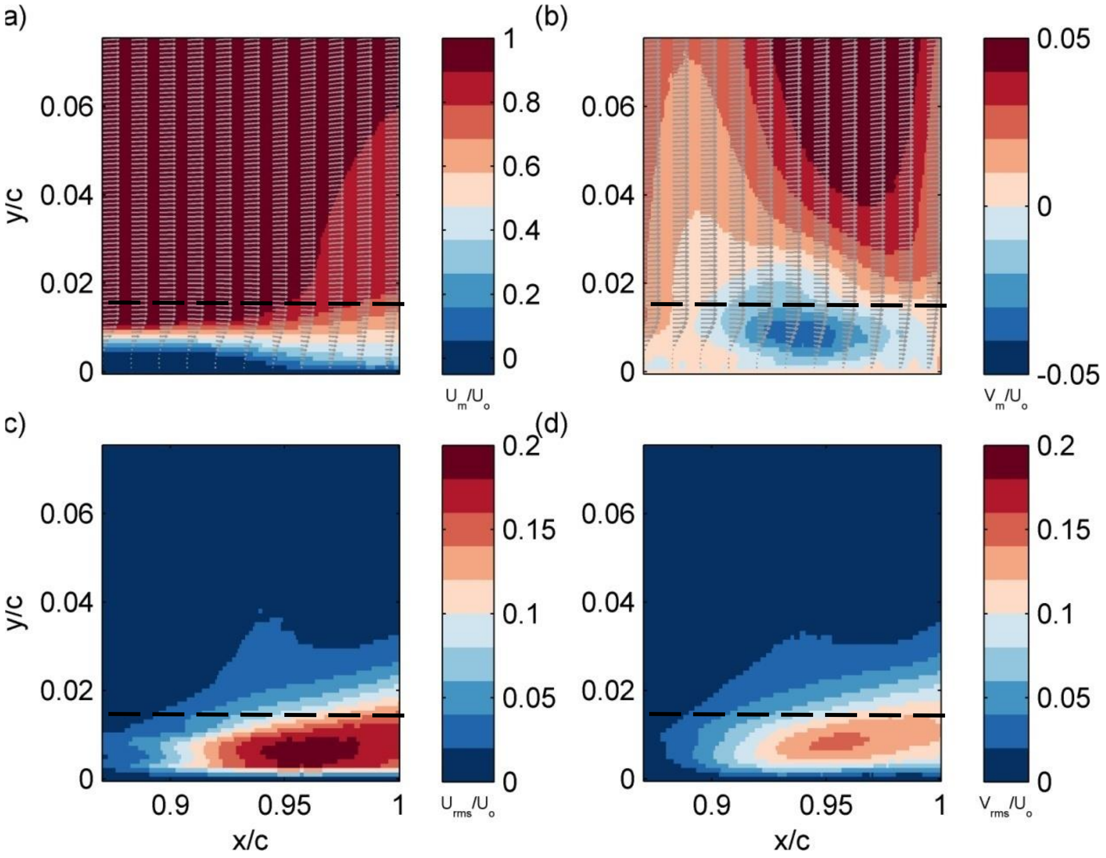

Figure 6-26: Mean and fluctuation plots at the tip of serration for configuration B – 2

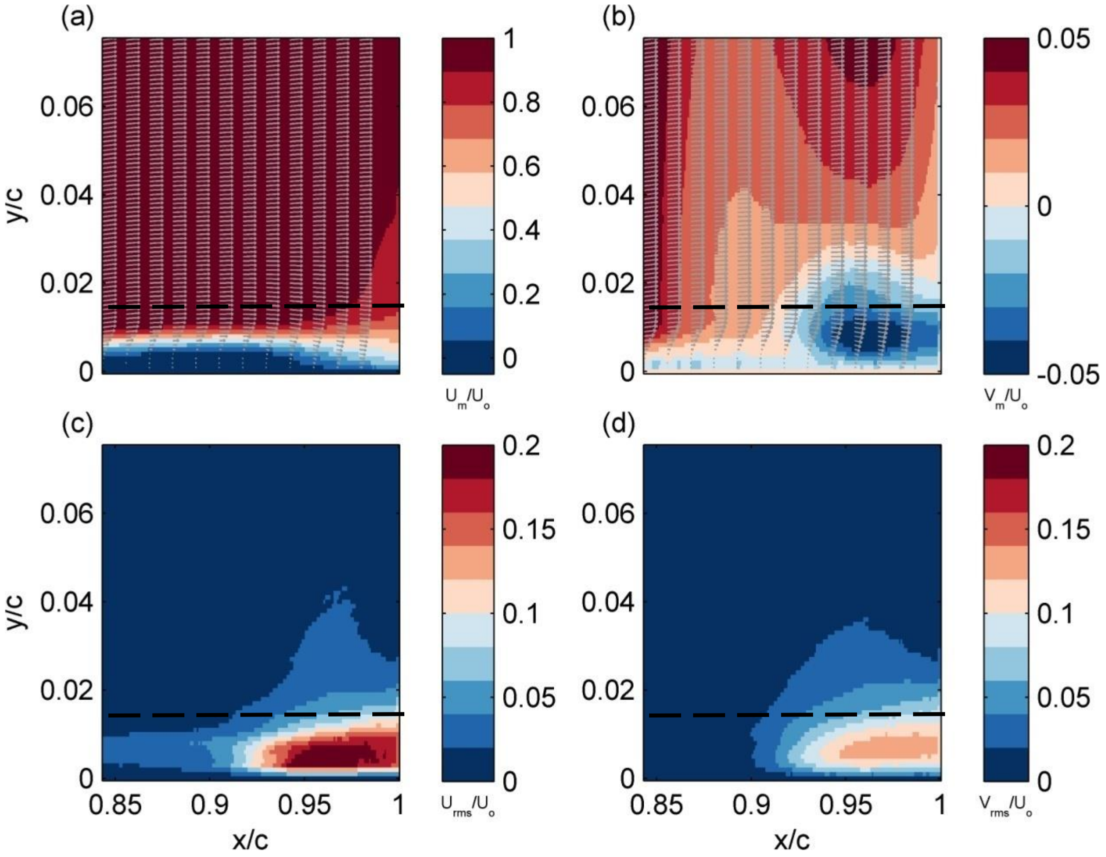

Figure 6-27: Mean and fluctuation plots at the root of serration for configuration B – 2

6.2.3.2 Spanwise correlations

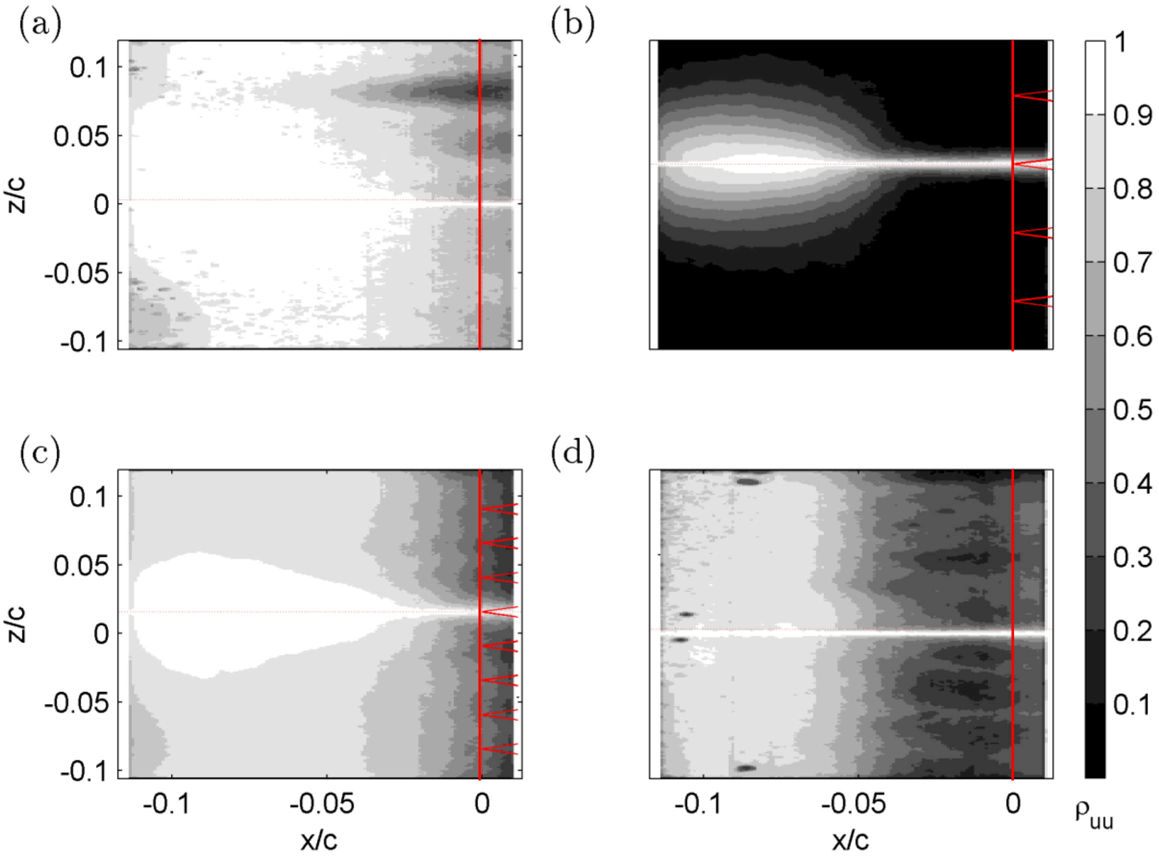

Figure 6-28: Contours of the cross-correlation coefficient ρ_{uu} of the unsteady velocity component u' for the different TE configurations (a) straight TE (b) serration 3 TE (c) serration 2 TE (d) flap TE at U = 25ms^{-1} measured at 3mm from the wing PS surface.

A span-wise velocity cross-correlation study is done to check the coherent structures and the turbulent nature of the flow. A span-wise location is chosen, root of the serrations, and the each velocity station in stream-wise on this location is cross-correlated with each velocity station of its span-wise counter-part. The cross-correlation function of the unsteady stream-wise velocity component (u) for zero time delay was computed between each of the stream-wise locations (x) of the domain at a reference span-wise station (z_0) (depicted with the red dashed line) in fig 6-28 and coinciding with the central span-wise station for configuration A-1 & D-1 and a serration root for configuration B-1 & C-1 and the other span-wise stations. The cross-correlation is then non-dimensionalized by the product of the standard deviations of the two signals as shown in equation 6.1, where the symbol N denotes the 4,500 vector fields and the '*i*' the time instant. Fig 6-28 (a) shows the span-wise correlated velocity structures in case of straight TE. The fig 6-28 (d) is highly uncorrelated span-wise upstream of TE, signifying the flow is already turbulent and thus completely attenuating tonal noise.

Correlation maps for serrations 2 and flap have partial span-wise correlated velocities, thus partial tonal noise attenuation. This analysis clearly shows the flow transitions to turbulent before the TE.

$$\rho_{uu}(x,z) = \sum_i^N \frac{u_i'(x,z_0).u_i'(x,z)}{u_{rms}(x,z_0).u_{rms}(x,z)} \tag{6.1}$$

7. Conclusions

An experimental study of the tonal noise phenomenon has been carried out in an open jet wind tunnel with the flow around the NACA 0018 airfoil (c=0.20m). Trailing edge (TE) modifications are employed on the wing to study their effects on the noise and on the flow domain. The acoustic emission experiments were conducted using far-field microphones between Reynolds numbers $1.32X10^5$ & $5.3X10^5$ with varying angles of attack (AoA).

- Tonal noise was detected for all the cases in the mentioned Reynolds number range at geometric AoA 4°, 7°, 10°, 13°. The role of PS and SS in noise generation is studied by forcing the boundary layer transition using roughness elements. The study showed, for all cases, the tonal noise is direct result of the flow characteristics on the PS.
- With increasing serration angle and wavelength, the noise attenuation increases.
- The same acoustic study is conducted with different trailing edge modifications in the above mentioned Reynolds number range at geometric AoA 7° keeping SS forcibly transitioned. It was found that the serration 3 ($2h = 20mm$ &$\lambda = 10mm$) attached to the TE of wing attenuates the tonal noise by 30db as compared to straight TE.
- Oil flow visualization technique with photochromic dye was used to study the effect of TE modifications on the PS upstream of the TE. The results obtained show that the TE modifications effect point of separation of the laminar separation bubble and hence the TE modifications effect the flow upstream of the TE of the wing. The separation point in case of serration-3 shifts upstream and the weak separation is observed as compared to other cases.
- The flow domain is studied at wall normal (orthogonal) and wall parallel (span-wise) planes by means of time resolved 2C-PIV techniques, for the selected case of U 25 ms^{-1} at AoA 7°, near TE. The span-wise PIV results show the TS-waves convecting downstream towards TE of the wing. Though for straight TE, the TS waves are span-wise coherent before interacting with TE. But for serration 3 case, span-wise PIV measurements showed lack of span-wise coherence and presence of turbulent spots. Presence of turbulent spots indicate the flow has transitioned to turbulent flow which in turn is the main cause of tonal noise attenuation.

- Other TE modifications' span-wise PIV results show the flow is more turbulent as compared to straight TE case. Vortex frequency analysis or spectral analysis of the time resolved span-wise PIV cements the above conclusion. Spectral analysis shown a perfect match of the radiated noise frequencies and the boundary layer waves till past the wake for the straight trailing edge. Instead the flow over the investigated serrations are of much more turbulent nature.
- The mean and fluctuation fields of the wall normal TR 2C-PIV show the difference in flow domain at tip and root of the serration. The span-wise change in flow characteristics in case of serrations can be attributed to the effective chord-length of the wing at each span-wise position.
- Further analysis of the flow, to understand the turbulence characteristics, through span-wise cross-correlation of u' for serration-3 give a clear picture of the span-wise un-correlated flow upstream of TE of the wing. Thus proving serrations attenuating the Tonal noise has direct effect on the upstream flow of the TE.

The study critically analysed the results published by Chong et al. 2014 and showed the serrations effect the flow upstream of the TE of the wing. The bypass transition, suggested by Chong et al. 2014, has not been observed but it is suggested that the span-wise variation of chord length due to TE serration is the reason for the early transition of the flow.

References

[1] R. W. Paterson, P. G. Vogt, M. R. Fink, and C. L. Munch, “Vortex Noise of Isolated Airfoils,” *J. Aircr.*, vol. 10, no. 5, pp. 296–302, 1973.

[2] C. K. W. Tam, “Secondary Ton,” vol. 55, no. 6, pp. 1173–1177, 2014.

[3] H. Arbey and J. Bataille, “Noise generated by airfoil profiles placed in a uniform laminar flow,” *J. Fluid Mech.*, vol. 134, pp. 33–47, 1983.

[4] M. S. Howe, “Aerodynamic noise of a serrated trailing edge,” *J. Fluids Struct.*, vol. 5, no. 1, pp. 33–45, 1991.

[5] M. V. Lowson, S. P. Fiddes, and E. C. Nash, “Laminar boundary layer aeroacoustic instabilities,” *Proc. 32nd AIAA Aerosp. Sci. Meet. Exhib.*, 1994.

[6] M. V Lowson, A. McAlpine, and E. C. Nash, “The generation of boundary layer instability noise on aerofoils,” *Proc. 36th AIAA Aerosp. Sci. Meet. Exhib.*, 1998.

[7] A. McAlpine, E. C. Nash, and M. V Lowson, “On the generation of discrete frequency tones by the flow around an aerofoil,” *J. Sound Vib.*, vol. 222, no. 5, pp. 753–779, 1999.

[8] T. Nakano, N. Fujisawa, and S. Lee, “Measurement of tonal-noise characteristics and periodic flow structure around NACA0018 airfoil,” *Exp. Fluids*, vol. 40, no. 3, pp. 482–490, 2006.

[9] G. Desquesnes, M. Terracol, and P. Sagaut, “Numerical investigation of the tone noise mechanism over laminar airfoils,” *J. Fluid Mech.*, vol. 591, pp. 155–182, 2007.

[10] Pröbsting, S., Serpieri, J. & Scarano, F., "Experimental investigation of aerofoil tonal noise generation." J. Fluid Mech. 747, 656–687, 2014.

[11] M. S. H. Boutilier and S. Yarusevych, “Separated shear layer transition over an airfoil at a low Reynolds number,” *Phys. Fluids*, vol. 24, no. 8, 2012.

[12] T. P. Chong and P. F. Joseph, “An experimental study of tonal noise mechanism of laminar airfoils,” *Proc. 15th AIAA/CEAS Aeroacoustics Conf.*, no. May, pp. 1–9, 2009.

[13] T. P. Chong and P. F. Joseph, “An experimental study of airfoil instability tonal noise with trailing edge serrations,” *J. Sound Vib.*, vol. 332, no. 24, pp. 6335–6358, 2013.

[14] J. W. Jaworski and N. Peake, “Aerodynamic noise from a poroelastic edge with implications for the silent flight of owls,” *J. Fluid Mech.*, vol. 723, pp. 456–479, 2013.

[15] D. Moreau, L. Brooks, and C. Doolan, “Experimental investigation of flat plate self-noise reduction using trailing edge serrations,” *Congr. Int. …*, pp. 1–10, 2012.

[16] D. J. Moreau and C. J. Doolan, “Noise-Reduction Mechanism of a Flat-Plate Serrated Trailing Edge,” *AIAA J.*, vol. 51, no. 10, pp. 2513–2522, 2013.

[17] L. E. Jones and R. D. Sandberg, “Numerical investigation of airfoil self-noise reduction by addition of trailing edge serrations,” *Engineering*, vol. 2010--3703, pp. 1–23, 2010.

[18] M. J. Kingan and J. R. Pearse, “Laminar boundary layer instability noise produced by an aerofoil,” *J. Sound Vib.*, vol. 322, no. 4–5, pp. 808–828, 2009.

[19] R. D. Sandberg and L. E. Jones, “Direct numerical simulations of low Reynolds number flow over airfoils with trailing-edge serrations,” *J. Sound Vib.*, vol. 330, no. 16, pp. 3818–3831, 2011.

[20] A. S. Hersh and R. E. Hayden, “Aerodynamic Sound Radiation from lifting Surfaces With and Without Leading-Edge Serrations,” *BBN Report.No. 2095*, 1971.

[21] T. F. Brooks, M. A. Marcolini and D. S. Pope, “T.F. Brooks and M.A. Marcolini, NASA Langley Research Center, Hampton,” 1984.

[22] S. Pope, “Turbulent Flows - S Pope (Cambridge, 2000)”, 2000.

[23] B. Plogmann, A. Herrig, and W. Würz, “Experimental investigations of a trailing edge noise feedback mechanism on a NACA 0012 airfoil,” *Exp. Fluids*, vol. 54, no. 5, 2013.

[24] W. A. Timmer, “Two-Dimensional Low-Reynolds Number Wind Tunnel Results for Airfoil NACA 0018,” *Wind Eng.*, vol. 32, no. 6, pp. 525–537, 2008.

[25] S. Pröbsting,"Airfoil self-noise, Investigation with particle image velocimetry", 2015

[26] Sandberg, R. D., Jones, L. E., Sandham, N. D. & Joseph, P. F., "Direct numerical simulations of tonal noise generated by laminar flow past airfoils." J. Sound Vib. 320, 838–858., 2009

[27] Raffel, M., Willert, C.E., Wereley, S., Kompenhans, J," A practical guide to Particle image velocimetry", Springer